1998-03-01

Acoustical emission source location in thin rods through wavelet detail crosscorrelation

Jerauld, Joseph G.

Monterey, California. Naval Postgraduate School

NAVAL POSTGRADUATE SCHOOL
Monterey, California

THESIS

ACOUSTICAL EMISSION SOURCE LOCATION IN THIN RODS THROUGH WAVELET DETAIL CROSSCORRELATION

by

Joseph G. Jerauld

March 1998

Thesis Advisor: Edward M. Wu

REPORT DOCUMENTATION PAGE

Form Approved
OMB No. 0704-0188

1. AGENCY USE ONLY *(Leave blank)*	2. REPORT DATE	3. REPORT TYPE AND DATES COVERED
	March 1998	Engineer's Thesis

4. TITLE AND SUBTITLE
ACOUSTICAL EMISSION SOURCE LOCATION IN THIN RODS THROUGH WAVELET DETAIL CROSSCORRELATION

5. FUNDING NUMBERS
Grant No. 32384-EG

6. AUTHOR(S)
Jerauld, Joseph G.

7. PERFORMING ORGANIZATION NAME(S) AND ADDRESS(ES)
Naval Postgraduate School
Monterey, CA 93943-5000

8. PERFORMING ORGANIZATION REPORT NUMBER

9. SPONSORING / MONITORING AGENCY NAME(S) AND ADDRESS(ES)
Engineering and Environmental Science Division
Army Research Office

10. SPONSORING/ MONITORING AGENCY REPORT NUMBER

11. SUPPLEMENTARY NOTES
The views expressed in this thesis are those of the author and do not reflect the official policy or position of the Department of Defense or the U.S. Government.

12a. DISTRIBUTION / AVAILABILITY STATEMENT
Approved for public release; distribution is unlimited.

12b. DISTRIBUTION CODE

13. ABSTRACT ***(maximum 200 words)***

Flaws in structural elements release strain energy in the form of stress waves that can be detected through acoustical emission techniques. The transient nature of a stress wave is analytically inconsistent to Fourier Transforms, and the wave characteristics under the effects of dispersion and attenuation deviate from the formal basis of the Windowed Fourier Transform. The transient solid body elastic waves contain multiple wave types and frequency components which lend themselves to the time and frequency characteristics of Wavelet Analysis. Software implementation now enables the exploration of the Wavelet Transform to identify the time of arrival of stress wave signals for source location in homogeneous and composite materials. This investigation quantifies the accuracy and resolution of two existing source location methods and develops a third technique using the Discrete Wavelet Transform on a windowed portion of the stress wave signal. A refined method for the spatial location of material damage induced stress waves can be used to directly monitor the safe-life of structures and provide a quantitative measure for the risk assessment of critical and aging structures. This investigation was partially supported by the Army Research Office.

14. SUBJECT TERMS	15. NUMBER OF PAGES
	151
	16. PRICE CODE

17. SECURITY CLASSIFICATION OF REPORT	18. SECURITY CLASSIFICATION OF THIS PAGE	19. SECURITY CLASSIFI- CATION OF ABSTRACT	20. LIMITATION OF ABSTRACT
Unclassified	Unclassified	Unclassified	UL

NSN 7540-01-280-5500

Standard Form 298 (Rev. 2-89)
Prescribed by ANSI Std. 239-18

Approved for public release; distribution is unlimited

ACOUSTICAL EMISSION SOURCE LOCATION IN THIN RODS THROUGH WAVELET DETAIL CROSSCORRELATION

Joseph G. Jerauld
Lieutenant Commander, United States Navy
B.S., California Polytechnic State University, June 1986
M.S., Naval Postgraduate School, September 1997

Submitted in partial fulfillment of the
requirements for the degree of

AERONAUTICAL AND ASTRONAUTICAL ENGINEER

from the

NAVAL POSTGRADUATE SCHOOL
March 1998

ABSTRACT

Flaws in structural elements release strain energy in the form of stress waves that can be detected through acoustical emission techniques. The transient nature of a stress wave is analytically inconsistent to Fourier Transforms, and the wave characteristics under the effects of dispersion and attenuation deviate from the formal basis of the Windowed Fourier Transform. The transient solid body elastic waves contain multiple wave types and frequency components which lend themselves to the time and frequency characteristics of Wavelet Analysis. Software implementation now enables the exploration of the Wavelet Transform to identify the time of arrival of stress wave signals for source location in homogeneous and composite materials. This investigation quantifies the accuracy and resolution of two existing source location methods and develops a third technique using the Discrete Wavelet Transform on a windowed portion of the stress wave signal. A refined method for the spatial location of material damage induced stress waves can be used to directly monitor the safe-life of structures and provide a quantitative measure for the risk assessment of critical and aging structures.
This investigation was partially supported by the Army Research Office.

DISCLAIMER

The views expressed in this thesis are those of the author and do not reflect the official policy or position of the Department of Defense of the U.S. Government.

Readers are also cautioned that the computer code in this thesis may not have been exercised for all cases of interest. While effort has been made, within the time available, to ensure that the program is free of computational and logical errors, additional verification should be applied. The use of this application is at the risk of the user.

TABLE OF CONTENTS

ACKNOWLEDGEMENT

I wish to thank my wife Lisa and my children Benjamin and Audrey for their support, patience and understanding during the conduct of this investigation. I would like to thank my advisor, Professor Ed Wu, for his guidance, intuition, and musical taste and for occasionally kicking me. As Vince Lombardi said, "The quality of a man's life is directly proportional to his commitment to excellence, no matter his field of endeavor."

I. INTRODUCTION

A. DAMAGE DETECTION AND FAILURE SITE LOCATION

In the design of aircraft and space structures, there is a requirement for high performance and low weight. As the designer estimates the loads and stresses, the classical approach is to use a factor of safety to ensure reliability and safety. Except for very simple structures, neither the service load (or load history) can be well defined, nor the methodology for calculating the limiting failure load well established. The ratio of calculated failure load to service load, or the calculated failure life to desired service life are utilized as safety factors. The magnitude of this factor of safety is often based on judgment and experience vice quantitative parameters. The ability of structural designers to maximize the strength to weight or stiffness to weight ratios is bounded by the safety factor and produces structures that are designed heavier and bulkier than the operating loads require to preclude catastrophic failure. Higher performance can be achieved if the structure is designed closer to operational load levels. Safety and reliability can still be assured if there is a system to monitor, detect and locate the onset of damage. In both metal and composite structures, flaws ultimately leading to failure begin at sizes which can easily escape current detection techniques. The small size of these initial failures enables them to be statistically spread throughout the structure, but spatial clustering can lead to catastrophic failure. Dislocations, cracks, delaminations, and fiber breakage all can lead to the failure of a structure. These point failures release strain energy which creates stress waves in the structure. Acoustical emission techniques detect stress waves by the particle motion that they create in the material itself. Most current source location techniques require operator input to calculate the source location for each signal, and do not calculate locations in real time. A large number of test signals must be made in order to accurately determine the location distributions for a given location method. To facilitate the processing of these signals, a method of determining the acoustic emission

source location that is free of continuous operator intervention is required for applications. An automated or semi-automated technique is more suitable for applications in aircraft or other high performance structures. Such a technique could be used by inflight data recorders and processing to warn aircrew of potential structural failure, or alert ground personnel to the locations for inspection and repair.

Alternately, the reliability of a structure may be assured by proof testing. Structural elements that pass proof testing are assumed to be safe at the operational load, when it may have transitioned to a less reliable state through the creation of new flaws in the proof testing process. With an effective damage detection and source location system, the element's worthiness at the operational load will be known. Risk of structural failure can be assessed based on information that is garnered from the structure. There can be a qualitative decision to inspect, repair or replace the structure of elements of the structure, or leave in service in the absence of any failures.

B. SIGNAL ANALYSIS OF STRESS WAVES

The localized failure site is analogous to the perturbation caused by a pebble in a still pond. On contact with the water surface, a transverse ripple wave is created on the surface. After the pebble penetrates the water surface, a compressive wave is created and propagates through the volume. An elastic solid under load is much the same. When a failure caused by a dislocation, a crack, or a fiber breaking in a composite occurs, the energy released propagates through the structure in the form of stress redistribution by elastic waves. There are two primary types of stress waves that propagate through the solid medium. When a solid medium is deformed, and released suddenly, both distortional, (shear deformation), and dilatational, (volume deformational), waves are produced. Particle motion parallel to the direction of propagation is characteristic of waves of dilatation, or longitudinal waves. Motion perpendicular to direction of propagation is representative of waves of distortion, or transverse waves. When a wave of either type impinges on a boundary of the solid, waves of both types will be generated

by the reflection (Kolsky, 1954). Structural materials are never perfectly elastic. The stress waves will attenuate, a loss in amplitude as it propagates through the medium, due to internal friction. Additionally, the stress waves do not exist as a single component of a single frequency. The many frequency components of both the longitudinal and transverse waves will each travel at different characteristic velocities through the solid. This phenomena is dispersion.

The critical parameter for determining the location of the source is the time of arrival of the wave, or a frequency component of that wave, at a sensor. Attenuation and dispersion affect the characteristics of the signal received at different sensors. The signals created by the stress waves are transitory, that is, the wave characteristics are different for different time or spatial windows. Fourier analysis transforms a stationary signal in the time domain to the frequency domain. The frequency spectrum, or presence of a frequency can be determined, but the time of arrival of that frequency cannot be resolved. Windowed Fourier transforms use a smaller but nevertheless fixed window, and evaluate the frequency content of the signal within that window. The transitory, non-stationary nature of the stress waves caused by the microscopic failure sites precludes the applicability of Fourier analysis. Wavelet signal processing techniques retain the time information that is lost in Fourier analysis. The signals are decomposed into a time-frequency basis that can determine the arrival and location of specific frequencies and transient phenomena. (Hess-Nielsen,1996)

C. SOURCE LOCATION TECHNIQUES

There are several methods which may be used to determine the time of arrival of a signal at a sensor, and each has strengths and limitations. The three degrees of freedom are amplitude, frequency, and time. Threshold Crossing, uses a preset level (voltage) as the time of arrival of the signal. When the signal strength reaches or exceeds this level, the time is marked, and a comparison is made to when the signal crossing that preset level at other sensors at different spatial locations. Gaussian Cross Correlation uses a

modulated cosine of one *a priori* selected frequency to determine the arrival time of the signal at a sensor. Correlation is carried out by sweeping (digitally) the modulated cosine pulse across the signals from each sensor, and the sum of the products of the two signals is calculated at each point. The peaks in the cross correlation functions correspond to the arrival of that frequency at the sensor (Ziola,1991). A third technique is explored in this investigation using Wavelet Detail Cross Correlation. A discrete wavelet transform is performed on the signals from each of the sensors. The reconstructed detail levels are then crosscorrelated to determine the difference in the time of arrivals at the sensors. A number of parameters were compared for the determination of location. The purpose of this investigation is to assess the feasibility of detecting the time of arrival of the acoustic emissions caused by the stress waves in homogeneous (steel) and heterogeneous composite (carbon fiber) rods, and to determine the location of the source of the acoustic emissions. Gish (1995) indicated a resolution to the location distribution on the order of the diameter of the sensing elements. This investigation is limited to one-dimensional cylindrical sample geometry of both homogeneous and composite materials. Steel and carbon fiber composite materials offer a wide range of varying propagation characteristics in attenuation and dispersion. They are chosen to broaden the applicability of the findings of this investigation. Only existing Wavelet Analysis methods are used, no new analytical techniques in the discrete wavelet transform are developed. Wave theory for thin rods is presented in Section II. The analytical bases for source location by threshold crossing, gaussian crosscorrelation, and wavelet detail crosscorrelation is described in detail in Section III. The experimental set up is given briefly in Section IV. The experimental results are given in Section V. Conclusions and recommendations are made in Section VI. Appendix A contains plots of representative signals, wavelet decompositions and crosscorrelations from the three test samples. Appendix B has the histograms of the location distributions, as well as the histograms of the best correlation level. Experimental method is given is greater detail in Appendix C. MATLAB script files written for the Wavelet Detail Cross Correlation and data analysis are given in Appendix D.

II. WAVE EQUATIONS IN GENERAL ANISOTROPIC SOLIDS

A. EQUATIONS OF MOTION

The set of governing equations for wave propagation in an isotropic solid is available in many text books of continuum - solid mechanics also in specialized books on stress waves. We develop herein the governing wave equations for homogeneous anisotropic solids for applications to composite materials.

For a general solid subjected to a time dependent surface traction $T_i^v(t)$, on a surface area A, with outward normal ν_j,(ν_j is taken to be independent of time for small deformation) at any instant, t, the *local* dynamic equilibrium between the external surface force and the internal stresses (σ_{ji}) adjacent to the surface is represented by the boundary condition:

$$T_i^v(t) = \sigma_{ji}(t)\nu_j . \qquad (1)$$

The *global* dynamic equilibrium for the entire body is maintained by summation of all the surface traction $T_i^v(t)$ on the external surface area A and the internal body forces within the internal volume to be balanced by the inertia force:

$$\int_A T_i^v dA + \int_V X_i dV = \rho \frac{d^2 x_i}{dt^2}, \qquad (2)$$

where X_i is field induced body force with dimension (wd) of [Force]/[Volume], ρ is the density wd [mass]/[Volume] and $\frac{d^2 x_i}{dt^2}$ is the acceleration in terms of the fixed inertia coordinates x_i (Eulerian coordinates). The boundary condition (1) is substituted into (2) and Divergence theorem applied (which must be in Lagrangian coordinates ξ_j, which moves with the body). Under the assumptions that density is time invariant, Equation (2) becomes:

$$\int_V \left(\frac{\partial \sigma_{ji}}{\partial \xi_j} + X_i - \rho \frac{d^2 x_i}{dt^2} \right) dV = 0$$

Assuming an arbitrary volume, then Newton's second law takes on a form in terms of the two different coordinate systems:

$$\frac{\partial \sigma_{ji}}{\partial \xi_j} + X_i = \rho \frac{d^2 x_i}{dt^2}. \qquad (3)$$

The Eulerian coordinates x_i which are fixed with an inertia system are related to Lagrangian coordinates ξ_i (which moves with the body by displacements u_i) by the kinematics relation:

$$x_i = u_i + \xi_i. \qquad (4)$$

The set of equations governing the dynamic behaviors of solid includes: the equations of motion, the displacement relating the Eulerian to the Lagrangian coordinates, the constitutive relation for materials responses between strain and stress, the kinematics relation between displacements and strain. Respectively, the set of governing equations are :

$$\frac{\partial \sigma_{ji}}{\partial \xi_j} + X_i = \rho \frac{d^2 x_i}{dt^2}, \qquad (5a)$$

$$x_i = u_i + \xi_i, \qquad (5b)$$

$$\sigma_{ij} = C_{ijpq} \varepsilon_{pq}, \qquad (5c)$$

$$\varepsilon_{pq} = \frac{1}{2} \left(\frac{\partial u_p}{\partial \xi_q} + \frac{\partial u_q}{\partial \xi_p} \right). \qquad (5d)$$

In the last equation, the strain-displacement relation is expressed in Lagrangian coordinates since rigid-body motion has been partitioned out, and higher order strain derivatives are not included.

In three dimensions ($i, j, p, q = 1,2,3$) this set of governing equations consists of 19 equations with 19 unknowns (X_i, x_i, u_i, σ_{ij}(symmetric), ε_{ij}(symmetric), t); the density ρ is taken to be a known constant, implying that it is not affected by the small deformation.

This set of coupled governing equations can be combined to a single equation of motion in terms of the displacements. This can be carried out first by substituting the strain-displacement relation (5d) into the stress-strain relation (5c) resulting in a constitutive relation in terms of displacement:

$$\sigma_{ij} = \frac{1}{2} C_{ijpq} \left(\frac{\partial u_p}{\partial \xi_q} + \frac{\partial u_q}{\partial \xi_p} \right).$$

Substituting this stress-displacement constitutive relation into the equation of motion while invoking symmetry in stress leads to (materials homogeneity is assumed, i.e. C_{ijpq} is not a function of spatial locations):

$$\frac{1}{2} C_{ijpq} \left(\frac{\partial^2 u_p}{\partial \xi_j \partial \xi_q} + \frac{\partial^2 u_q}{\partial \xi_j \partial \xi_p} \right) + X_i = \rho \frac{d^2 x_i}{dt^2} \qquad (6)$$

The Eulerian derivative operators can be expressed, in terms of the Lagrangian derivative operators by the chain-rule employing equation (5b):

$$\frac{\partial}{\partial x_j} = \frac{\partial \xi_k}{\partial x_j} \frac{\partial}{\partial \xi_k} = \left(\delta_{kj} - \frac{\partial u_k}{\partial x_j} \right) \frac{\partial}{\partial \xi_k}.$$

For infinitesimal displacement u_i during a time period $t_o \le t < t_1$, $\left(\delta_{kj} - \frac{\partial u_k}{\partial x_j}\right) \underset{u_k \to 0}{\Rightarrow} \delta_{kj}$

leading to the simplifications:

$$\frac{\partial}{\partial x_j} = \frac{\partial}{\partial \xi_j} + \text{higher order terms in } u_i .$$

As a result, for small displacements, the Eulerian and Lagrangian coordinate derivative operators are equivalent except for higher order terms in displacements u_k. The set of 19 coupled equations can be represented into a single equation in Eulerian coordinates (equation 6):

$$\frac{1}{2} C_{ijpq}\left(\frac{\partial^2 u_p}{\partial x_j \partial x_q} + \frac{\partial^2 u_q}{\partial x_j \partial x_p}\right) + X_i = \rho \frac{d^2 x_i}{dt^2} . \qquad (6E)$$

Alternatively, equation of motion in Lagrangian coordinates is:

$$\frac{1}{2} C_{ijpq}\left(\frac{\partial^2 u_p}{\partial \xi_j \partial \xi_q} + \frac{\partial^2 u_q}{\partial \xi_j \partial \xi_p}\right) + X_i = \rho \frac{d^2 u_i}{dt^2} . \qquad (6L)^*$$

Expanding for the two dimensional case (i = 1; j,p,q = 1, 2) , (6L) becomes the general anisotropic equation of motion in the i=1 direction:

$$C_{1111}\left(\frac{\partial^2 u_1}{\partial \xi_1^2}\right) + \frac{1}{2} C_{1112}\left(\frac{\partial^2 u_1}{\partial \xi_1^2} + \frac{\partial^2 u_2}{\partial \xi_1 \partial \xi_2}\right) + \frac{1}{2} C_{1121}\left(\frac{\partial^2 u_2}{\partial \xi_1 \partial \xi_2} + \frac{\partial^2 u_1}{\partial \xi_1^2}\right)$$

$$+ C_{1122}\left(\frac{\partial^2 u_2}{\partial \xi_1 \partial \xi_2}\right) + \frac{1}{2} C_{1211}\left(\frac{\partial^2 u_1}{\partial \xi_2 \partial \xi_1} + \frac{\partial^2 u_2}{\partial \xi_2 \partial \xi_1}\right) + \frac{1}{2} C_{1212}\left(\frac{\partial^2 u_1}{\partial \xi_2 \partial \xi_1} + \frac{\partial^2 u_2}{\partial \xi_2^2}\right)$$

$$\frac{1}{2} C_{1221}\left(\frac{\partial^2 u_2}{\partial \xi_2^2} + \frac{\partial^2 u_1}{\partial \xi_2 \partial \xi_1}\right) + C_{1222}\left(\frac{\partial^2 u_2}{\partial \xi_2^2}\right) + X_1 = \rho \frac{d^2 u_1}{dt^2} \qquad (7)$$

For the orthotropic case in the absence of field induced body force, $X_i = 0$ (e.g., in a gravitational field, the implied assumption is that the particle motions do not lead to large elevation changes). ($C_{1112} = C_{1121} = C_{1211} = C_{1222} = 0$) equation (7) yields

$$C_{1111}\left(\frac{\partial^2 u_1}{\partial \xi_1^{\,2}}\right) + C_{1122}\left(\frac{\partial^2 u_2}{\partial \xi_1 \partial \xi_2}\right) + \frac{1}{2}\left(C_{1212} + C_{1221}\right)\left(\frac{\partial^2 u_1}{\partial \xi_2 \partial \xi_1} + \frac{\partial^2 u_2}{\partial \xi_2^{\,2}}\right) = \rho \frac{d^2 u_1}{dt^2} \qquad (8)$$

Both forms of the above equations of motion are appropriate for stress wave analysis because the particle motions associated with the stress wave are small. Time dependent displacement functions which satisfy Equation (7) provide wave velocity associated with the particle motions. However, insight into amplitude decay is not contained in this formulation since the constitutive relations used herein do not include descriptions of internal dissipation.

*For isotropy, if the Lame constants λ and μ are used respectively to characterize the volumetric and deformational stiffness, Replacing the constitutive relation (5d) in this form, Equation (6L) reduces to the Navier Equation:

$$\left(\mu + \lambda\right)\left(\frac{\partial^2 u_p}{\partial \xi_j \partial \xi_q}\right) + \mu\left(\frac{\partial^2 u_q}{\partial \xi_j \partial \xi_p}\right) + X_i = \rho \frac{d^2 u_i}{dt^2},$$

$$\text{where } C_{1111} = \lambda + 2\mu \text{ and } C_{1122} = \lambda$$

B. ONE DIMENSIONAL WAVE PROPAGATION IN ANISOTROPIC SOLIDS

One dimensional solutions to the Equation of Motion Eq (7) can be obtained by semi-inverse method. That is, a kinematically admissible displacement function is *a priori* assumed and the satisfaction of the equation of motion and the boundary

conditions are *a posterori* demonstrated. Two kinematically admissible displacement functions are examined: i) for particle motion is parallel to direction of propagation and ii) for particle motion is perpendicular to the direction of propagation.

1. Longitudinal Wave Propagation

A one-dimensional wave can be induced by distributed force T_1 applied parallel the outward normal ν_1 of a free surface for a short time duration. The induced displacement is assumed to be:

$$\left.\begin{aligned} u_1 &= f(\xi_1, t) \\ u_2, u_3 &= 0 \end{aligned}\right\} \qquad (9)$$

That is, ξ_1 is the direction of propagation and u_1, the particle motion, is *parallel* to the direction of propagation; all other displacement components are zero. By substitution of Eq.(9) into Eq.(7), the second and third equations (i=2, i=3) are identically satisfied for orthotropic materials leaving the first equation as the only equation:

$$\frac{\partial^2 u_1}{\partial \xi_1^2} = \left(\frac{\rho}{C_{1111}}\right)\frac{d^2 u_1}{dt^2}. \qquad (10)$$

For small deformation (10) can be written in terms of the Eulerian coordinates

$$\frac{d^2 u_1}{dt^2} = C_L{}^2 \frac{\partial^2 u_1}{\partial x_1^2},$$
$$C_L{}^2 := \left(\frac{C_{1111}}{\rho}\right) = \left(\frac{\lambda + 2\mu}{\rho}\right)$$

which has a solution of the form:

$$u_1 = f(x_1 - C_L t) + F(x_1 + C_L t),$$

where C_L is the longitudinal wave velocity.

2. Transverse Wave Propagation

A second one-dimensional wave can be induced by distributed force T_2 applied perpendicularly to the outward normal ν_1 of a free surface for a short time duration. The induced displacement is assumed to be:

$$\left.\begin{aligned} u_1 &= 0 \\ u_2 &= g(\xi_1, t) \\ u_3 &= 0 \end{aligned}\right\} \qquad (11)$$

That is, x_1 is both the direction of propagation and the particle motion, u_2, is *perpendicular* to the direction of propagation; all other displacement components are zero. Upon substitution of eq. (11) into eq. (7), the first equation and third equation are identically satisfied leaving the second equation as the only equation

$$\frac{d^2 u_2}{dt^2} = C_T{}^2 \frac{\partial^2 u_2}{\partial \xi_1^2},$$

$$C_T{}^2 = \left(\frac{C_{1212}}{\rho}\right) = \left(\frac{\lambda}{\rho}\right)$$

with a solution of the form:

$$u_2 = g(\xi_1 - C_T t) + G(\xi_1 + C_T t)$$

where C_T is the transverse wave velocity.

III. SOURCE LOCATION TECHNIQUES

A. CHARACTERISTICS OF TRANSIENT SIGNAL ANALYSIS TECHNIQUES

At the instance of occurrence of a localized damage, the strain energy is released which induces stress waves. The time of arrival of the transient stress waves at different spatial locations can be used to locate the source of the damage. The propagation of stress waves produces particle motions which can be detected by analog transducers (on a free surface) and recorded digitally as implemented by several commercially available instrumentation packages (the Fracture Wave Detector is used in this investigation). Here, only the motion perpendicular the free surface is sampled. At a fixed spatial location, the mapping of samplings of particle motion (converted to voltage) results in a function of time. Conversely, at a fixed time, sampling by transducers in different spatial locations maps the results in a function of space. The sampling functions of time and space can be modeled by stress wave equations of the simpler homogeneous elastic case; a more general homogeneous anisotropic elastic case is presented herein. Other known and observed phenomena, such as dispersion , the velocity of propagation is a function of wavelength, and attenuation, the decrease in amplitude during propagation, are not well modeled (Davies, 1956). Because of the limitations of the analytical models of the underlying physical phenomena, the time of arrival of the samples of transient stress waves has to be cast in the context of identification of stochastic processes. The sampling recorded is viewed as information available on one of the ensemble sample functions of the particle motion. Based on the axiomatic heuristics that the accuracy of the identification is proportional to the degree of utilization of the information, we seek a method which maximizes the usage of information sampled toward the identification of the time of arrival of the stress waves.

1. Basic Features of Stress Waves and Stress Wave Sampling

From the derivation of the stress wave equations, there are two classes of stress waves: first, the longitudinal stress wave associated with particle motions parallel to the direction of propagation, second, the transverse stress wave associated with particle motions perpendicular to the direction of propagation. In a two dimensional solid, both the longitudinal and transverse modes are excited from a local damage. Even under an experimentally controlled excitation, the indentation and sudden release from the breakage of a pencil lead, both waves are generated from the minute deviation from geometric symmetry. Dispersion leads to wavefront change, attenuation leads to amplitude decrease. Also from the derivation of the wave equations, the propagation speed of the longitudinal wave is higher than that of the transverse wave. Therefore in the absence of total attenuation, the longitudinal wave will arrive before the transverse wave. The observation on attenuation is that the transverse wave attenuates faster than the longitudinal. The comparison of time of arrivals for location calculations must be obtained by correlating the samplings of waves of the same mode; i.e. the longitudinal wave to the longitudinal wave, or the transverse to the transverse.

2. Signal Analysis Characteristics

The three techniques used in this investigation for determining the time of arrival of the stress wave each have different fundamental functions, domains of analysis and applicability, and degree of information utilization. Threshold Crossing is based on a single point in the sample space, does not use any frequency information, and is applicable to non-stationary signals. Threshold Crossing is a logical 'greater than or equal to.' Gaussian Cross Correlation, is similar to the Fourier Transform and the Windowed Fourier Transform. A Fourier Transform is a sum of sines and cosines that has as its domain time from minus to plus infinity. The Fourier Transform utilizes the entire sample for frequency information, but is not applicable to non-stationary signals like stress waves. The Windowed Fourier Transform is also a sum of sines and cosines, but its domain is a moving window of fixed size from t_0 to t_1. Within this window the

same countable discrete frequency determination can be made as in the Fourier Transform. The Windowed Fourier Transform is applicable to signals that are stationary on the scale of the window, and is applicable to transient stress waves by an *a priori* selection of window size. Gaussian Cross Correlation is a special case of the Windowed Fourier Transform. Instead of a fixed window in time, the window is fixed in frequency. A single *a priori* frequency is modulated by a Gaussian pulse. GCC uses the content of that frequency within the entire sample space. A small Gaussian window will give a high resolution in time, but loss of information on lower frequency components. A large window will give better frequency information, but less time resolution. The Wavelet Transform is a function of a special wave shape with a fixed number of oscillations called a mother wavelet. The domain extends and contracts with the scaling of the mother wavelet, and with the scaling, the frequency component changes. Lower frequency as the scale is extended, higher frequency as the scale is contracted. The Wavelet Transform is applicable to strict-sense non-stationary signals in time, space and frequency, and utilizes the entire frequency content of the entire sample space. The *a priori* selection of the mother wavelet only affects the efficiency of the signal reconstruction.

B. THRESHOLD CROSSING

Threshold Crossing, also known as First Threshold Crossing, is the most rudimentary technique in determining time of arrival in Acoustical Emission. The FWD software allows a variable setting for the threshold voltage which is used to determine the first arrival time. The exceedance of the sample data over that preset value is defined as the first arrival of the stress wave. The sensor which records first arrival triggers the event recording and digitization. If the stress wave of a single mode and its velocity is known, the calculation of the location based on the difference in arrival time for each of the sensors is straightforward. The actual velocity is determined by iteration of the input velocity to position the central tendency of multiple signals under the first sensor. The location in the signal where the threshold is crossed may not be in the same place at each

sensor. Since only one single point of the entire data sample is utilized to determine the time of arrival, there are two major limitations to TC. One is the selection of the threshold value. If the threshold value is set too low, any noise is the signal will produce an under estimation of the time of arrival. Conversely, if the threshold value is set too high, the presence of attenuation will reduce the amplitude of the longitudinal mode below the threshold and the time of arrival will be based on the transverse mode. The second limitation is that in the presence of dispersion, the wavefront shape is altered which results in a different portion of the wave being used for the time of arrival. Figure 1 is signal number 50 from the 1/8 in. diameter steel rod data. The upper signal is sensor #1, the lower signal is from sensor #3. Figure 2 is zoomed in to show the arrival of the longitudinal wave and the threshold voltage of 0.005 v. The upper signal, sensor #1, exceeds the threshold voltage in the initial dilatation of the longitudinal wave. For sensor #3, the lower signal in Figure 2, the initial rise of the longitudinal wave does not cross the threshold, and the time of arrival is calculated from the second part of the longitudinal wave. The difference in the time of arrival should be 34 microseconds (μs) (56 μs - 22 μs), instead the arrival of the wave at sensor #3 is 59.4μs. This difference, 37.4 μs vice 34 μs, led to a 8 mm error in the 175 mm distance calculation between sensor #1 and #3. There is a trade-off in the setting of the threshold voltage level. If it is to low, the signal can trigger on the random noise in the system. If it is too high, the threshold crossing may occur in different portions of the signal, as seen in Figure 2. The gain setting on the preamplifiers and signal conditioning modules also affects TC performance. A gain setting that is high can trigger false signal recordings, and can easily cause time of arrival to be calculated from the random noise. A low gain setting may prevent the wave from exceeding the threshold and can lead to miscalculation of location.

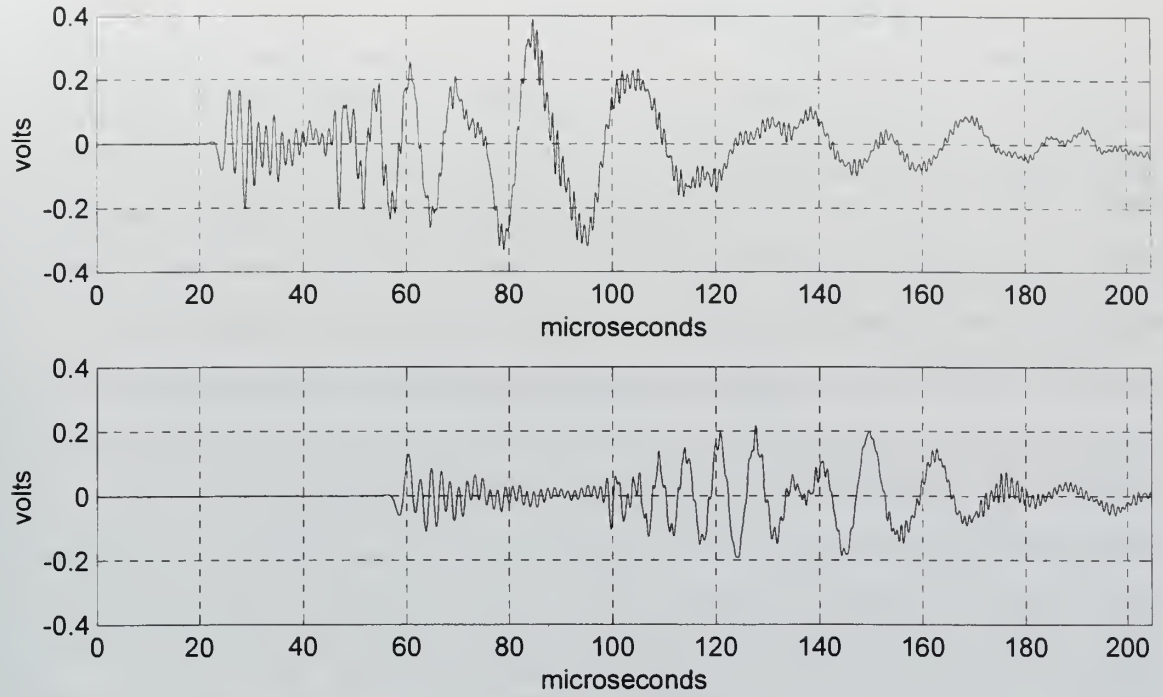

Figure 1. 1/8 in. Steel Rod Signal no. 50 Sensor #1 (upper) and #3 (lower)

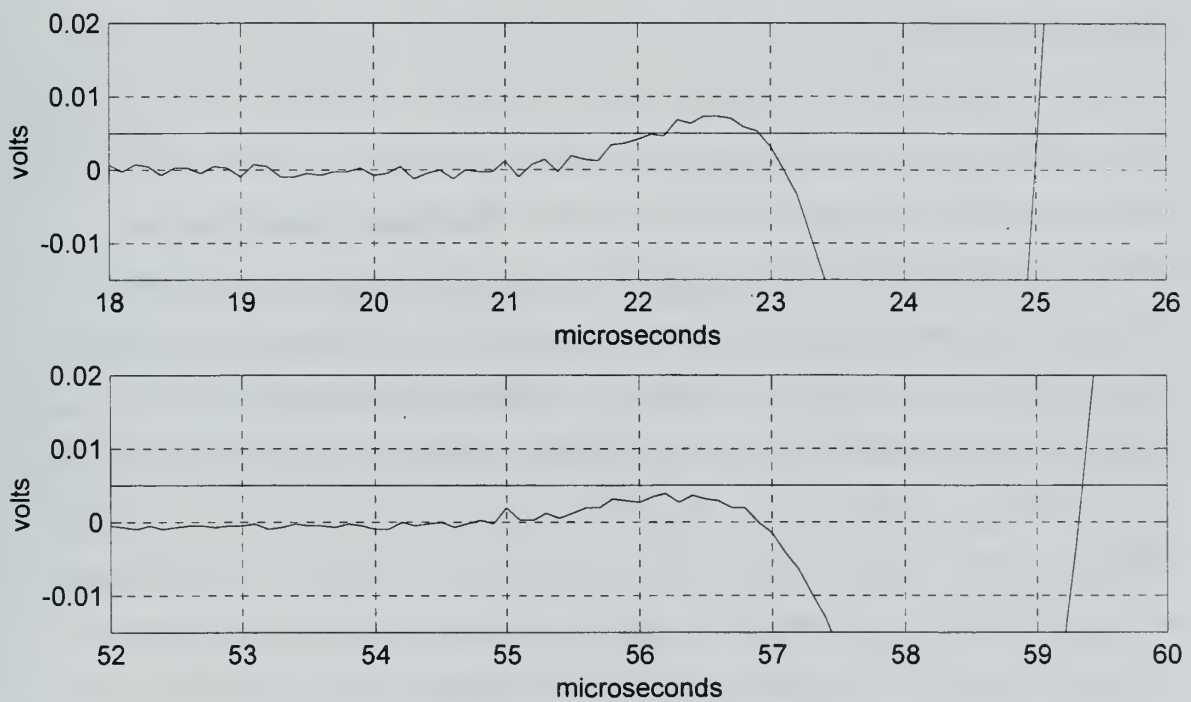

Figure 2. 1/8 in. Steel Rod Signal no. 50 Sensor #1 and #3 Threshold Crossing

C. GAUSSIAN CROSS CORRELATION

Gaussian Cross Correlation (GCC) is a variation of the Windowed Fourier Transform by Digital Wave Corporation. The technique was developed by Dr. Steven M. Ziola at Naval Postgraduate School (Ziola,1991). The core of the technique is based upon the premise that a single frequency from the output of all the sensors can be used to determine the arrival time of the wave at the sensors. GCC takes a frequency that is selected by the user, and amplitude modulates that frequency by a Gaussian envelope. The frequency that is modulated should be an average of the dominant frequencies of the waveform. The maximum of the crosscorrelation of the signals, the signal from the sensor and the modulated pulse, is the expected value of the time of arrival. Briefly, one signal is digitally swept across the other. There is a shift applied to one of the signals, and the product of the two signals at each shift value is calculated. In MATLAB terminology, it is the sum of the vectorized product of the signals at all the points where the signals overlap. The value of the crosscorrelation function at that value of the shift is the sum of all the products of the point for point multiplication. The amplitude modulation of the cosine gives it a single maximum, which means that there may be a more distinct location where the crosscorrelation function is a maximum. If there is more that one location in the waveform where the modulated frequency is present, there may be more than one peak in the crosscorrelation function. The amount of shift when the modulated cosine and the signal from different sensors crosscorrelates the best is then compared to the crosscorrelation from the other sensors. The difference in time between the peaks of the crosscorrelation functions is then difference in the time of arrival between those two sensors. GCC uses one frequency component of the entire signal, not just one point in the signal like TC. The technique requires foreknowledge of the single dominant frequency content of the signal. In the presence of reflections, the correlation peak may correspond to the part of the signal containing the reflection. If the chosen frequency is contained in both the longitudinal and transverse waves, the crosscorrelation function will have multiple peaks. The location parameter is the peak of the

crosscorrelation function. It is important to recognize that only an idealized sinusoidal excitation can produce a single frequency stress wave and a single mode, longitudinal or transverse. Even the idealized input requires the absence of dispersion. In an impulse-like excitation, as from actual material damage, or our controlled lead-break experiment, the stress wave always contains multiple frequencies.

D. WAVELET DETAIL CROSS CORRELATION

To find the location of a failure site consistently and with the least iteration by an operator, the location parameter used in the Wavelet Detail Cross Correlation technique and the methods for choosing the best correlation became the focus of this research. The wavelet transform gives different domains for interpretation of the time of arrival by the use of all, most, or some of the information in the sample set. The pragmatic approach to finding the location would be to analyze each signal individually, much like the Threshold Crossing and Gaussian Cross Correlation methods. To get to an automated procedure, and perhaps more importantly, to use a statistically significant number of test signals, the algorithm used in locating the failure site needs minimize operator intervention.

1. Wavelet Transform

The transient nature of a stress wave is analytically inconsistent to a Fourier Transform, and in the presence of dispersion and attenuation deviates from the formal bases of the Windowed Fourier Transform However, all the above characteristics of stress waves lend themselves to Wavelet Analysis. With the software implementation available through the MATLAB Wavelet Toolbox (by The MathWorks Inc.), it is now possible to explore using the wavelet transform to identify the time of arrival of stress wave signals. A wavelet is a small wave that is zero outside of some defined interval, and has a zero mean. The wavelet used in this investigation is the 'db4' wavelet. The choice of the 'db4' wavelet over any of the other db wavelets or any of the other families

of wavelets was purely subjective. The choice was motivated by its resemblance the leading edge of the longitudinal wave in the 3/8 in. diameter steel rod.

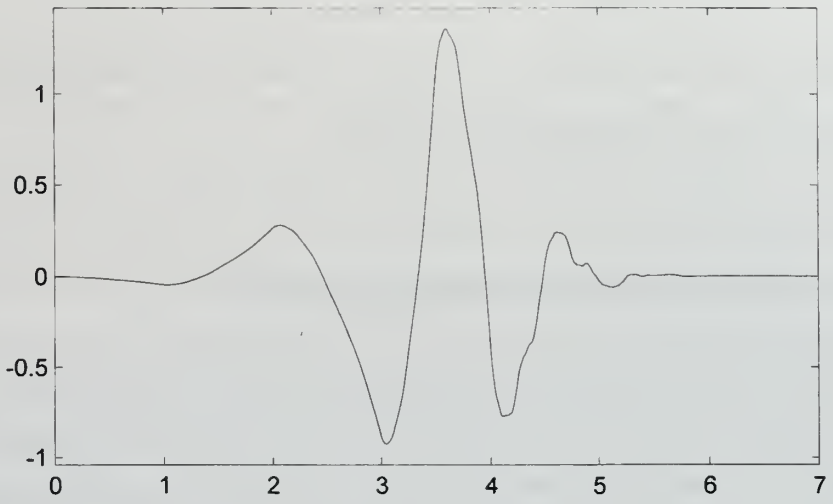

Figure 3. 'db4' Wavelet

The wavelet function is shifted, or translated, over all or part of the signal that is being analyzed. It is also scaled, the function is stretched or compressed, to focus on various components within the signal. The time-frequency domain is replaced in the Wavelet Transform by the time-scale domain. Scaling in the wavelet sense is simply stretching or compressing the wavelet. When the wavelet is elongated, it is a longer wavelength and lower frequency. When the wavelet is compressed, it is a shorter wavelength and hence higher frequency. The scaling function, Φ, gives the relationship between each of the discrete scales.

$$\Phi_{j,k}(t) = 2^{j/2}\Phi\left(2^{j}t - k\right)$$

Figure 4 shows the sum of a single cycle of Sin(t) and two cycles of Sin(2t). The same summation curve is plotted in Figure 5. Because of the two distinct sine curves, there are two distinct frequency components in each of the curves in Figure 5. The higher the scale, as in Figure 5a, the lower the frequencies. The lower the scale, as in Figure 5b, and Figure 5c, the higher the frequencies contained within the curves. As can be observed, scale is proportional to the inverse of frequency.

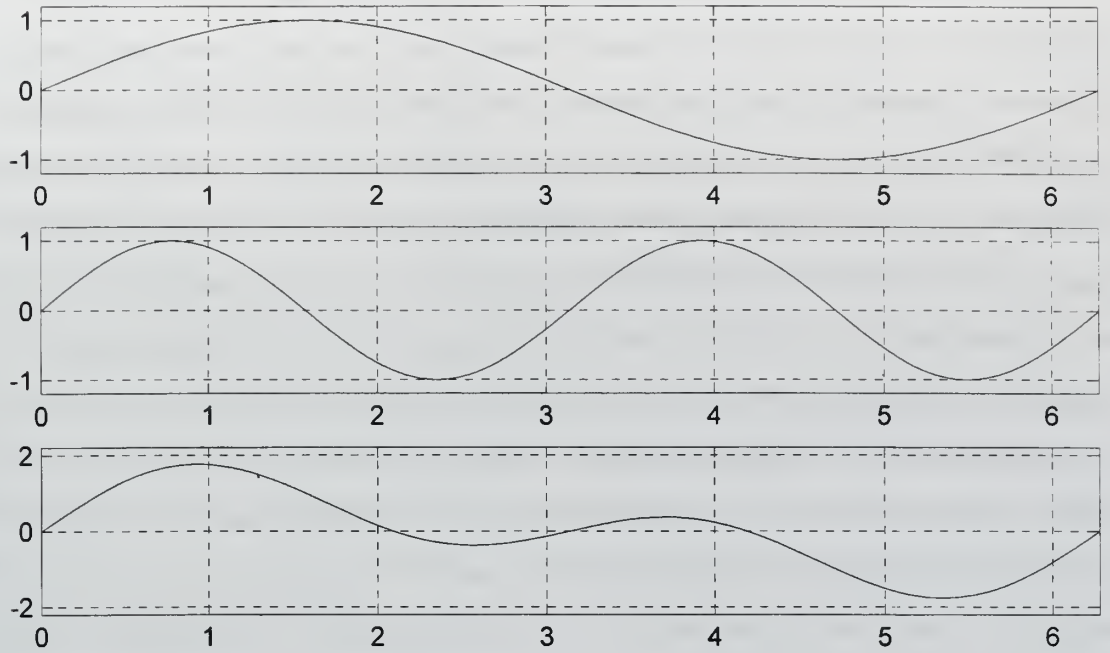

Figure 4. Sum of Two Sine Waves

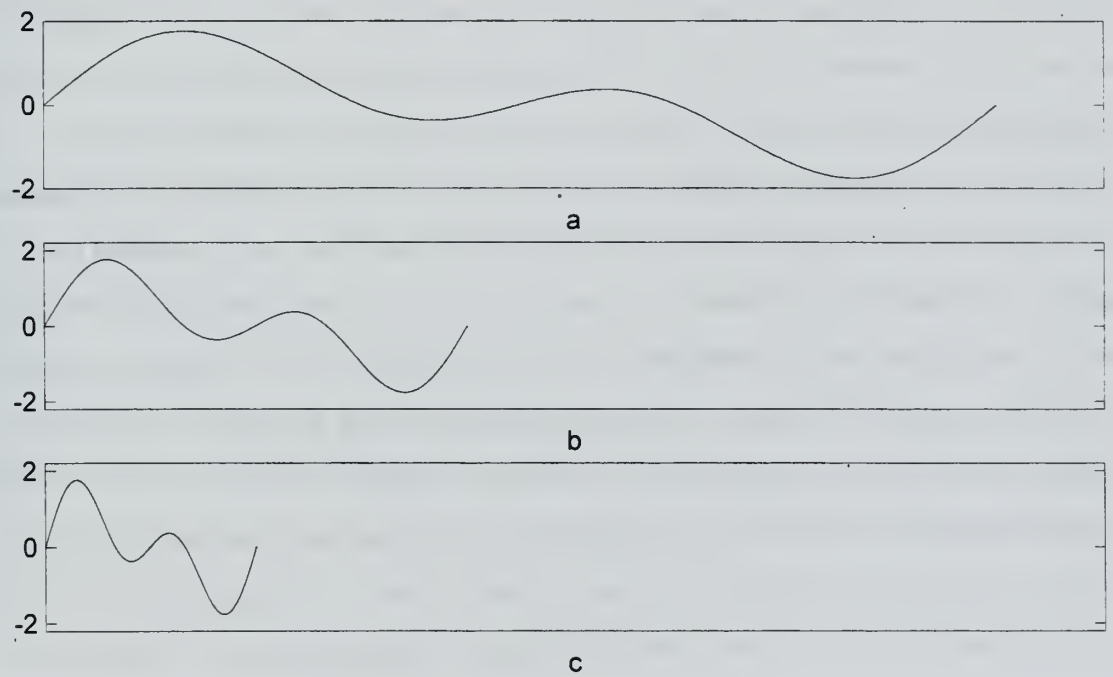

Figure 5. Effect of Scaling on Frequency of Sum of Sines

The wavelet is also translated. The translation of any function F(t) is F(t-k), where k is the amount of shift. A wavelet is scaled and translated over the range of the function or signal that is being transformed. There are two types of wavelet transforms, discrete and continuous. A continuous wavelet transform uses every scale up to a selected maximum value. The discrete wavelet transform utilizes scales of the wavelet that are based on powers of two. The term in the scaling function, Φ, is 2^j, where j is an integer value. If the sine wave in Figure 5a overlapped a signal, the amount that the signal resembled the long sine wave could be calculated. The sine wave would then shift and the resemblance at that location calculated. This process is repeated for all the chosen scales. The resemblance of the signal to the wavelet at a particular scale is actually the correlation of that portion of the signal to the wavelet. The value of the correlation is a number called the wavelet coefficient of either the approximation or the details. Smaller scale factors pick out higher frequency components, larger scale factors pick out lower frequency components. The signal can be broken into its constituent frequency components by reconstruction or synthesis. The scale, the location of the translated wavelet, the wavelet function, and the value of the wavelet coefficient at that translation are then used to assemble the portion of the original signal that lies within the frequencies at that particular wavelet scale. At a given level, the higher scale, lower frequency components of a signal are called the approximations. The lower scale, higher frequency contents are known as the details. A discrete wavelet transform can be repeated on a signal. The transform is performed at a larger scale on the approximations left over from the first level of the wavelet transform. The Wavelet Detail Cross Correlation technique performs an eight level discrete wavelet decomposition using the 'db4' wavelet on the signal received by each of the sensors on the steel or carbon fiber rods. After the discrete wavelet transform is performed, the eight details are reconstructed and each detail is a portion of the signal at progressively lower frequency bands. The signal in Figure 6 is signal number 89 from the carbon fiber rod data set. The uppermost plot is the raw data from sensor one, with the eight detail levels from the discrete wavelet transformation below. The time scale is shared for all curves and labeled on the bottom plot. The

longitudinal wave arrives at 25 μs (microseconds) and the transverse wave at 100 μs. The uppercase letter L indicates the approximate arrival of the longitudinal wave, and the uppercase letter T indicates the approximate arrival of the transverse wave. It can clearly be seen that the eight detail levels below the original signal contain information that corresponds to one or both of these waves. Detail level one is primarily the noise in the system. Details two, three, four and five have the frequency components of the longitudinal wave arriving at 25 μs. Level five also contains some of the transverse wave. Detail levels six through eight show the arrival of the transverse wave at 100 μs. The remaining approximation after the eight level decomposition is not plotted, as it is effectively a flat line. The trade-off between more decomposition and computation time did not make sense past the eighth level. This discussion is also applicable to the additional wave forms for the large and small steel rods given in Appendix A. The important difference is that the small steel rod has a less distinctive transverse wave mode. This is consistent with the physical consideration that the stress wave is the smaller diameter rod approaches a one dimensional propagation, and the transverse wave is suppressed.

Figure 6. Carbon Fiber Rod Signal no. 89 Sensor #1, Eight Level Decomposition

2. Location Parameter

After the discrete wavelet transform has created the details of the original signal, the next step is to crosscorrelate the details between transducers at different spatial locations. Each of the details from the signals from sensor #2, #3 and #4 are crosscorrelated with the corresponding detail level from the decomposition of the signal from sensor #1. These operations result in eight crosscorrelation functions for each sensor pair, sensors #1 and #2, sensors #1 and #3, and sensors #1 and #4. Figure 7 shows the crosscorrelations of carbon fiber rod signal no.89 sensors #1 and #4. The crosscorrelation functions are displayed in increasing order of detail level from top to bottom, which corresponds to decreasing frequency. The magnitude of each plot is plus or minus one. The different levels of decomposition do not have the same magnitudes and the values of the crosscorrelation functions could not be compared directly. In order to preclude biasing the results toward signals of large amplitude by simply choosing the largest maximum among the eight, the crosscorrelation functions are normalized by the energy of the details being crosscorrelated. They are normalized such that if the two details being crosscorrelated are exactly the same, the maximum value of the crosscorrelation function would be one. Among the eight crosscorrelation functions, the best crosscorrelation is used to determine the difference in the time of arrival at each sensor. In order to make an initial step towards semi-automation, the location parameter and best correlation parameter were varied. In time/frequency analysis, a priori knowledge of a signal makes it possible to choose the most relevant representations among the many possibilities (Gade,Gram-Hansen,1997). The goal is to improve the location calculation from the TC and GCC results, without the limitations of either. The determination of which crosscorrelation function to use is the essence of the problem. The variable is the difference in the time of arrival of the signal at each sensor. There are eight answers available, and the correct answer is obtainable from one or more of them. From a probabilistic viewpoint, the signals from each sensor are stochastic variables that have an underlying distribution.

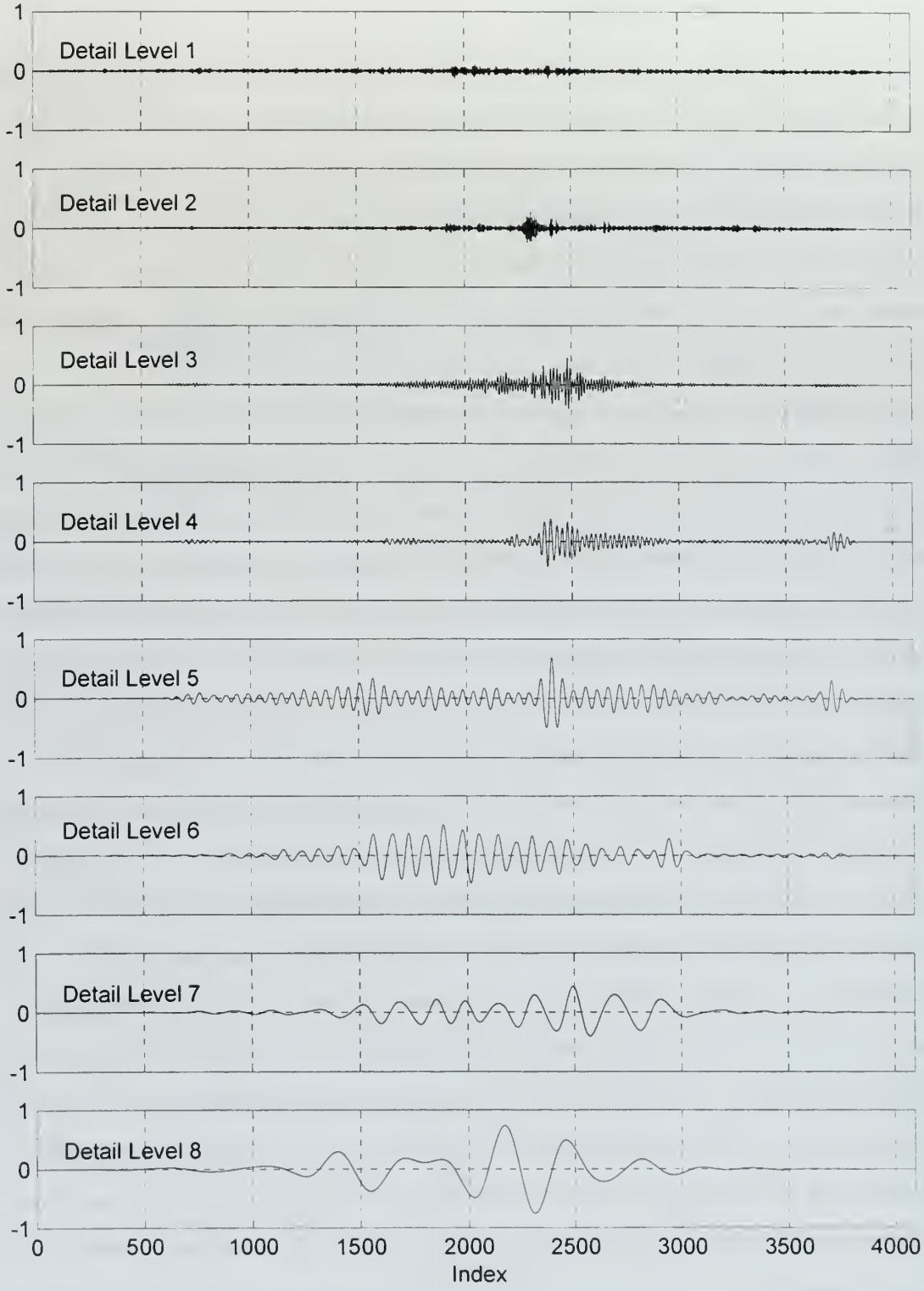

Figure 7. Crosscorrelation Functions of Carbon Fiber Rod Signal no. 89 Sensors #1 and #4

The value of each point within the signal will obey the same distribution as any other point in the signal. The location parameter in threshold crossing is the point in the signal where a preset voltage is exceeded. This puts all the emphasis on a single point in the data. Gaussian crosscorrelation uses a single frequency as the location parameter. The whole data set is checked for this frequency, and the highest value in the crosscorrelation function is used. GCC uses more of the total information available in the signal to determine the location.

To determine which of the eight crosscorrelation functions was the best, the variance of the absolute value of the function was calculated. When the absolute value of the crosscorrelation function is taken, the function takes on the form of a distribution. The statistical properties of the absolute value of the crosscorrelation function would be used to determine the best correlation level, and the time of arrival of the stress wave at that level. It is apparent from the detail levels in Figure 6 that there are many frequency components in the longitudinal and transverse waves. Because of dispersion, each of these frequencies will travel at a different speed. Consistent calculation of location requires using the same detail level to the maximum extent. A pragmatic approach would be to select a detail level, and use that level exclusively. This places all the weights on that frequency regime, and the variability in distance from the source and details of the source can change the presence of that frequency. For example, breakage or dislocation near the surface of a structure could cause a major difference in the stress wave from the wave created by a flaw in the interior of the structure. In studying the many crosscorrelation functions generated in this effort, the function that appears to the human eye to correlate best rises in amplitude to a single distinct maximum, then returns toward zero. If the criteria of minimum variance in the absolute value is used, then the signals that have a more deterministic appearance would be used for the calculation of location. The effect on the best correlation calculation by zeroing the lower five to forty five percent based on the maximum value was established. Another parameter explored for choosing the best crosscorrelation function was the minimum of the variance divided by the maximum value of the correlation. This change kept phenomena such as a single

random spike in the noise in detail level one from determining the time of arrival. To determine the effects of basing the location on a single detail level, the location calculation based on the maximum value of the crosscorrelation function of a single detail level was investigated. Finally, the effect of windowing the signal to isolate the longitudinal and transverse waves was explored. From the windowed signals, the Wavelet Detail Cross Correlation was performed. The beginning of the window is the arrival of the longitudinal wave at the triggering sensor. The pre-trigger settings available in the FWD software were zero percent of the capture length and 12.5 percent. This is the amount of data that is kept in a continuous buffer to preclude missing the initial portion of a triggering signal. The need for setting the left side of the window could be satisfied by more flexible software which would allow a one or two percent pre-trigger. The right side of the window was set to allow either: i) all the data in the signal, or ii), to end before the arrival of the transverse wave. Both the longitudinal and transverse waves were isolated by the windowing. The effect of using a single stress wave mode was established. These attempts are based on the desire to use as much time-frequency information from the signal as possible. If the location determination is calculated from a greater amount of time-frequency information rather than just one point or one frequency, then a change in one component or amplitude will have a reduced effect.

IV. EXPERIMENTAL SETUP

A. OBJECTIVE AND SCOPE

The objective of this investigation is to determine the accuracy and resolution of locating the time of arrival of stress waves through Threshold Crossing, Gaussian Cross Correlation, and Wavelet Detail Cross Correlation. The Experimental scope is narrowed down to one-dimensional experiment without reflections to reduce experimental variables. Within the one-dimensional scope, the parameters are widened to extend the generality of the observations and conclusions. The parameters investigated are:

1. Materials Homogeneity
2. Effect of Plane Wave - diameter effect
3. Signal Amplification

B. EQUIPMENT

The test signals were captured and analyzed on acoustical emission equipment purchased from the Digital Wave Corporation. A pentium 133 Mhz personal computer, two dual channel Filter Trigger Modules, four wideband preamplifiers, and one of two sets of four wideband sensors, make up the system, and were connected in accordance with the FWD users guide. The FWD 12 bit software was used to capture the signals, which were made on the ends of the test specimen with Pentel 0.3 millimeter (mm) mechanical pencil and H lead. The test focused on the location of failure sites in one dimension, therefore steel and carbon fiber rods were used as test specimen. Two steel drill rods, one 3/8 inch diameter, and one 1/8 inch diameter, and one 0.158 inch diameter carbon fiber rod were used. The steel rods, nominally three feet in length, had the ends machined to remove the strain hardened area. The carbon fiber rod was purchased in

bulk, and a four feet section was cut and dressed for the test article. The wideband sensors were purchased in two sizes. The large transducers are 3/8 inch, (9.5 mm) in diameter, and the small transducers are 0.20 inches, (5.08 mm) in diameter. The large transducers were only used on the 3/8 inch steel rod. The small transducers were used on the 1/8 in. diameter steel and 0.158 in. diameter carbon fiber rod. The large and small transducers, were held onto the test articles by transducer holders that were made from round plexiglass stock. Silicon vacuum grease and small dental rubber bands were used to maintain the contact force between the transducers and the test specimen. All signals were made in four channel mode, that is, they had four sensors recording signals. The memory length used was 2048 data points, with a digitization rate of 10 megahertz (Mhz). The highest frequency observed (in detail level two) was 2.22 Mhz. The gain for the 3/8 in. diameter steel rod was 41 decibels (db). The gain for the 0.158 in. diameter carbon fiber rod was 47 db. To explore the effect of gain on the location calculation, the gain setting was changed in the 1/8 in. diameter steel rod data set. The gain for the first 50 signals in the 1/8 in. diameter steel rod was 43 db, and for the second 50 was 41 db. One hundred signals on the large steel rod were made first, followed by the signals on the small steel rod, and finally one hundred signals on the carbon fiber rod. Signal 17 from the 3/8 in. diameter steel rod data, and signal 61 from the 1/8 in. diameter steel rod data were not used due to file corruption, leaving 99 signals in the large and small steel rod data sets. The Fracture Wave Detector (by Digital Wave Corp.), and the MATLAB Wavelet, Statistics, and Signal Processing Toolboxes were used on the acquisition and analysis of the test signals. The experimental method is described in detail in Appendix C.

C. TEST SIGNALS

Each of the signals was analyzed with the Threshold Crossing and Gaussian Cross Correlation methods within the FWD software. Each file was then exported as comma

delimited ASCII text, and opened in a spreadsheet, to enable the file to be formatted to tab delimited ASCII text. The only role of the spreadsheet program was to convert the files to a format that could be read by MATLAB. There are two locations where a test signal can be made on a cylindrical rod. The signal can be made on the end or on the edge. Kolsky (1953) demonstrates how a either a longitudinal or transverse wave mode impinging on a boundary will reflect as both types of waves. Signals made at the end of the rod will begin as a longitudinal wave, and then excite transverse waves. Signals made anywhere on the edge will initiate as transverse waves and excite longitudinal waves. This method has the advantage that the test signals can be made anywhere on the rod, and internal to the sensor arrangement. Signals made at the end of the rod must be made external to the sensors, however this is the signal form that is likely to be encountered in an actual failure. The test signals were made at the end of the rod for this reason. The parameter measured by the location algorithms is the time of arrival of the stress wave at the sensors. When the signal comes from outside the sensors, the difference in the arrival times between sensors maps into the distance between the sensors. The force applied by the pencil lead at the end of the rod deforms the end slightly, and when the lead breaks, the deformation is quickly released, and the stress waves propagate down the rod. The physical layout of the transducers was identical on all three rods and is shown in Figure 8. The pencil lead breaks were made on the free end to the left of the sensor array. Metric units are used in all calculations to facilitate comparisons with the FWD location methods. The 1/8 in. and 3/8 in. diameter steel rods were nominally 910 mm in length. The carbon fiber rod used was a nominal 1200 mm in length.

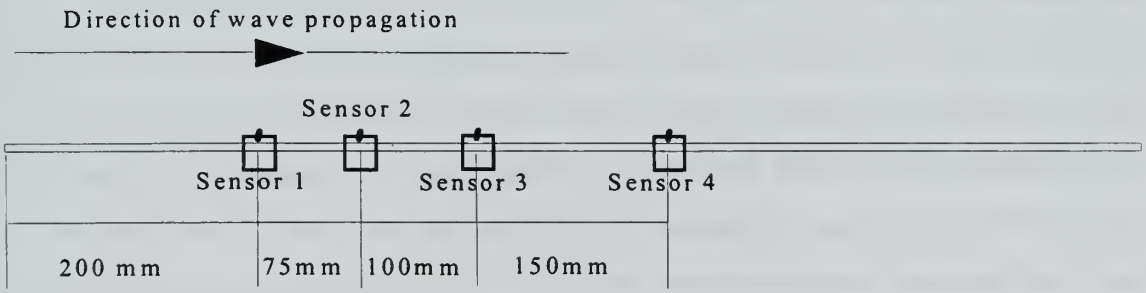

Figure 8. Test Specimen Setup

Critical to the consistent, repeatable calculation of distance is the elimination of reflections. Earlier thesis research (Gish,1995) had used a 3/8 inch diameter steel rod 206 mm in length. The velocity of the longitudinal wave was found to be 5135 meters per second (m/s). The signal travels 206 mm in 40.12 μs. To eliminate as many potential sources of error, the location algorithms need to use the best possible signal, and by eliminating reflections, it simplifies the processing. As the longitudinal wave front travels down the rod, it attenuates. When the wave is reflected from the end, the amplitude will double and reverse direction back up the rod. The sensors are not directionally sensitive, they are unable to discriminate between left or right running waves. The increase in amplitude from the reflection may be used as the arrival time in a threshold crossing location determination. The FWD software used in the acquisition of the signals can be utilized to eliminate the capture of reflected signals. The memory length / channel is the total number of data points digitized per channel for every wave form captured. The digitization rate is the frequency at which analog to digital conversion takes place. The duration of data captured is the memory length divided by the digitization rate. The duration of data captured must be long enough to allow the slower moving transverse wave the reach the final sensor, but short enough to preclude the reflection of the faster longitudinal wave returning to that same sensor. The memory length of 2048 data points, and digitization rate of 10 Mhz. gave a duration of captured of 204.8 microseconds. This length of time in conjunction with the length of the rod past the final sensor eliminated reflections. The waves detected by the sensing elements will be characterized, and some key features will be discussed. Figure 9 is an example signal from sensor #1 for the 3/8 in. steel rod. The first pulse with a peak at 28 μs is the longitudinal wave. The higher frequency, larger amplitude waveform is the transverse wave with the time of arrival at approximately 45 μs. Figure 10 is an example signal from sensor #4, for the 3/8 in. steel rod. The longitudinal wave arrives at 90 μs, the transverse wave at 150 μs. The source signal for the plots of Figures 9 and 10 are the same, and the salient points to note are the increase in separation between the longitudinal and transverse waves from Figure 9 to Figure 10, and the decrease in amplitude of both

waveforms as they propagate down the rod. Recalling from Figure 8 that sensor #4 is farther away from the source than sensor #1, the increase in the separation of the time of arrival of the two wave modes (in Figures 9 and 10) is a graphical illustration of the greater velocity of the longitudinal wave. The distance between sensors #1 and #4 is 325 mm. The signal has traveled a total distance of 525 mm when it has reached sensor #4. The decrease in amplitude illustrates the effect of attenuation, and the somewhat subtle change in the wave form illustrates the effect of dispersion. Attenuation can be seen clearly in Figures 1 and 2. Dispersion is more difficult to envision. The different frequency components of either the longitudinal wave or the transverse wave will travel at different velocities. The wave front shape will change as dispersion affects the signal. The main pulse of a longitudinal wave will become distorted, and will be followed by a train of oscillations of higher frequency (Kolsky, 1953). This phenomena may be observed in the sensor #4 signal of Figure 10, where the waves between 100 μs, and 140 μs were caused by the dispersion of the longitudinal wave.

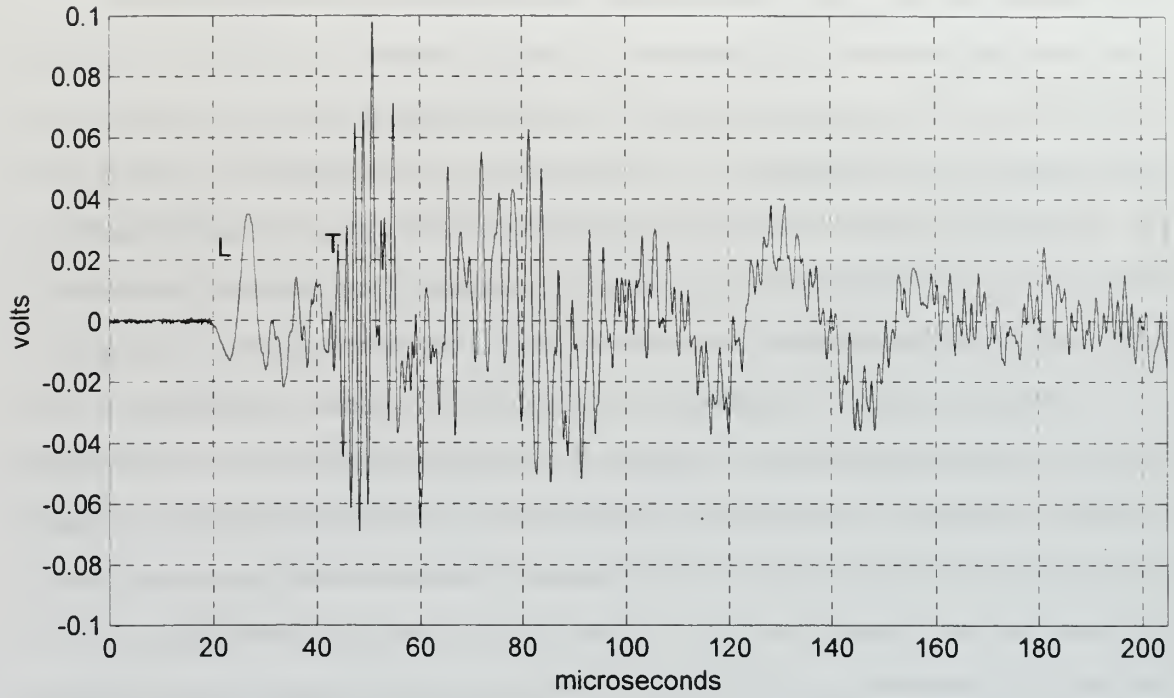

Figure 9. Example 3/8 in. Diameter Steel Rod Signal from Sensor #1

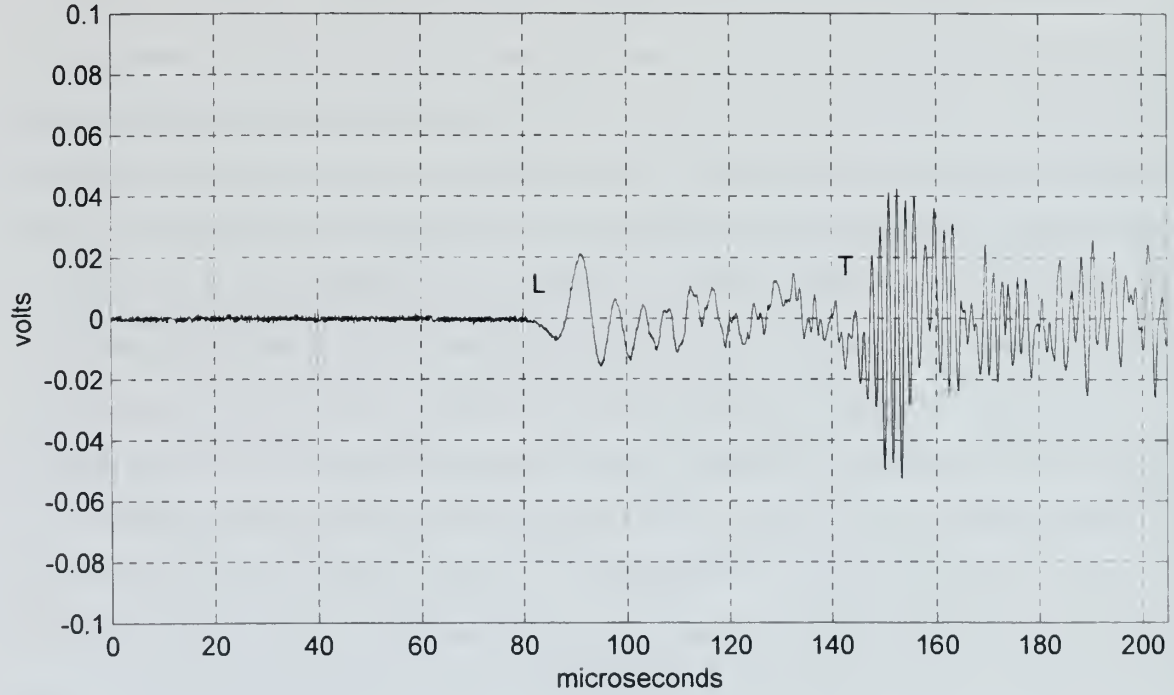

Figure 10. Typical 3/8 in. Diameter Steel Rod Signal from Sensor #4

For a longitudinal wave, the lower frequency components will travel faster than the higher frequencies. Transverse waves are the opposite, the lower frequencies travel slower than higher frequencies. Velocity becomes independent of wavelength, therefore frequency, when the wavelength is on the order of the diameter of the rod or greater. For long wavelength signals, both the longitudinal and transverse waves travel with the same velocity. The signals made in this research are in the dispersive region. For all three rods, 0.005 volts threshold was used. Additionally, the software allows for one or two dimensional locations, however one dimensional location was used exclusively. The coordinates of the sensors and velocity of the expected waveform are used in the calculation of source location. Sensor #1 is the reference channel. The location of sensor #1 is preset to 0.0 meters (m), and the locations of the other sensors are in relationship to sensor #1. Sensors #2, #3, and #4 were set to 0.075 m, 0.175 m, and 0.325 m respectively. Each acoustic event was captured and saved individually, and all the source location techniques used the same signals. Once again, because of the choice to have an initial longitudinal pulse, the signal had to be made outside of the sensors. The location calculation will calculate the distance between sensor pairs. If the calculation is correct, the FWD software will display the location under the first sensor. The script files used for the Wavelet Detail Cross Correlation and location analysis are given in Appendix D.

V. EXPERIMENTAL RESULTS

For each method of determining location, a histogram of the location calculations for the signals was made. For all the methods, the data from sensors #1 and #2 was used to center the distribution by adjusting the velocity used in the calculations, and then the data from the other sensor pairs was plotted using that velocity. The preliminary goal for the locations in all calculations was to have all the calculations fall within the diameter of the transducers. The plots of the location distributions are included in Appendix B.

A. LARGE (3/8 IN.) STEEL ROD

1. Signal Characterization

The wavelet decomposition of the stress waves generated in the 3/8 inch diameter steel rod reveals the structure of the longitudinal and transverse waves in terms of the frequency components contained within the details. Detail level one is primarily system noise, but there is some transverse wave information. Detail levels two, three and four contain the high frequency components of the transverse wave, there is a small portion of detail level four that has the longitudinal wave. Levels five, six, seven and eight have the longitudinal wave. In general, the clearest component of either wave occurs in detail level three, which is a nicely modulated frequency that resembles a football going sideways. The large steel bar appears to exhibit multi-modal vibration, especially in detail level five, a component of the longitudinal wave.

2. Threshold Crossing Locations

The threshold voltage was 0.005 volts. The first 50 signals in the data set were used to calculate the velocity of the wave. The wave velocity calculated was 5135 m/s. The signal source external to the sensors makes the calculated location actually the

distance between the sensors. If the distance between the sensors, 75 mm, is accurately calculated, the location is placed at zero. The mean value of the distribution is 0.12 mm, with a standard variation of 0.20 mm. The TC locations for sensors #1 and #2 are all within ±0.5 mm. The mean for sensors #1 and #3 is -0.17 mm with a standard deviation of 0.26 mm. The mean for sensors #1 and #4 is 0.44 mm with a standard deviation of 7.54 mm. The large increase in the standard deviation for the farthest sensor pair is due largely to a single location calculation at 75 mm, which illustrates the limitation to threshold crossing. The distance calculated was 250 mm vice the actual 325 mm.

3. Gaussian Cross Correlation Locations

The frequency which was modulated in the gaussian wave was calculated by picking the cleanest frequency from the wavelet decomposition detail level three. The frequency was calculated to be 588,235 Hz. The velocity used was 4715 m/s. Sensors #1 and #2 had a mean of 0.02 mm, with a standard deviation of 0.22 mm. Sensors #1 and #3 had a mean location of -1.17 mm and a standard deviation of 0.58mm. Sensors #1 and #4 had a mean location of -0.85 mm, with a standard deviation of 7.62 mm. Again, the change in the magnitude of the standard deviation in the furthest sensor pair was cause by a single location calculation at 74 mm. This was in signal no.78, the same signal which had a large calculation error in threshold crossing.

4. Wavelet Detail Cross Correlation Locations

The first parameter used for choosing the best correlation from the eight crosscorrelation functions, was the minimum second moment of area, or variance, of the absolute value of each crosscorrelation function. From the main MATLAB script file, *wavedetxcor.m*, a call to the function *wavedetcorstat.m*, calculated the centroid and variance of the absolute value of each crosscorrelation function. This call to the statistics function was repeated at each weighting factor, the amount of the signal that was set to zero. For example, if the weighting factor was 0.20, each data point less than or equal to 20 percent of the maximum value was set to zero. The weighting factor horizontally windowed the crosscorrelation function, and used the higher relative crosscorrelation

values in the variance and centroid calculations. The histograms of the crosscorrelation functions with the smallest variance for weighting factors of 0, 0.05, 0.10, 0.15, 0.20, 0.25, 0.30, 0.35, 0.40, and 0.45, are given in Appendix B. By basing the variance on the entire crosscorrelation function, weighting factor equal to zero, the detail level of best crosscorrelation has a peak of 28 (out of 49) occurring at level two for sensors #1 and #2, 41 at detail level three for sensors #1 and #3, and 40 at detail level four for sensors #1 and #4. As the weighting factor increases, more of the lower portions of the signal are zeroed. For the crosscorrelations between sensors #1 and #2, and sensors #1 and #3, the effect is to make the dominant peak in the histogram occur in detail level three. In general, the magnitude of the highest peak in the histogram increases with small weighting factors. In the cross correlation of sensors #1 to #4, small weighting factors moved the dominant peak from level four to level three, but for factors greater than 0.10, the peak disappeared, then moved into level two. At the time the signals were made, the possibility that one of the transducers was faulty needed to be investigated. The sensors in position three and four were switched. If sensor #4 was bad, then the spread in the histogram of the crosscorrelation of the far sensor pair as weighting factor increased would move to the crosscorrelation between sensor #1 and the new sensor #3. If the spreading did not occur, then it was due to the physical layout of the sensors, on a node of one of the wavelengths, or some other unresolved phenomena. The histograms of the best correlation level for signals 51 to 100 exhibited the same tendencies as the first 50 signals, and are included in Appendix B. The changing frequency band that accompanied the detail levels was thought to introduce too much variability in the location calculations. The parameter for choosing the best correlation changed to the minimum of the variance divided by the maximum value. The effect of this parameter change can be seen most clearly histogram for the first fifty signals. The same signals were reprocessed using the new criteria. The zero weighting factor histogram peak was 31 for sensors #1 and #2, 45 for sensors #1 and #3, and 35 for sensors #1 and #4. It must be emphasized, that this was for the first 50 signals only. All the histogram peaks occurred in detail level three. The effect of small weighting factors did not worsen the values for sensors #1 and #3, and improved the other

two sensor pairs. The parameters for the location calculations chosen were to use a weighting factor of 0.20 to zero the bottom twenty percent of the signal, base the best correlation on the minimum of the variance divided by the maximum value of the crosscorrelation function, and calculate the location based on the centroid of the signal greater than the value of the weighting factor, the top eighty percent of the signal.

The distribution of locations was centered by the same methods previously used in threshold crossing and gaussian cross correlation. The velocity calculated was 2742.5 m/s. The mean location calculation for the crosscorrelation between sensors one and two was -0.002 mm, and the standard deviation was 10.12 mm. The mean for sensors one and three was -12.15 mm, and the standard deviation was 10.21 mm. The mean for sensors one and four was -24.76 mm with a standard deviation of 15.40 mm. With a preponderance of the locations coming from detail level three, the slower velocity corresponded with the slower transverse wave. When the maximum of crosscorrelation function for detail level three was used for the location parameter, sensors one and two had a mean location of 0.01 mm and a standard deviation of 6.85 mm. Sensors one and three mean location was 5.78 mm with a standard deviation of 5.39 mm. The final sensor pair had a mean of 6.85, with a standard deviation of 13.82 mm. The location distributions for these parameters may be found in Appendix B, Figure B.7 through Figure B.21. To bound the variability due to the changing detail levels possible in the preceding effort, the maximum of detail level three's crosscorrelation function was used as the next location parameter for the large steel rod. The effect of simply basing the location on the maximum of the crosscorrelation at detail level three can be seen in Figures B.22, B.23, and B.24. The location distribution accuracy and resolution is improved by a factor of two. Table 1 summarizes all the large steel rod location distributions.

Table1. Summary of 3/8 Inch Diameter Steel Rod Location Calculations

	Sensors 1 and 2		Sensors 1 and 3		Sensors 1 and 4	
Method	Mean	Std Dev.	Mean	Std Dev.	Mean	Std Dev.
TC	0.116 mm	0.205 mm	-0.168 mm	0.263 mm	0.443 mm	7.535 mm
GCC	0.020 mm	0.217 mm	-1.170 mm	0.058 mm	-0.848 mm	7.617 mm
WDXC	-0.002 mm	10.115 mm	-12.154 mm	10.206 mm	-24.762 mm	15.405 mm
Det. 3 Max.	0.006 mm	6.849 mm	5.780 mm	5.392 mm	6.850 mm	13.823 mm

Figure 11 is a normal distribution plot using the parameters obtained in the three Threshold Crossing calculations. Figure 12 is a normal distribution from the Gaussian Cross Correlation calculations. In Figures 11 and 12 the disparity in the distribution for sensor #1 to #4 is largely due to a single extremely inaccurate calculation in the distance between the sensor pair. Figure 13 gives the normal distribution for the Wavelet Detail Cross Correlation using the location minimum of the variance divided by the maximum value to determine the best crosscorrelation function. Figure 14 is the location distribution for the locations as determined by selecting detail level three maximum value as the location parameter. Figure 15 is the data from sensor #1 to sensor #2 for TC, GCC, and the two methods using WDXC thus far discussed. Figure 15 plots the location distributions for sensors #1 and #3. Figure 16 plots the location distributions for sensors #1 and #4.

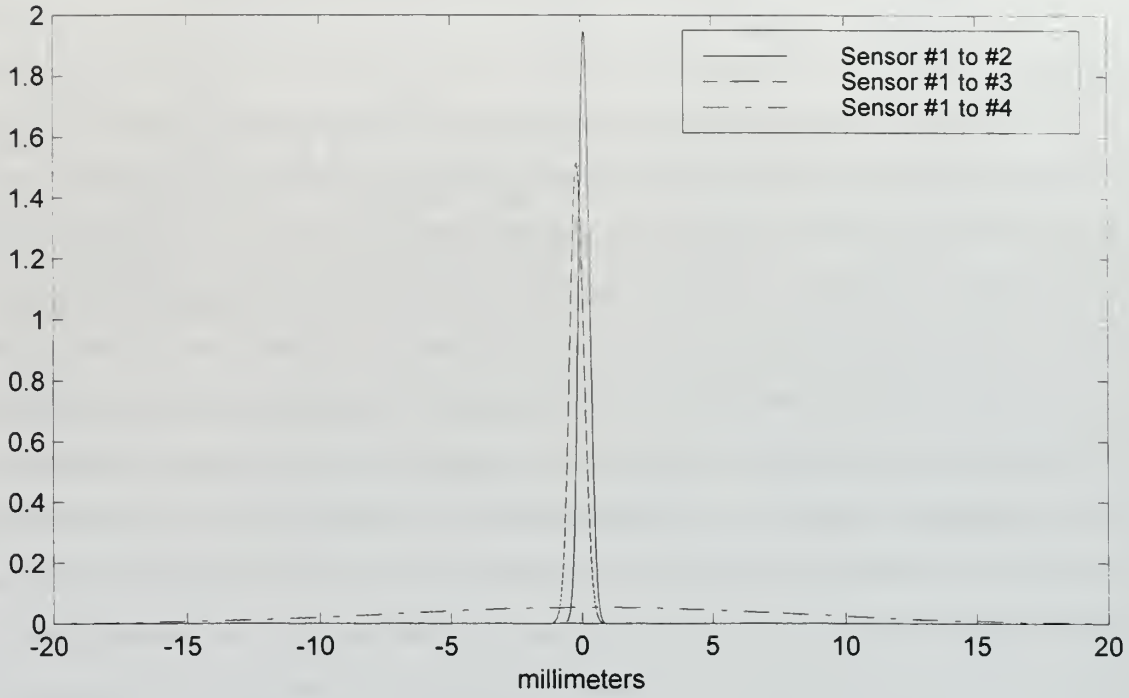

Figure 11. Normal Distribution Plots of Large Steel Rod Theshold Crossing Locations

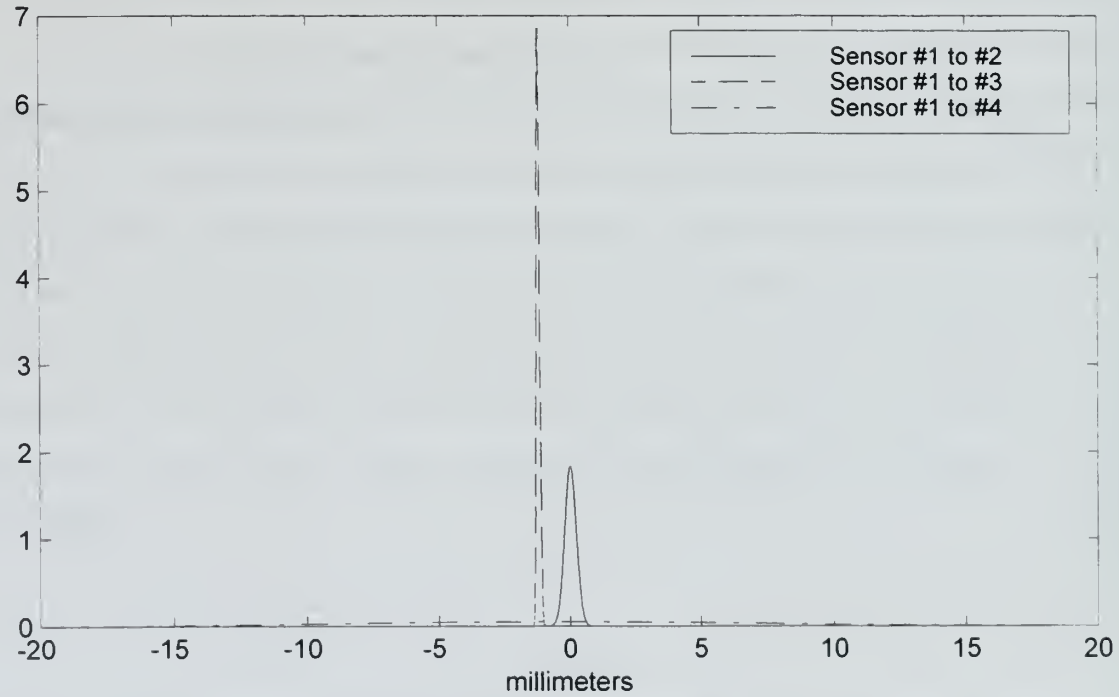

Figure 12. Normal Distribution Plots of Large Steel Rod Gaussian Cross Correlation Locations

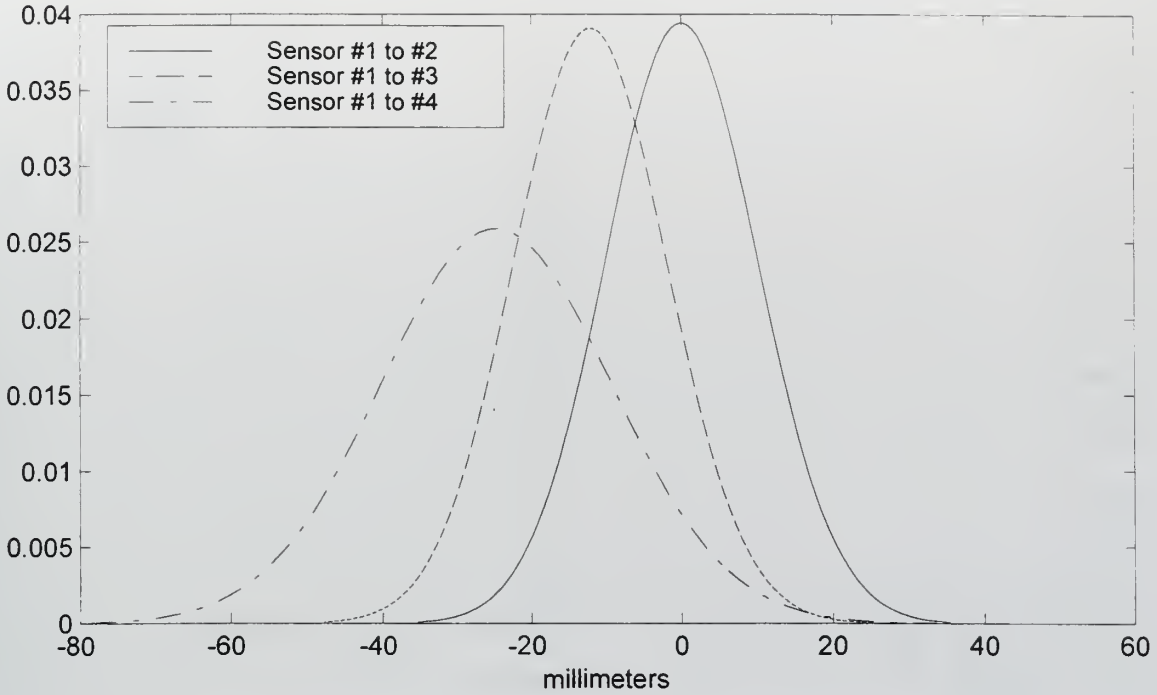

Figure 13. Normal Distribution Plots of Large Steel Rod Wavelet Detail Cross Correlation Locations

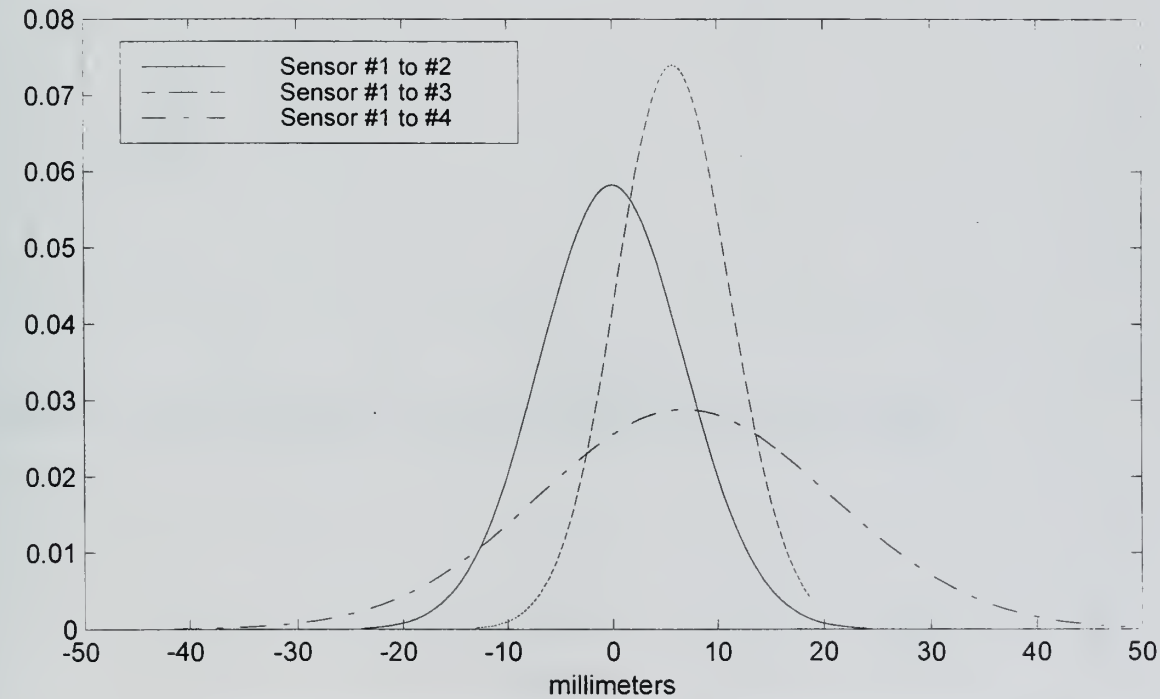

Figure 14. Normal Distribution Plots of Large Steel Rod Cross Correlation of Detail Level Three Locations

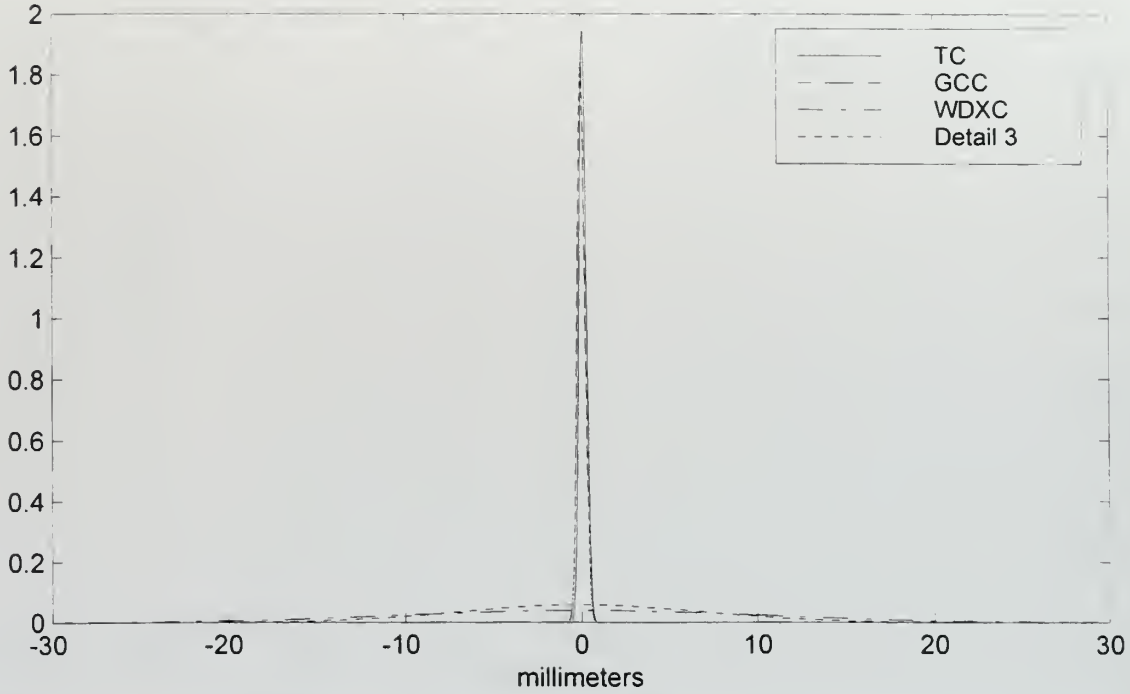

Figure 15. Normal Distribution Plots of Large Steel Rod Sensor #1 to #2 Locations

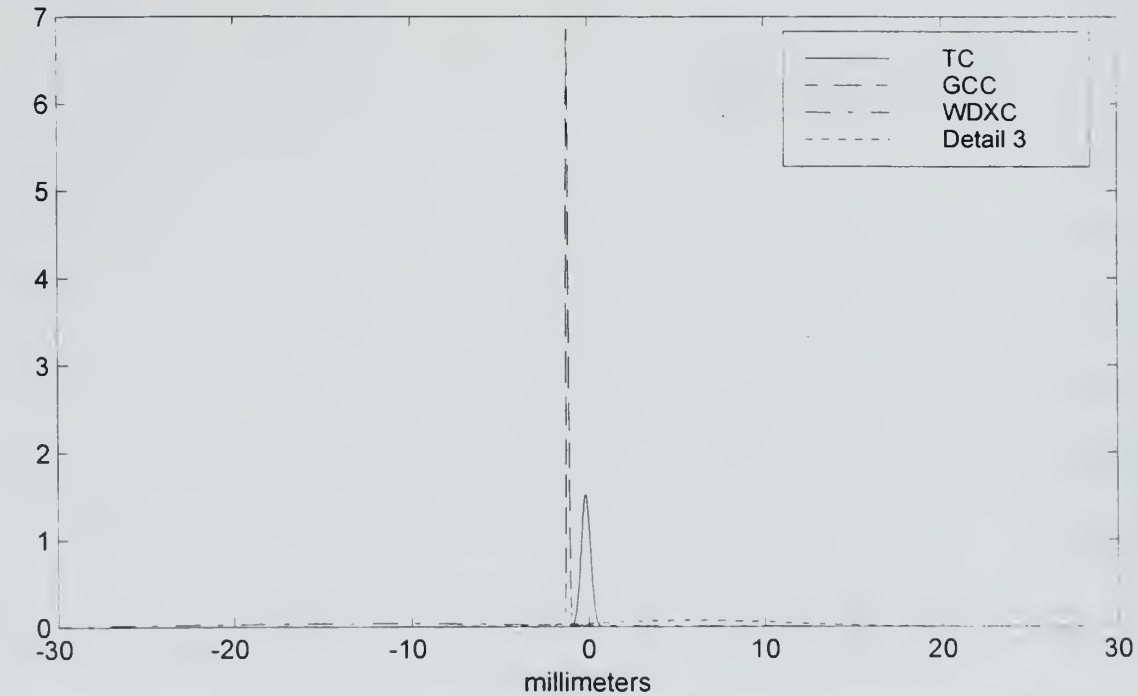

Figure 16. Normal Distribution Plots of Large Steel Rod Sensor #1 to #3 Locations

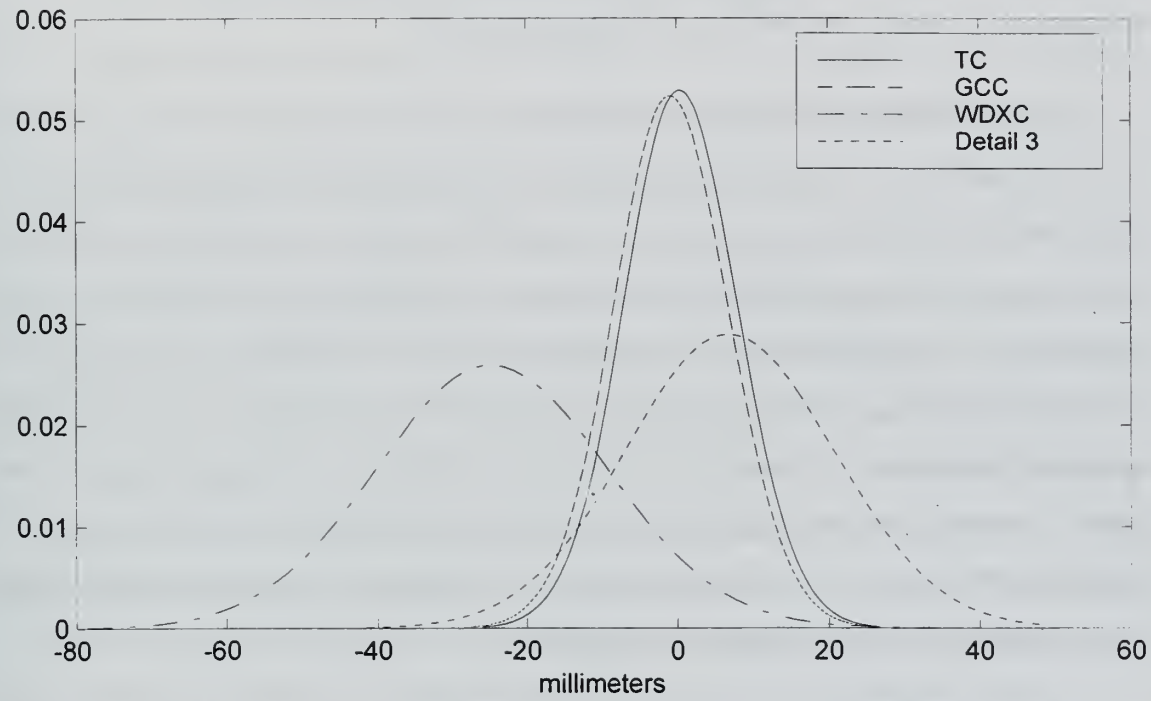

Figure 17. Normal Distribution Plots of Large Steel Rod Sensor #1 to #4 Locations

B. SMALL (1/8 IN.) STEEL ROD

1. Signal Characterization

The wavelet decomposition of the 1/8 inch diameter steel rod was in many ways the complement to the 3/8 in. diameter steel rod. The detail level one was still the noise with some components of the transverse wave. The longitudinal wave is contained in the frequencies of levels two, three, four, and five, with the transverse wave in details three, four, five, six, and seven. The smaller rod is equally stiff in the direction of motion , but more compliant in the out of plane direction. The same magnitude of test signal force creates a greater degree of transverse motion. The transverse wave is much more dominant in the small steel rod than in the large steel rod.

2. Threshold Crossing Locations

The threshold voltage was again 0.005 volts. The first fifty signals were made with 43 decibels of gain, and the next fifty with 41 db of gain. The velocity was 5135 m/s. The mean and standard deviation for sensors #1 and #2 was -0.09 mm and 0.69 mm respectively. For sensors #1 and #3, the mean location was -0.62 mm, with a standard deviation was 1.26 mm. The mean location for sensors #1 and #4 was -0.63 mm and the standard deviation was 1.25 mm. The vast majority of the signals, greater than 96 percent, were located by the threshold crossing algorithm within the width of the small transducers. The difference in the gain setting in the data had no discernible effect on the location calculation in the threshold crossing mode.

3. Gaussian Cross Correlation Locations

The frequency which was modulated was 588,235 hertz. The velocity calculated to center the sensor one distribution was 4715 m/s. The mean for sensors #1 and #2 was -1.86 mm, with a standard deviation of 18.57 mm. The velocity was calculated based on the first fifty signals, which had a mean of 0.00 mm. The second set of fifty signals had a mean of -3.80 mm. Sensors #1 and #3 had an overall mean of -1.76 mm with a standard

deviation of 0.87 mm. The first fifty signals in sensors #1 and #3 had a mean of -2.60 mm. The mean for the second fifty signals was -0.90 mm. Sensors #1 and #4 had an overall mean of -5.30 mm, with a standard deviation of 1.95 mm. Signals no. 1 through no. 50 had a mean of -7.20 mm for sensors #1 and #4. Signals 51 through 100 had a mean -3.40 mm. The overall effect of the gain difference was to separate the signal subsets by two to four millimeters. In two cases, sensors #1 and #2, and sensors #1 and #3, the higher gain setting calculation was closer to the correct answer than the lower gain. For sensors #1 and #4, the lower gain setting was closer by almost four millimeters.

4. Wavelet Detail Cross Correlation Locations

When there is no weighting factor applied to the crosscorrelation functions for the small steel rod, the histogram for the detail level of the best correlation is bimodal at detail levels two and four. For sensors #1 and #2, the peak is 57 (out of 99) at level two and 40 at level four. Sensors #1 and #3 have at level two a peak of 42, and the peak is 42 at level four as well. The final sensor pair, sensors #1 and #4 have only seven at detail level two, but 73 at detail level four. This appeared to be a potential result of the gain difference, but when the signals were broken into the data subsets by gain setting, the same bimodality existed. The effect of weighting factor on best correlation detail level was to raise the peak in level four for the first two sensor pairs, but to decrease the level four peak and raise the level two peak value for sensors #1 and #4. A weighting factor of 0.10 was used in the 1/8 inch steel rod, mostly for the reduction in calculating the location based on level five through seven crosscorrelations, which represents the transverse wave components. The wavelet detail cross correlation technique will have poor results for the small steel bar because the level most often used for location calculation, detail level four, contains frequency information from both the longitudinal and transverse waves. The velocity used was 3552.82 m/s, which is in the longitudinal wave range.

The mean location for sensor #1 and #2 was -0.01 mm, with a standard deviation of 21.47 mm. Sensors #1 and #3 had a mean of 23.28 mm, and a standard deviation of 43.28 mm. The mean for sensors #1 and #4 was -28.54 with a standard deviation of 43.47 mm. The results are summarized in Table 2.

Table 2. Summary of 1/8 Inch Steel Rod Location Calculations

	Sensors 1 and 2		Sensors 1 and 3		Sensors 1 and 4	
Method	Mean	Std Dev.	Mean	Std Dev.	Mean	Std Dev.
TC	-0.091 mm	0.693 mm	-0.623 mm	1.263 mm	-0.634 mm	1.250 mm
GCC	-1.869 mm	18.573 mm	-1.759 mm	0.874 mm	-5.328 mm	1.947 mm
WDXC	-0.008 mm	21.470 mm	23.281 mm	43.284 mm	-28.281 mm	43.473 mm

Figure 18 shows the normal distribution plots using for the TC locations. Figure 19 shows the GCC location distributions. Figure 20 plots the Wavelet Detail Cross Correlation locations based on the detail level with the minimum of the variance divided by the maximum value. Figure 21 is the comparison for sensors #1 and #2 for the three methods. Figure 22 compares sensors #1 and #3. Figure 23 compares sensors #1 and #4. Figures 18 through 23 use the parameters in Table 2.

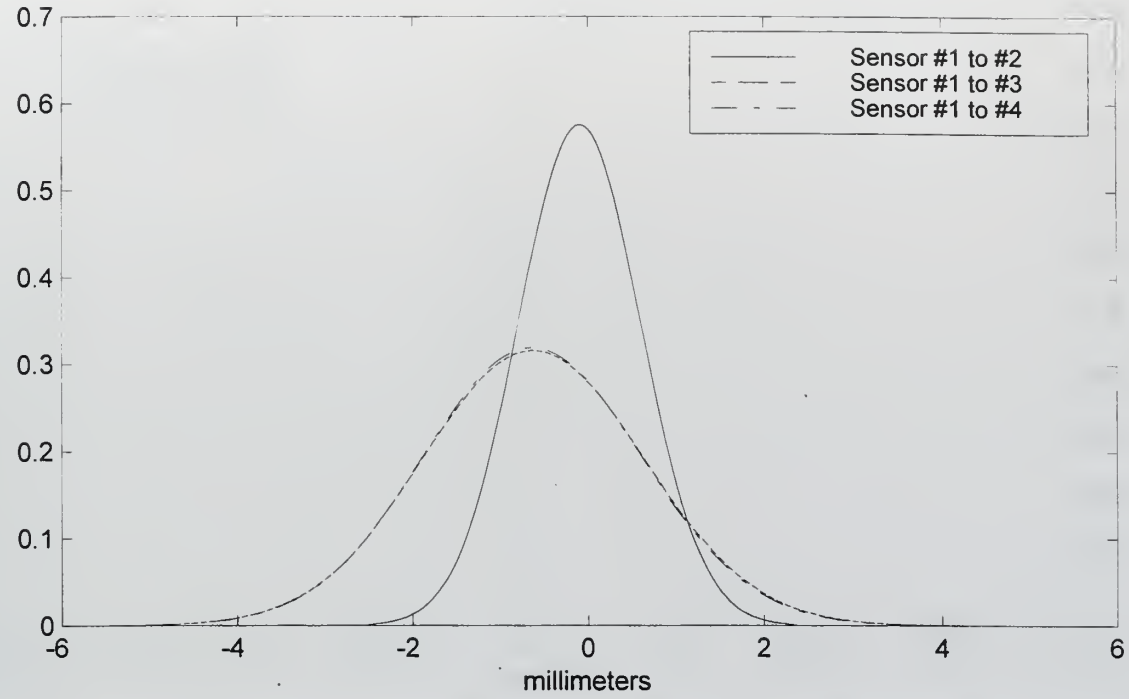

Figure 18. Normal Distribution Plots of Small Steel Rod Theshold Crossing Locations

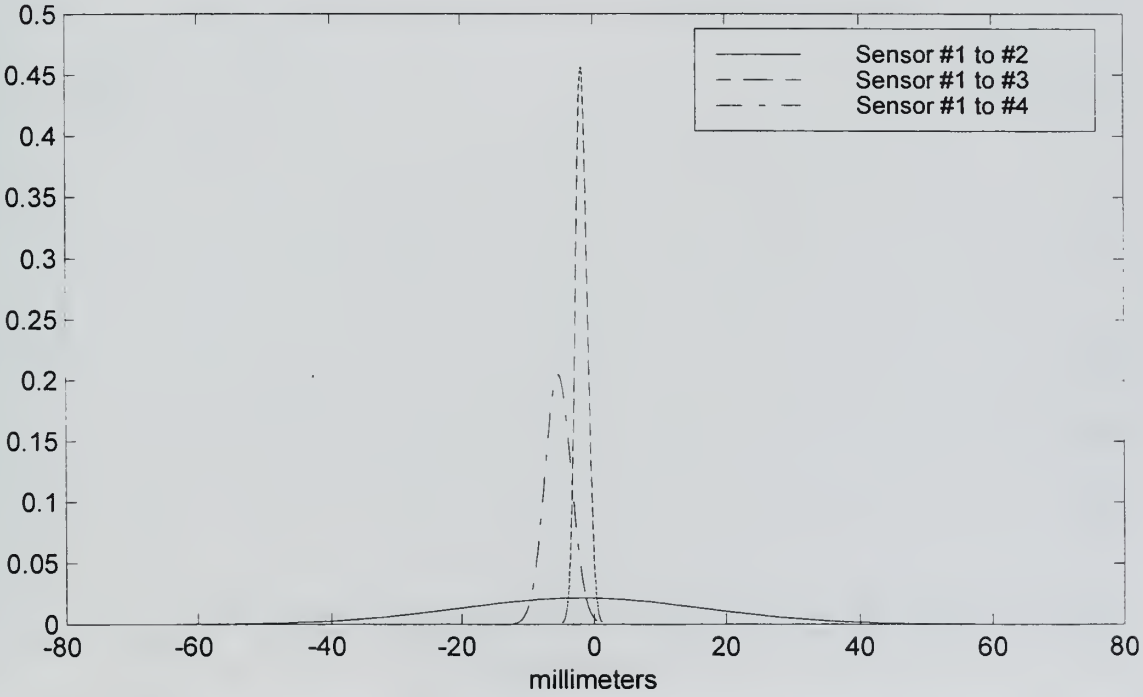

Figure 19. Normal Distribution Plots of Small Steel Rod Gaussian Cross Correlation Locations

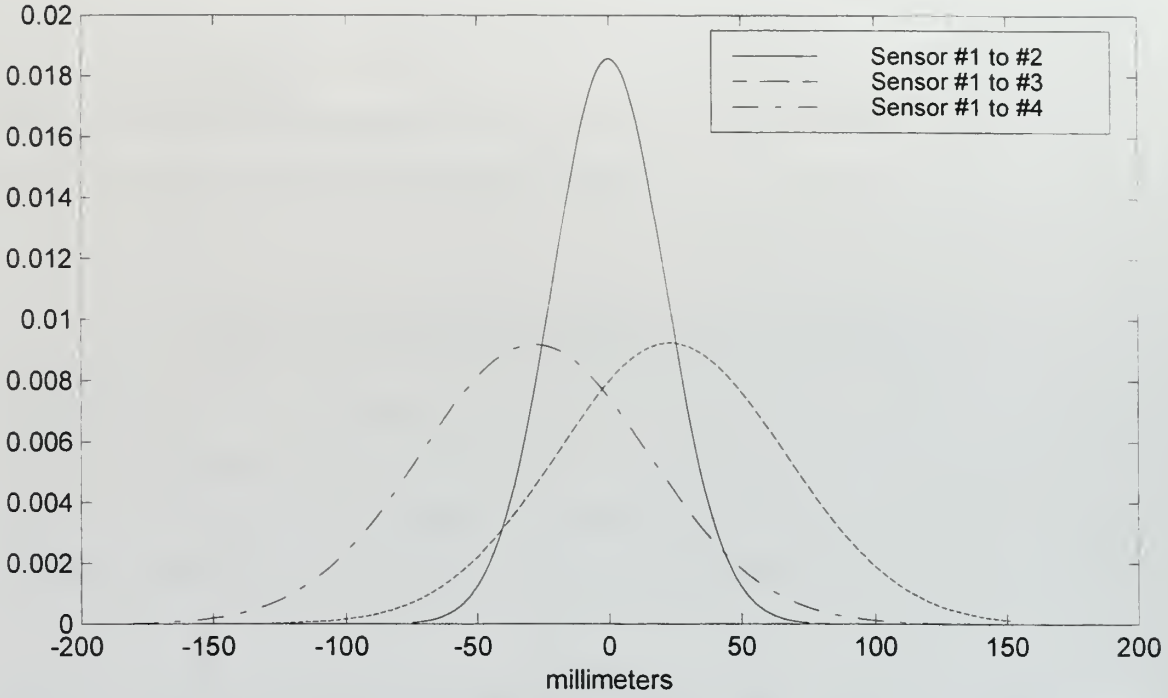

Figure 20. Normal Distribution Plots of Small Steel Rod Wavelet Detail Cross Correlation Locations

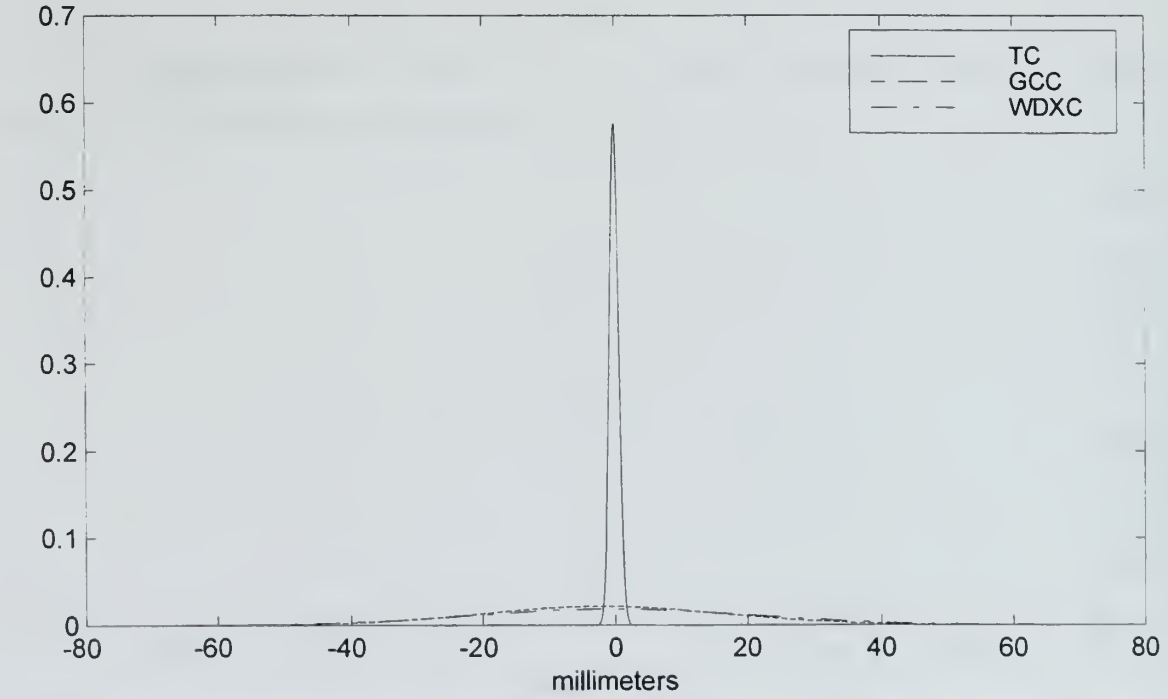

Figure 21. Normal Distribution Plots of Small Steel Rod Sensor #1 to #2 Locations

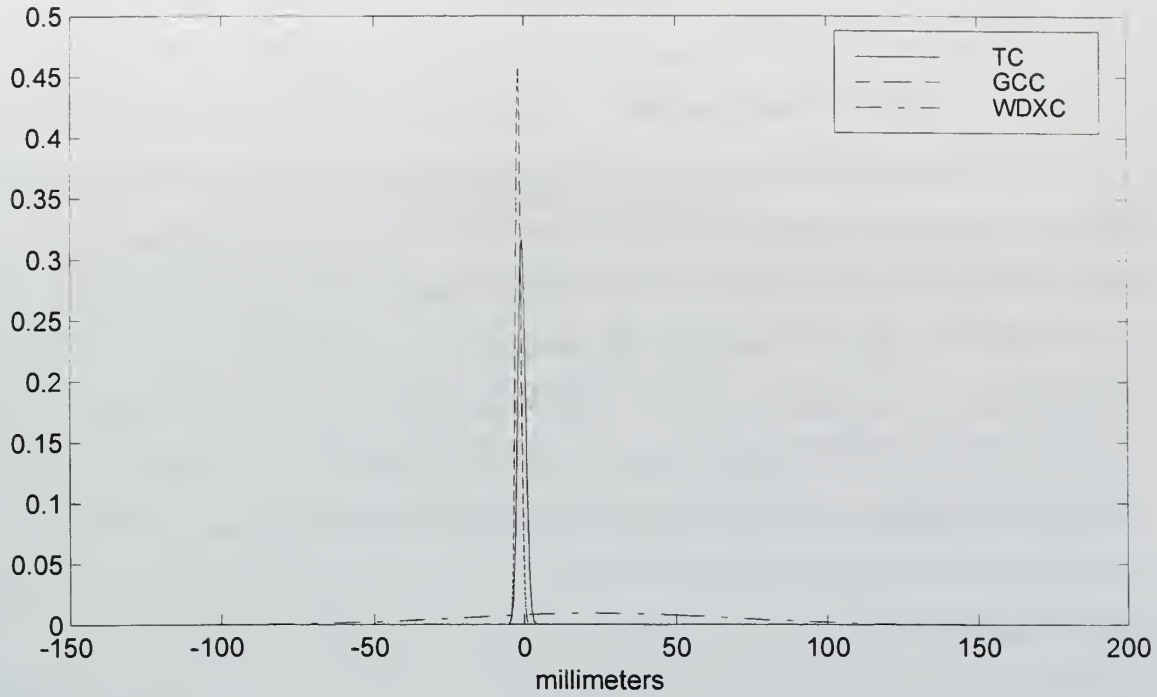

Figure 22. Normal Distribution Plots of Small Steel Rod Sensor #1 to #3 Locations

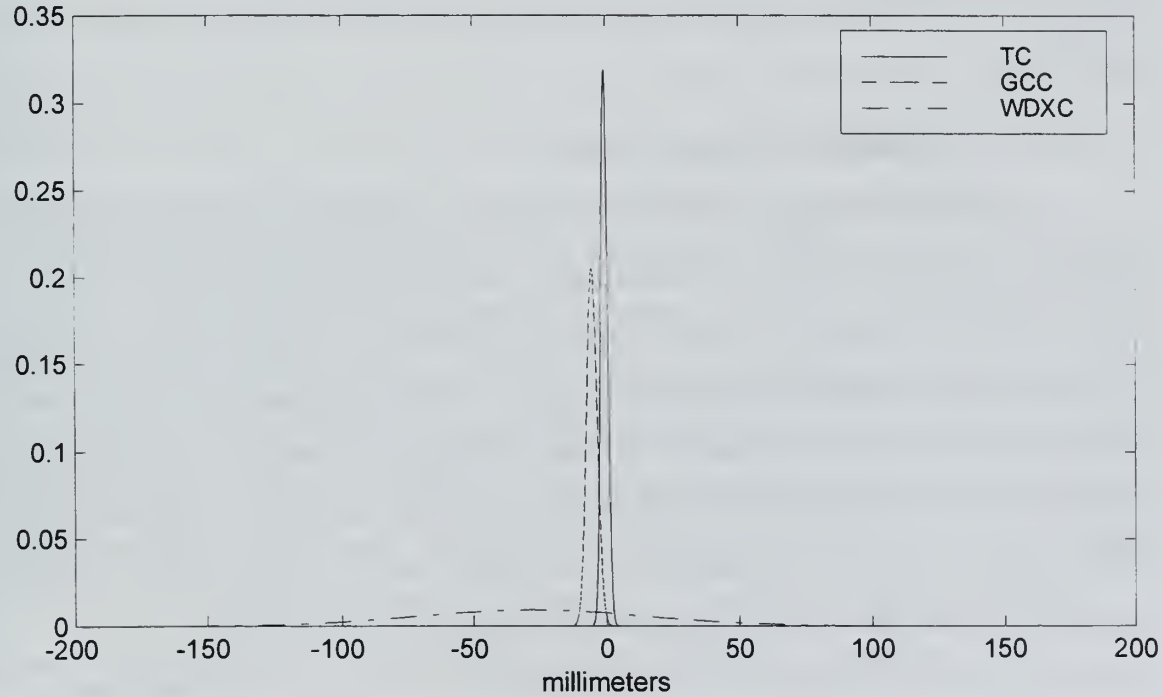

Figure 23. Normal Distribution Plots of Small Steel Rod Sensor #1 to #4 Locations

C. CARBON FIBER ROD

1. Signal Characterization

The most notable feature of the stress waves in the carbon fiber rod is the velocity difference between the longitudinal and the transverse waves. The longitudinal wave arrives at sensor #1 at approximately 25 μs, and the transverse wave arrives at almost 100 μs. At sensor #3, 325 mm further from the source, the longitudinal wave arrives at 45 μs, while the transverse appears at 190 μs. The transverse wave does not get to sensor #4 within the 204.8 μs memory length. The wavelet decomposition reveals a greater degree of order to the signals. The leading edge of the longitudinal wave appears distinctly in detail levels two through six in all the sensors, and in detail level seven as well from the signals from sensors three and four. The arrival of the transverse wave can be seen in detail levels five through eight, but the absence of the transverse wave in sensor #4 limits its observability. Detail level five and six contain nearly equal amounts of the longitudinal and transverse waves. Figure 6 in Section III shows the eight detail levels from signal no.89 from the carbon fiber rod data set, and additional examples are given in Appendix A.

2. Threshold Crossing Locations

The threshold voltage was 0.005 volts. The velocity used to center the first fifty signals was 9300 m/s. Sensors #1 and #2 had a mean location calculation of -0.77 mm, with a standard deviation of 3.11 mm. Sensors #1 and #3 had a mean location calculation of -9.80 mm and a standard deviation of 2.87 mm. The mean for sensors #1 and #4 was -9.67 mm, with a standard deviation of 2.94 mm. The location histograms are included in Appendix B. The calculation of location for the second and third sensor pairs had nearly identical means and standard deviations. If the velocity used was slightly different, these distributions would have both had mean values nearly zero, with the majority of the locations within the diameter of the small transducers, ± 2.54 mm. This is likely due to attenuation of the longitudinal wave. The first rise of the wave possibly triggered sensor

#1 and sensor #2, but the attenuation delayed triggering sensors #3 and #4 until the second rise of the longitudinal wave. Figure 2 in Section III shows this phenomena displayed in the large steel rod stress wave.

3. Gaussian Cross Correlation Locations

The frequency modulated by the gaussian pulse was 625,000 hz. The velocity which centered the distribution for sensors #1 and #2 was 7024.32 m/s. The mean for sensors #1 and #2 was 0.34 mm, and the standard deviation was 15.21 mm. For sensors #1 and #3, the mean location calculation was 7.17 mm with a standard deviation of 6.52 mm. Sensors #1 and #4 had a mean location value of 22.85 and a standard deviation of 11.05 mm. The histograms of the location distributions show that the increase in the standard deviation is caused by the variation of most of the signal, not a single signal with an extremely bad location calculation. The location histograms are included in Appendix B.

4. Wavelet Detail Cross Correlation Locations

The histograms of the crosscorrelation with the minimum value of the variance divided by the maximum of the respective crosscorrelation function for the carbon fiber rod shows the effect of weighting factor clearly. The zero weighting factor is spread over detail levels two, three, and four. By zeroing the bottom twenty percent of the crosscorrelation functions for sensors #1 and #2, the peak in detail level two went from 47 to 84. In the crosscorrelation functions of sensors #1 and #3, the peak in detail level three raised from 55 to 74. There was a decrease in the peak for sensors #1 and #4, which lowered from 93 to 84. The velocity used for the calculation of location through WDXC was 6865.74 m/s. Sensors #1 and #2 had a mean location calculation of 0.00 mm with a standard deviation of 9.28 mm. The second sensor pair, sensors #1 and #3, had a mean of 1.73 mm, but a standard deviation of 24.62 mm. The final pair of sensors, #1 and #4, gave a mean location of -88.57 mm and a standard deviation of 19.86 mm. The windowed results give the results of windowing the raw signal at the arrival of the longitudinal wave from the left side, and ending the window before the transverse wave

arrived. When the signal was windowed, Sensor #1 and #2 had a mean of 0.00 mm with a standard deviation of 0.39 mm. Sensors #1 and #3 had a mean of 0.00 mm and a standard deviation of 0.46 mm. Sensors #1 and#4 had a mean of 0.00 mm and a standard deviation of 0.09 mm when the windowed Wavelet Detail Cross Correlation was utilized. It is important to note the order of magnitude decrease in the standard deviation for all the sensor pairs through the use of the window to capture the longitudinal wave. Based on the known phenomena of dispersion in composites, the velocities for the calculation of the three windowed location means were based on the velocity for that detail level. The windowed results came from detail level six for sensors #1 and #2, and from detail level five for the other two sensor pairs. The results of the location distributions for the carbon fiber rod are given in Table 3.

Table 3. Summary of Carbon Fiber Rod Location Calculations

	Sensors 1 and 2		Sensors 1 and 3		Sensors 1 and 4	
Method	Mean	Std Dev.	Mean	Std Dev.	Mean	Std Dev.
TC	-0.773 mm	3.112 mm	-9.795 mm	2.865 mm	-9.668 mm	2.937 mm
GCC	0.344 mm	15.212 mm	7.174 mm	6.514 mm	22.825 mm	11.050 mm
WDXC	0.000 mm	9.281 mm	1.726 mm	24.617 mm	-88.572 mm	19.861 mm
Windowed	0.000 mm	0.388 mm	0.000 mm	0.459 mm	0.000 mm	0.092 mm

Figure 24 shows the normal distribution plots using for the TC locations. Figure 25 shows the GCC location distributions. Figure 26 plots the Wavelet Detail Cross Correlation locations based on the detail level with the minimum of the variance divided by the maximum value. The windowed Wavelet Detail Cross Correlation locations are given in Figure 27. Figure 28 is the comparison for sensors #1 and #2 for the four methods. Figure 29 compares sensors #1 and #3. Figure 30 compares sensors #1 and #4. Figures 24 through 30 use the parameters in Table 3.

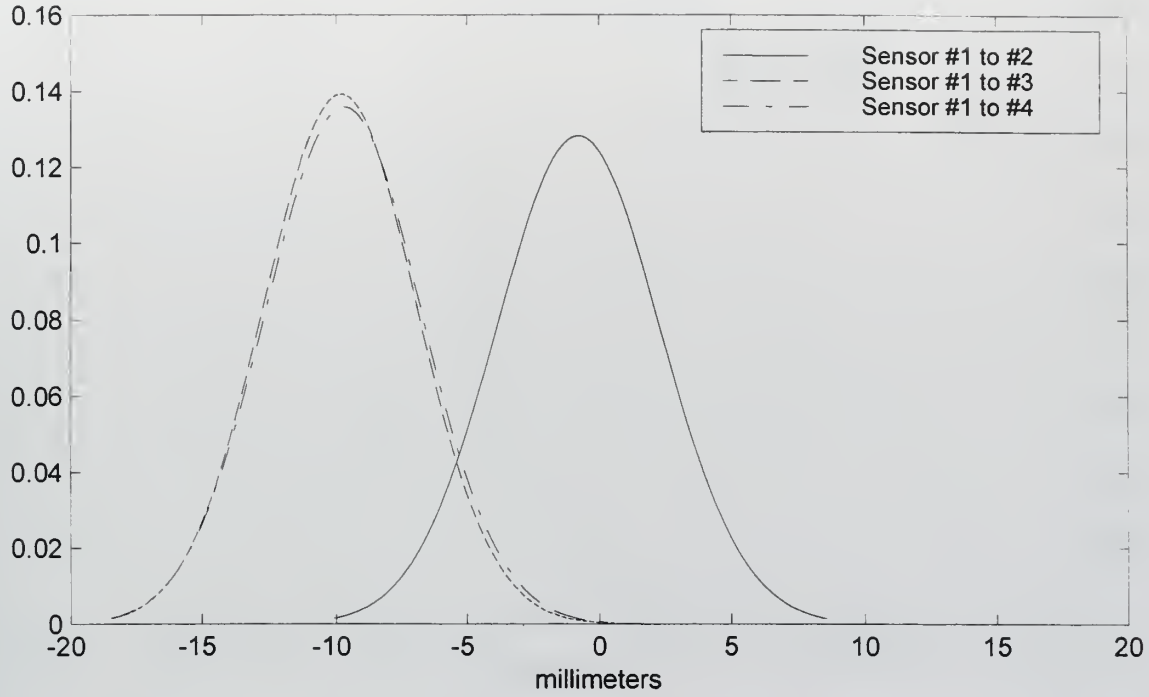

Figure 24. Normal Distribution Plots of Carbon Fiber Rod Theshold Crossing Locations

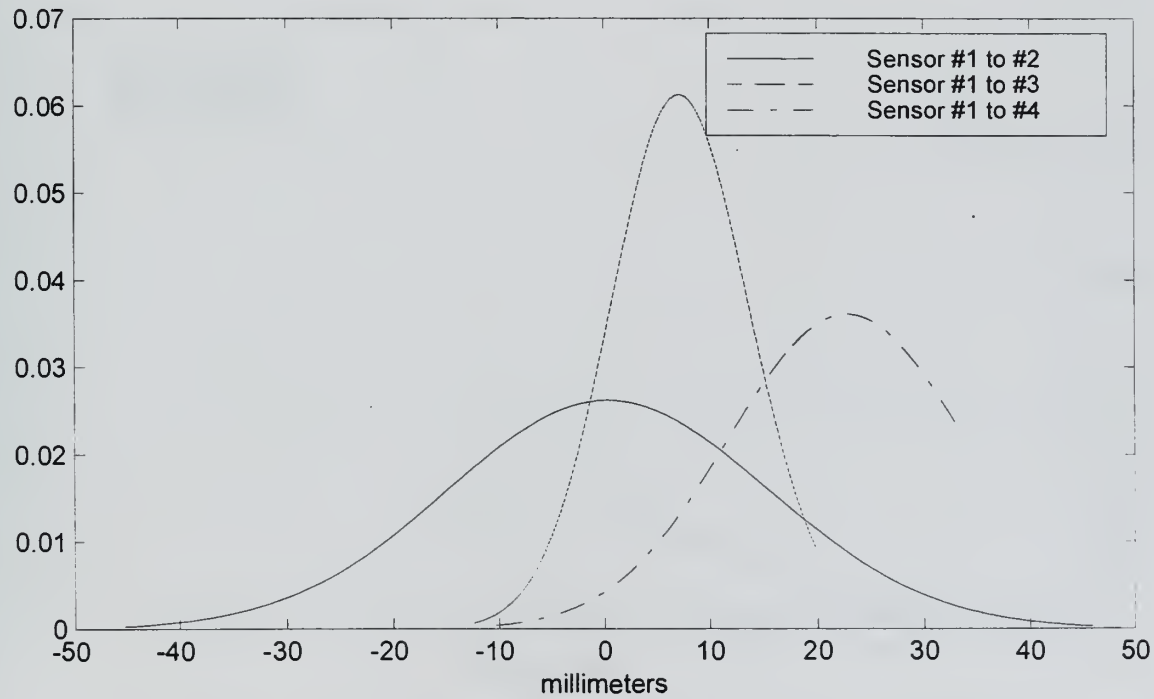

Figure 25. Normal Distribution Plots of Carbon Fiber Rod Gaussian Cross Correlation Locations

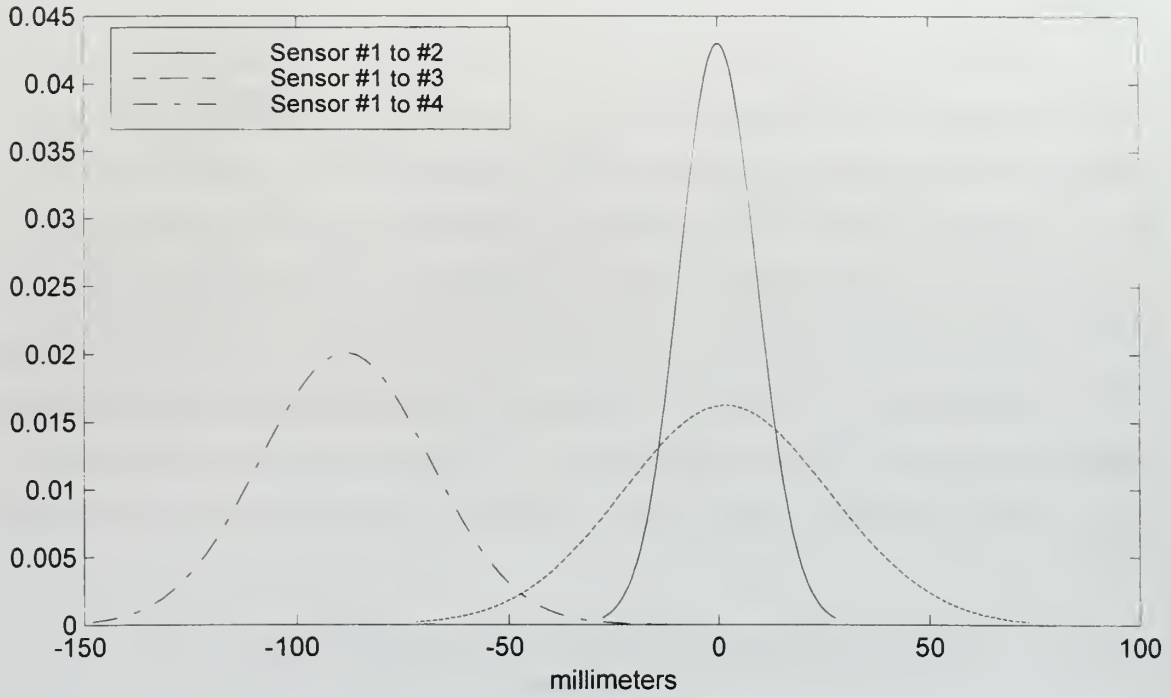

Figure 26. Normal Distribution Plots of Carbon Fiber Rod Wavelet Detail Cross Correlation Locations

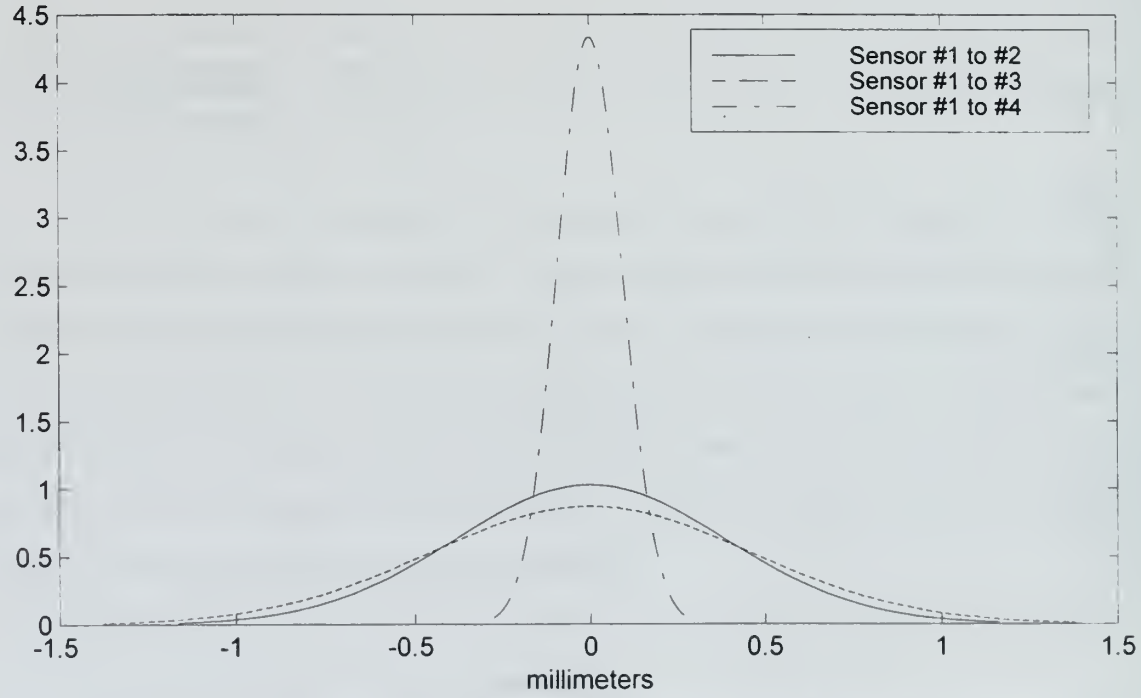

Figure 27. Normal Distribution Plots of Carbon Fiber Rod Windowed Wavelet Detail Cross Correlation Locations

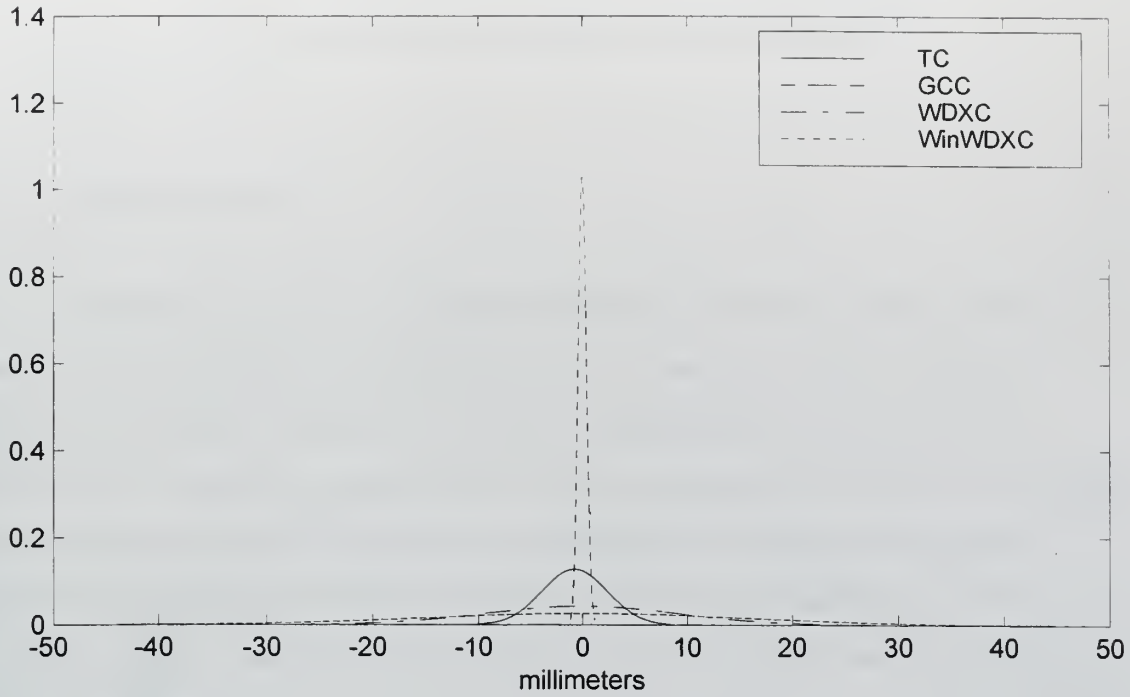

Figure 28. Normal Distribution Plots of Carbon Fiber Rod Sensor #1 to #2 Locations

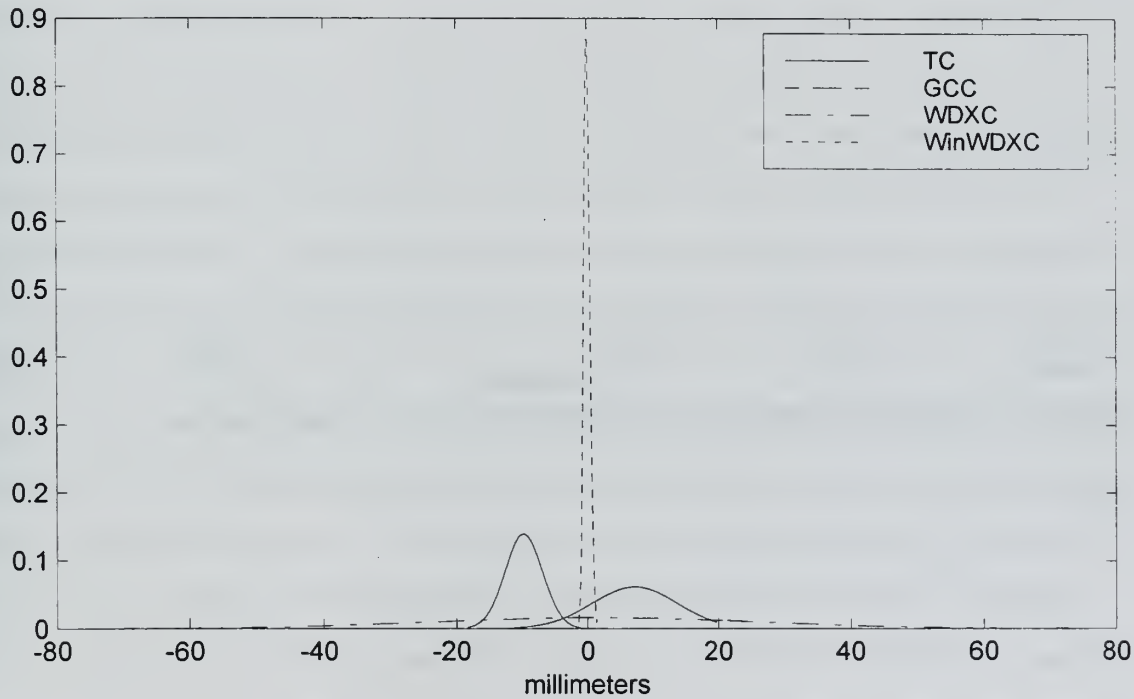

Figure 29. Normal Distribution Plots of Carbon Fiber Rod Sensor #1 to #3 Locations

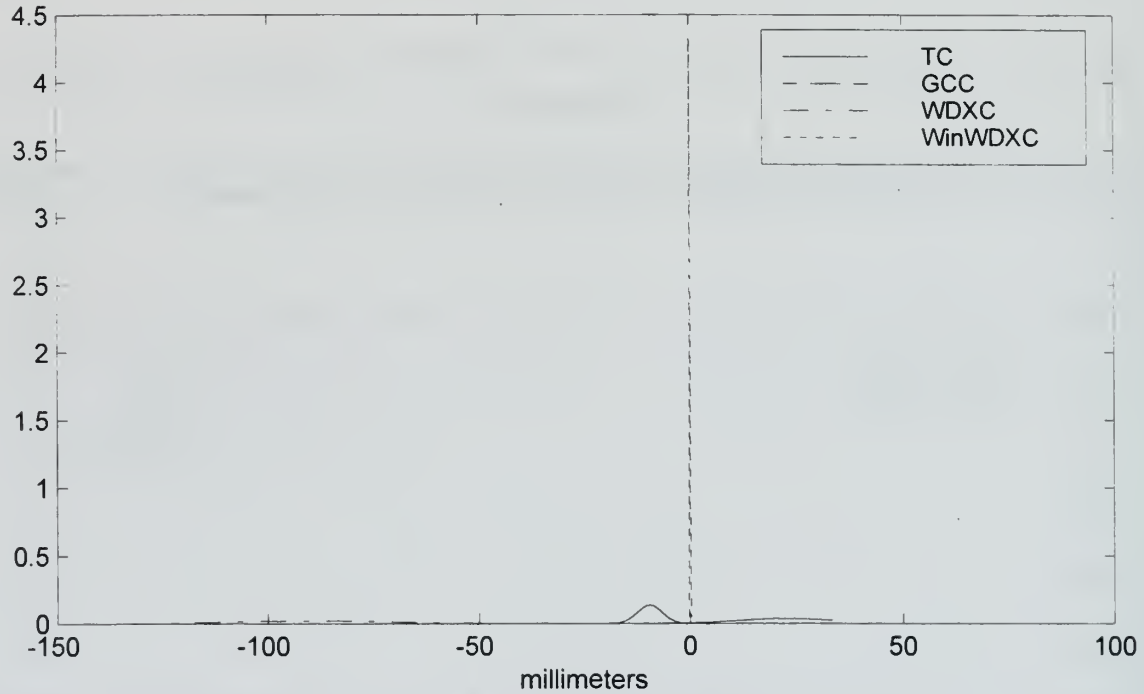

Figure 30. Normal Distribution Plots of Carbon Fiber Rod Sensor #1 to #4 Locations

VI. CONCLUSIONS AND RECOMMENDATIONS

A. CONCLUSIONS

A damage source location system would actively monitor structural reliability and provide assurance against catastophic failure. The acoustical emission techniques examined herein detect passively, but require varying degrees of interpretation and intervention. Threshold Crossing uses the minimum amount of the available information, and is therefore potentially erroneous in the presence of attenuation and dispersion. Within the scope of this investigation into time of arrival determination for source location analysis in one-dimensional cylindrical bars, Threshold Crossing gave good performance with outliers in the location calculations (see Figures 11, 18, 24 in Section V for the distribution plots, and Figures B.1, B.2, B.3, B.25, B.26, B.27, B.40, B.41, and B.42, in Appendix B for the location histograms). Fourier decomposition of elastic stress waves is not applicable due to the non-stationary nature of the signal. A Windowed Fourier Decomposition can be windowed with multiple frequencies, with the time resolution associated with the window width. Gaussian Cross Correlation uses a single frequency modulated by a Gaussian envelope, with the window width fixed by the modulated frequency. The results determined in this investigation for GCC source location were fair with outliers, largely due to the effects of dispersion (Figures 12, 19, 25 in Section V, Figures B.4, B.5,B.6, B.28, B.29, B.30, B.43, B.44, and B.45 in Appendix B). The time and frequency resolution of the Wavelet Transform offer very promising results. The 'db4' wavelet was chosen because of its physical similarity with the leading edge of the longitudinal wave. The maximum value of the crosscorrelation for single detail level was used in the homogeneous case with fair results (Figure 14 in SectionV, Figures B.22, B.23, B.24 in Appendix B). When the determination of the time of arrival is based on the mean of the absolute value of the crosscorrelation, the results are poor for both homogeneous and heterogeneous materials (Figures 13, 20 and 26 in Section V, and

Figures B.19, B.20, B.21, B.37, B.38, B.39, B.52, B.53, and B.54 an Appendix B), due to the difference in the velocity characteristic of each detail level and the variation in the mean of the absolute value of the crosscorrelation function. Windowing the signal to isolate one or both waves appears to be extremely promising for source location. Because of the velocity difference between the longitudinal and transverse waves, only the longitudinal wave propagates into undisturbed medium, while the transverse wave propagates into the disturbance created by the longitudinal wave. The source location results for a Windowed Wavelet Detail Cross Correlation are very good (Figure 27 in Section V, and Figures B.55, B.56, B.57 in Appendix B). This technique was applied to the carbon fiber signal data because it is the worst case for signal propagation due to attenuation and the wave guide effect of the fibers. When the location methods are ranked on the basis of variance and central tendency, the Windowed Wavelet Detail Cross Correlation is better than Threshold Crossing , Gaussian Cross Correlation, and the other Wavelet methods investigated herein. For homogeneous materials, the Windowed Wavelet Detail Cross Correlation was not attempted, and Threshold Crossing was better that Gaussian Cross Correlation and Wavelet Detal Cross Correlation. In heterogeneous materials, the Windowed Wavelet Detail Cross Correlation demonstrated better accuracy and resolution than any of the other techniques investigated, and was the only method which did not lose any accuracy or resolution as a function of spatial distance.

B. RECOMMENDATIONS

Recommendations for further research in stress wave time of arrival determination with the Windowed Wavelet Detail Cross Correlation are:

1. Implement a Gaussian edge on the window.
2. Modify the windowing method to account for the velocity of the wave and the known geometry of the sensor placement. Start the window at the trigger at the triggering sensor, but delay the start of the window slightly to effectively

have the leading edge of the longitudinal wave at the beginning of the data window for all sensors.

3. Determine source location resolution and accuracy in two-dimensional thin plates.
4. Research construction of a wavelet from the stress wave itself for comparison to the signals from the other sensors, that is, an acoustic fingerprint.
5. Analyze steel rod data for comparison to other methods with the homogeneous material.
6. Further determine the effects of attenuation through the use of Aluminum specimen.

APPENDIX A. REPRESENTATIVE SIGNALS FROM THE TEST RODS

The Plots in Appendix A are examples from the three different specimen. Each specimen, the large steel (3/8 inch diameter), small steel (1/8 inch diameter), and carbon fiber rods have a group of plots on the following pages. There are three different types of graphs. The first type is an example of the four channel raw signal. The second type is the reconstructed wavelet details from each individual sensor. The third type is the crosscorrelation function generated when each detail level from sensors #2, #3, and #4 is crosscorrelated with the same detail level from sensor #1. The large steel rod plots are followed by the small steel rod plots, and finally the carbon fiber plots.

The plot of the raw signal from each sensor is in a four row by one column subplot on a single page. The signals are ordered from top to bottom, with sensor #1 on the top, and sensor #4 on the bottom. The units on the vertical axes are volts, and the horizontal axes are datapoints, which is proportional to time by the inverse of the digitization rate. A data point of 200 when divided by the digitization rate of 10,000,000 datapoints/second corresponds to 20 microseconds. On the graph of each signal, the uppercase letter, L, indicates the approximate leading edge of the longitudinal wave, and the uppercase letter, T, indicates the estimation of the leading edge of the transverse wave. Figures A.1, A.9 and A.17 are the three raw signal plots.

Examples of the reconstructed wavelet details are Figures A.2 through A.5 for the large steel rod, Figures A.10 through A.13 for the small steel rod, and Figures A.18 through A.21 for the carbon fiber rod. Each individual page of this type of plot contains an eight row by one column subplot. The eight level discrete wavelet transform and detail reconstruction generates eight different detail levels from each sensor's raw signal. Detail level one, the noise in the system, has not been plotted, in its place, the original raw signal from that particular sensor. The horizontal axis label are combined on the bottom subplot. The vertical axes units are volts, and the horizontal axis units are

datapoints. The top subplot, the raw signal, is labeled with an uppercase L and T to denote the estimation of the arrival of the longitudinal and transverse waves respectively. Each specimen's reconstructed details sum to equal the raw signal. The components of both the longitudinal and transverse waves can be found in one or more of the details. Each specimen responds slightly differently and the type of wave in any given detail level is the same for all the signals of a given specimen, but may be different for each type of specimen.

The final type of plot is the detail crosscorrelation functions. Figures A.6 through A.8 for the large steel rod, Figures A.14 through A.16 for the small steel rod, and figures A.22 through A.24 for the carbon fiber rod are examples of the crosscorrelation functions generated. Each figure contains an eight row by one column subplot. The units of the horizontal axis are index, which is indicative of the amount of shift between the two signals at that particular point. The vertical axes are dimensionless. The crosscorrelation functions of the wavelet details are ordered from top to bottom, with the crosscorrelation function of detail level one at the top, and the crosscorrelation function of detail level eight on the bottom. The location of the highest crosscorrelation between and two details will be the largest relative maximum on that crosscorrelation function. The signals plotted reflect the entire 2048 datapoints recorded, and do not reflect the windowing of the detail level at the arrival of one wave form or the other.

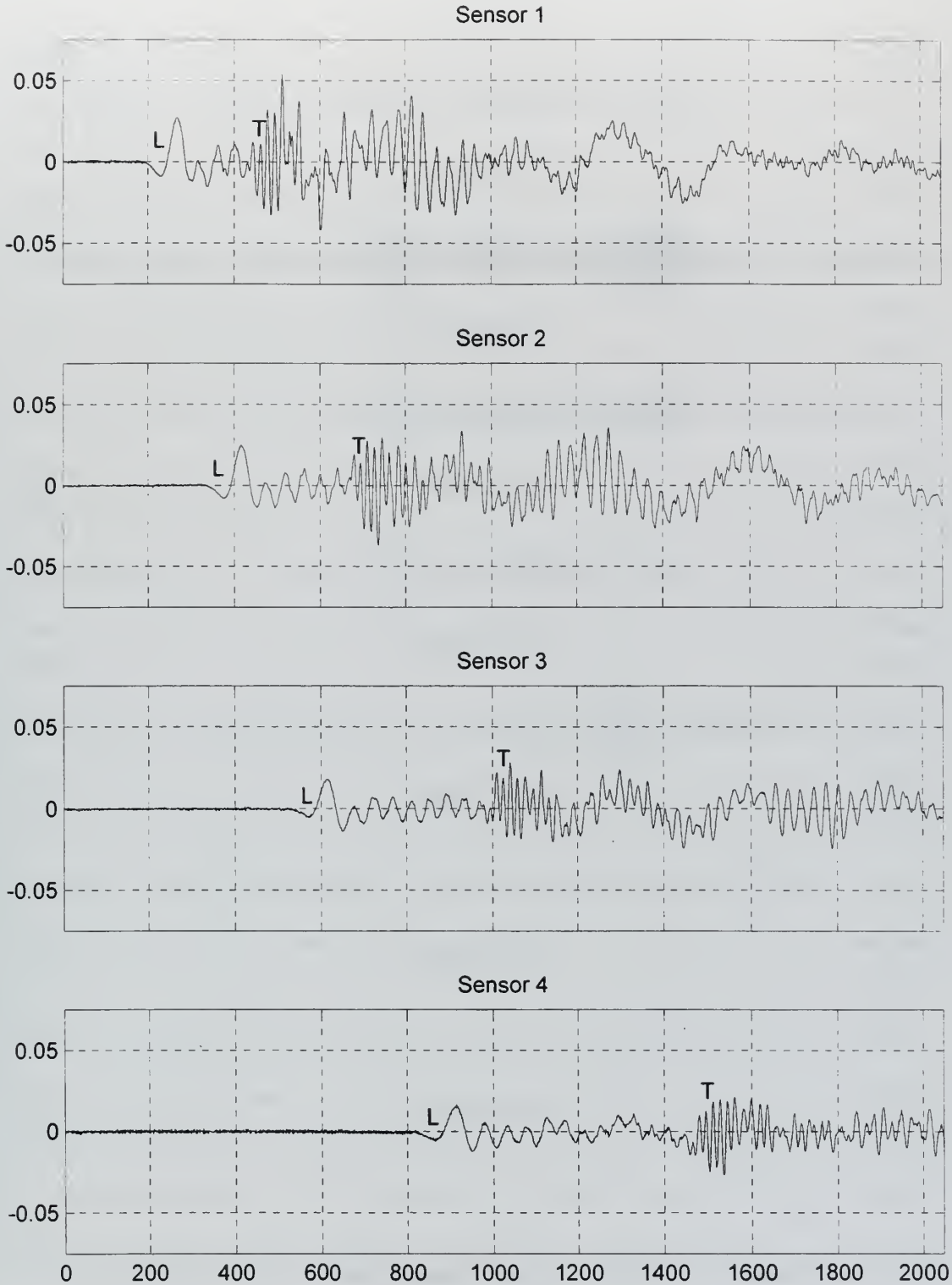

Figure A.1. Large Steel Rod Signal no. 23 Sensors #1 through #4

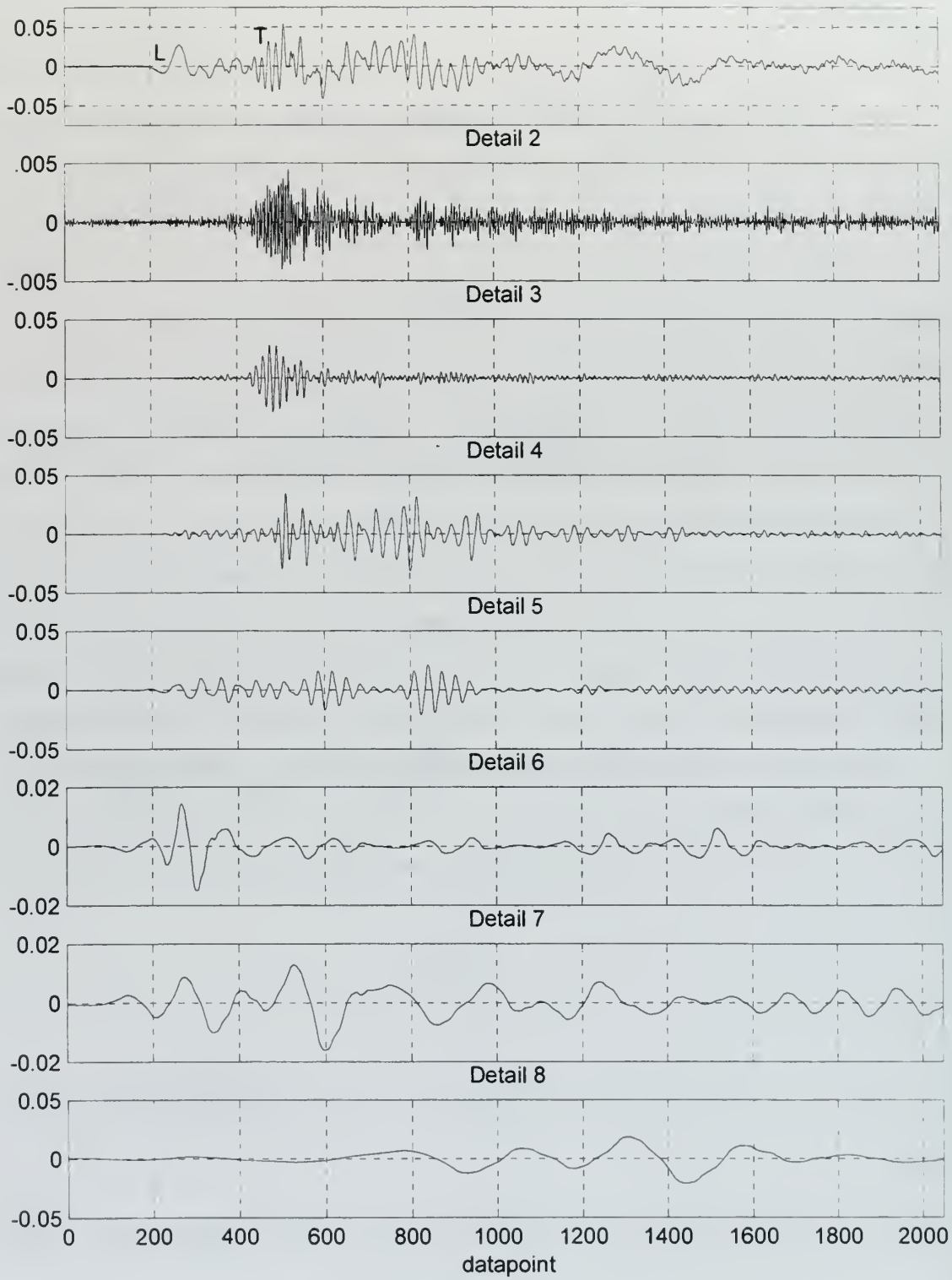

Figure A.2. Large Steel Rod Signal no. 23 Sensor #1 with Wavelet Details 2 through 8

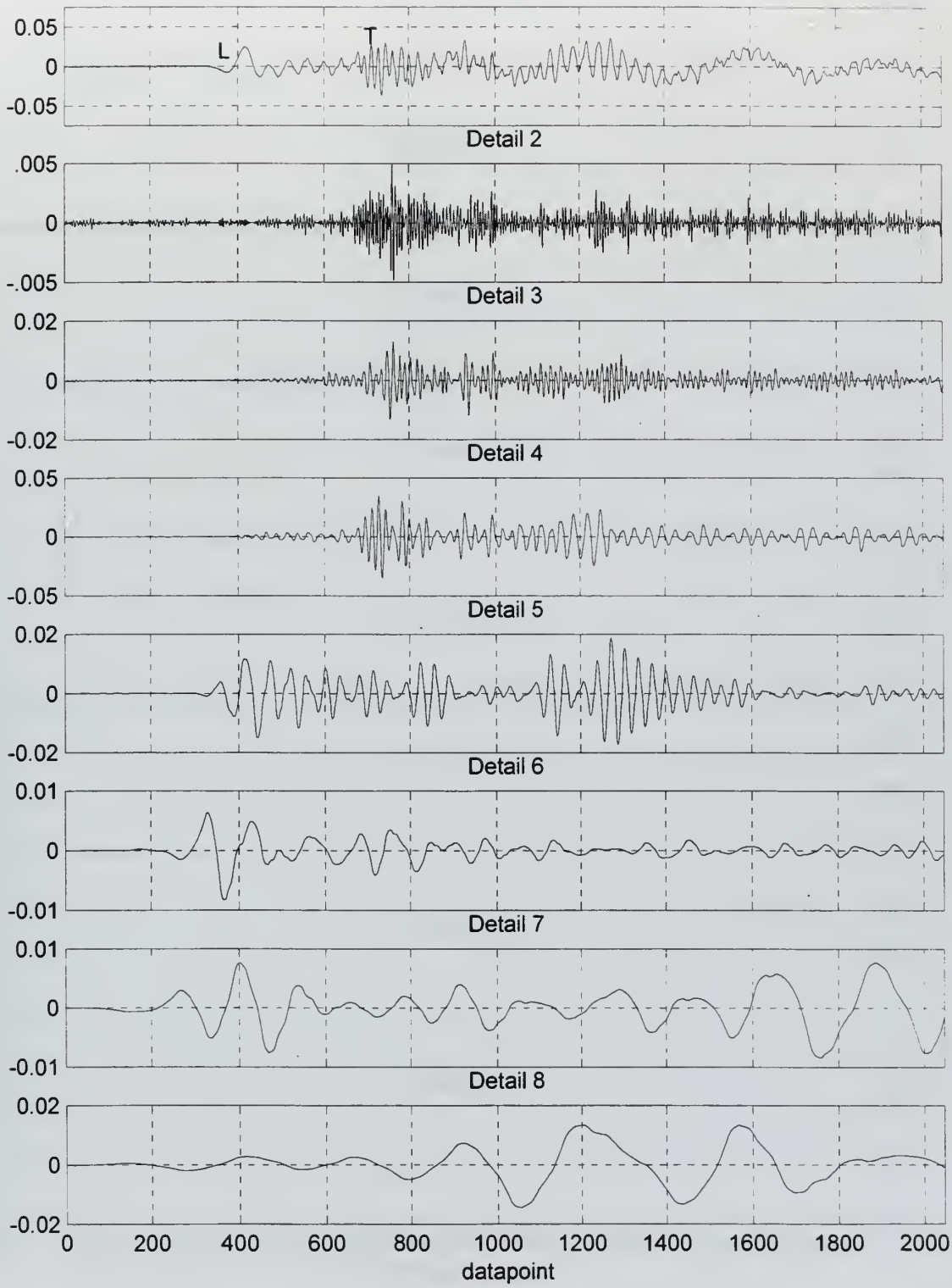

Figure A.3. Large Steel Rod Signal no. 23 Sensor #2 with Wavelet Details 2 through 8

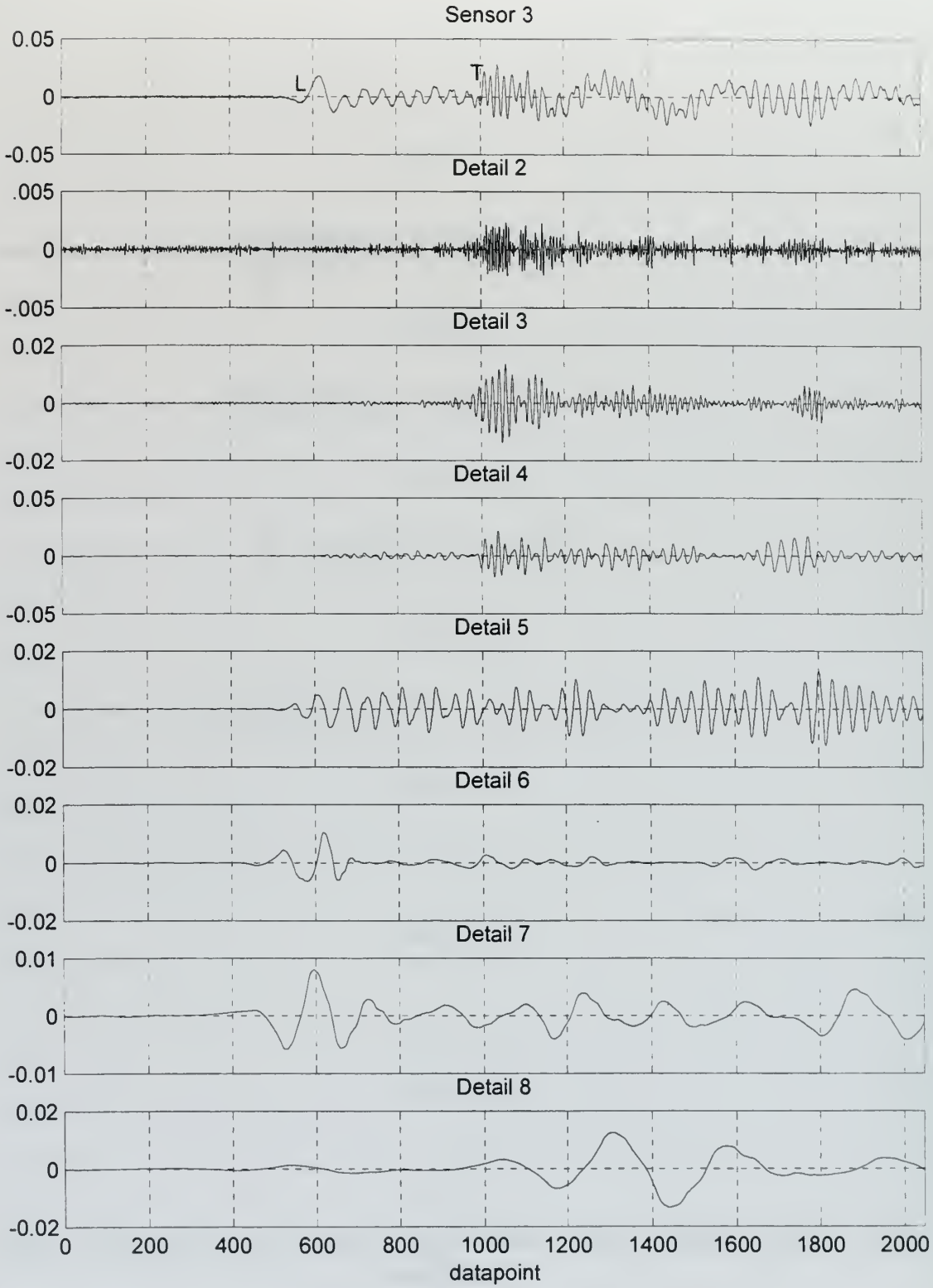

Figure A.4. Large Steel Rod Signal no. 23 Sensor #3 with Wavelet Details 2 through 8

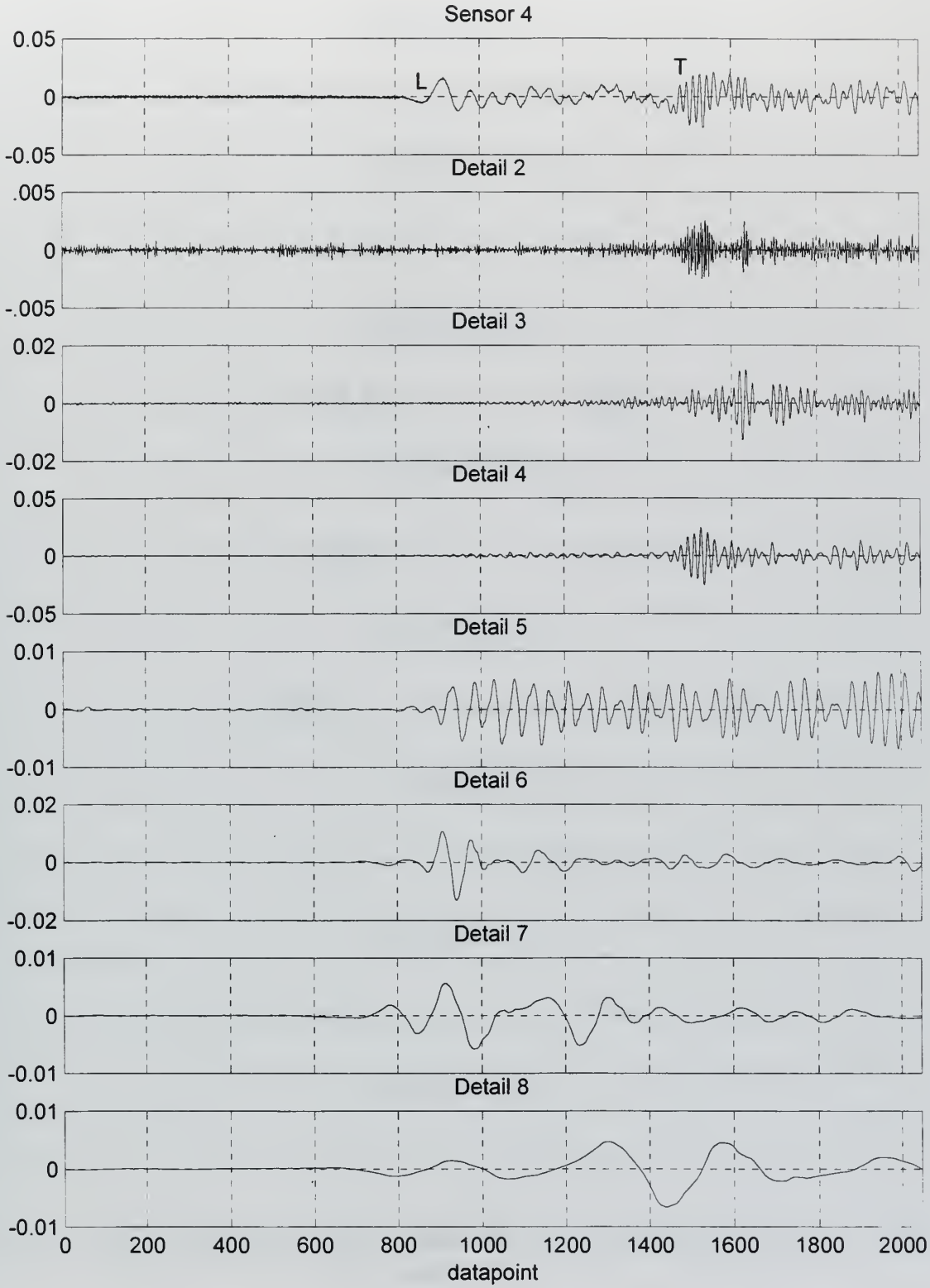

Figure A.5. Large Steel Rod Signal no. 23 Sensor #4 with Wavelet Details 2 through 8

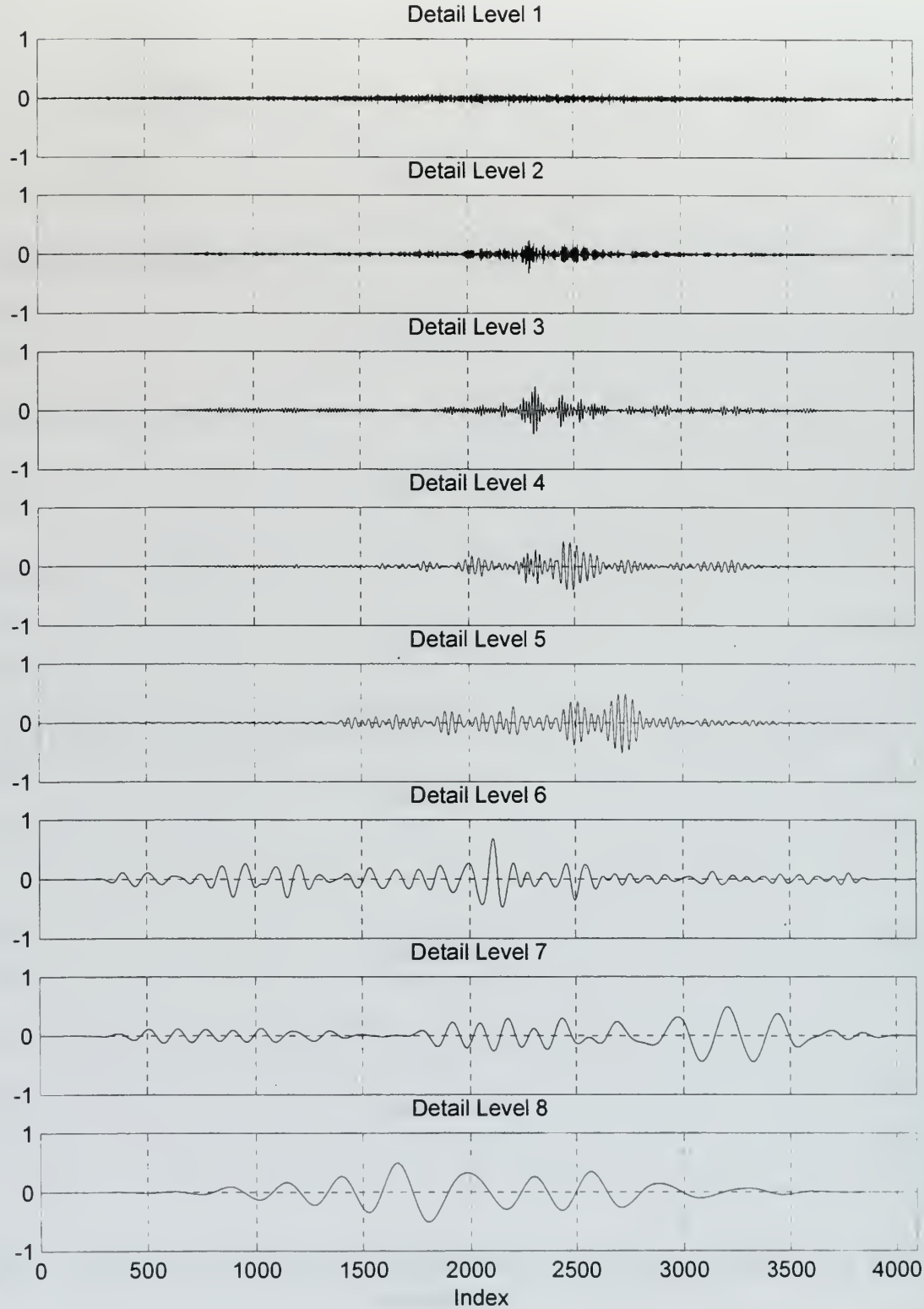

Figure A.6. Large Steel Rod Signal no. 23 Crosscorrelation of Details for Sensor #1 to #2

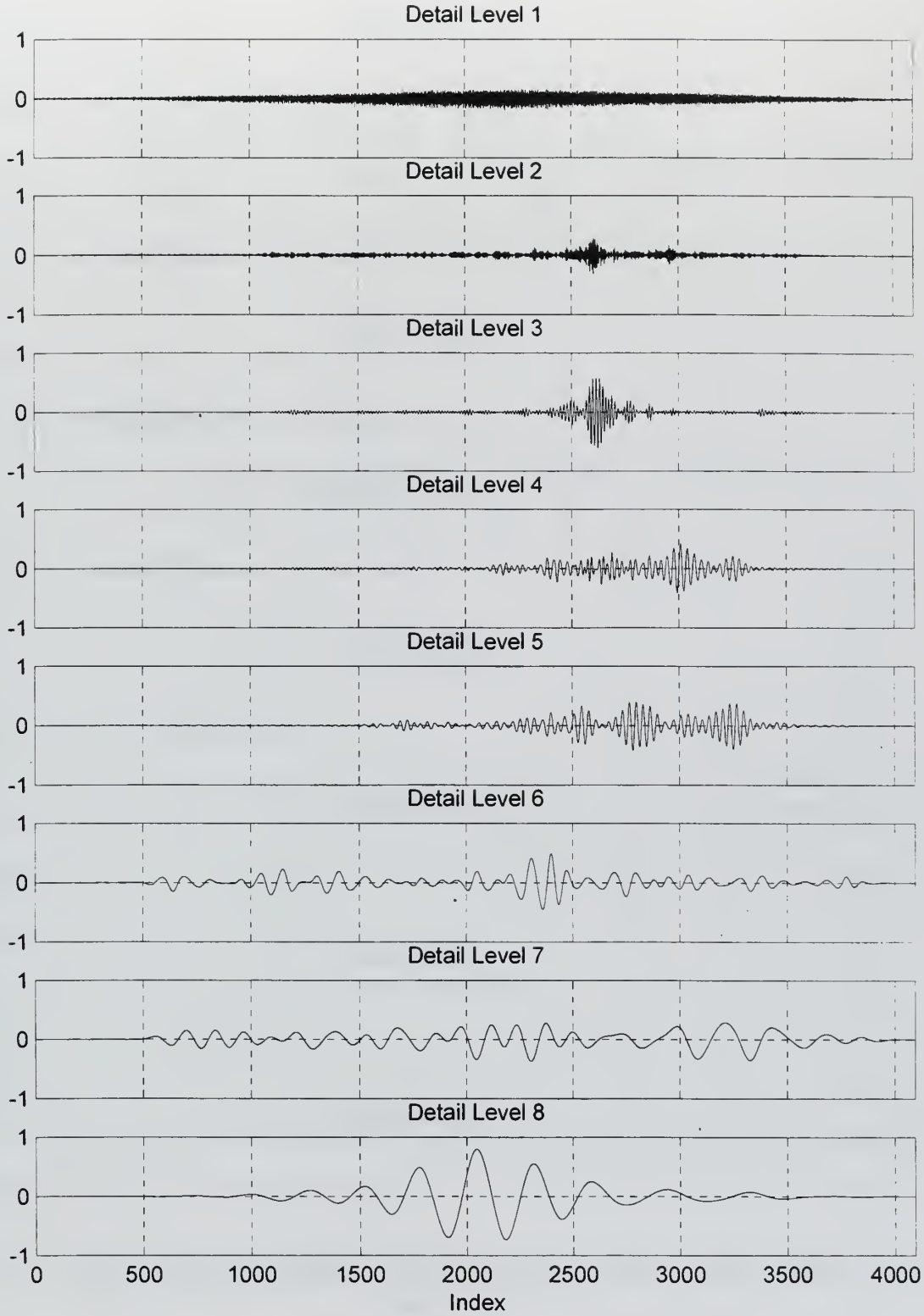

Figure A.7. Large Steel Rod Signal no. 23 Crosscorrelation of Details for Sensor #1 to #3

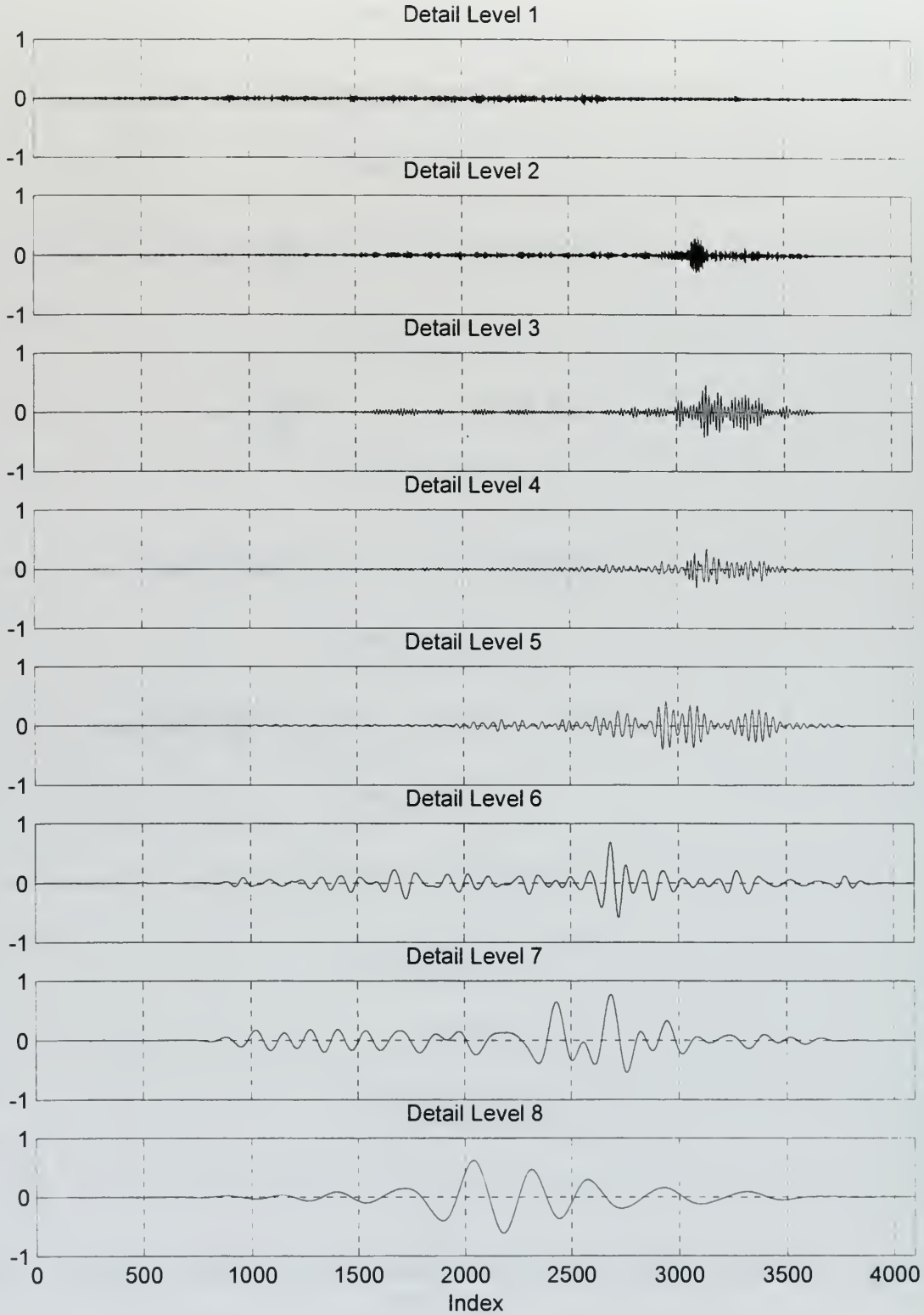

Figure A.8. Large Steel Rod Signal no. 23 Crosscorrelation of Details for Sensor #1 to #4

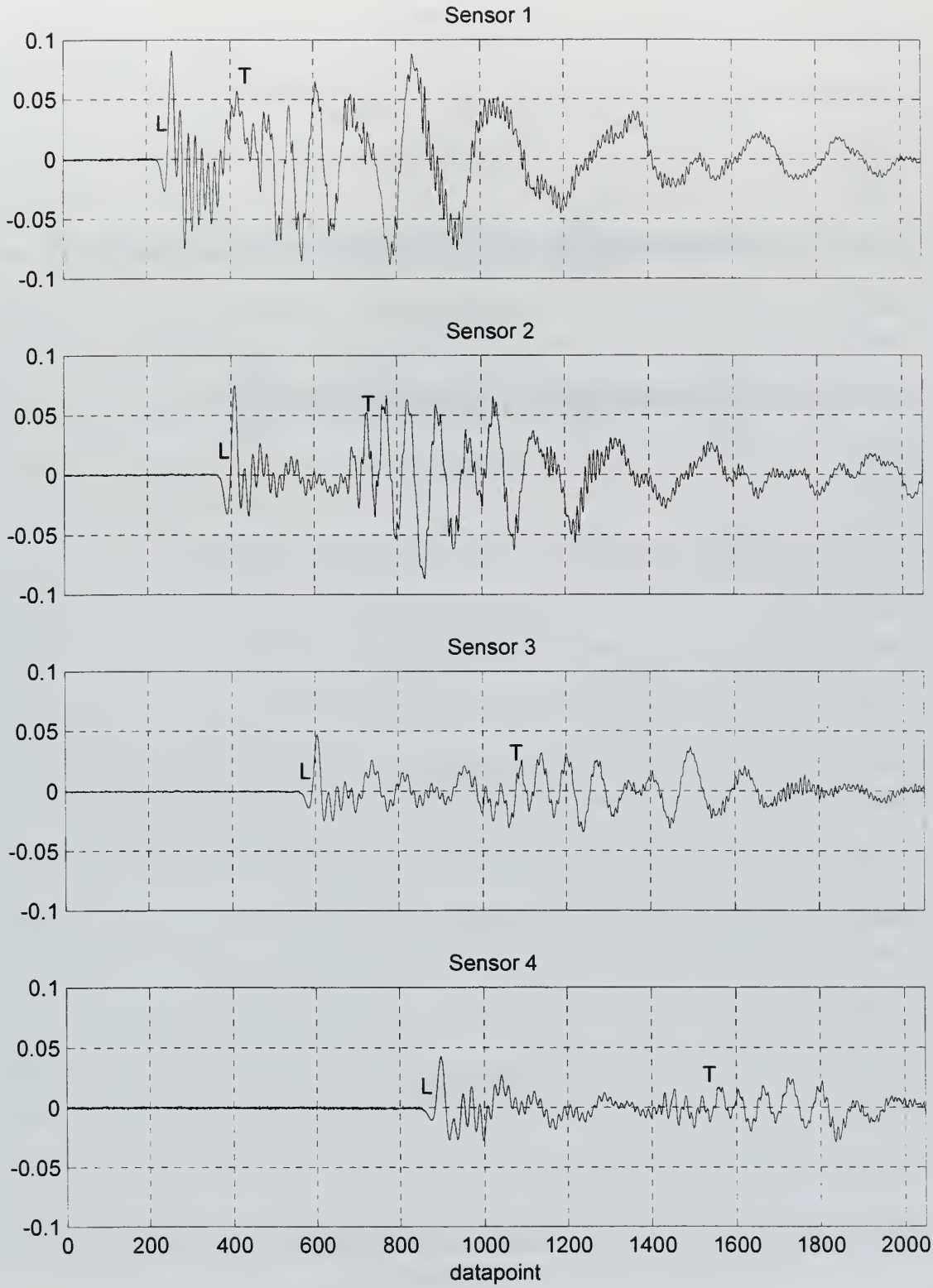

Figure A.9. Small Steel Rod Signal no. 61 Sensors #1 through #4

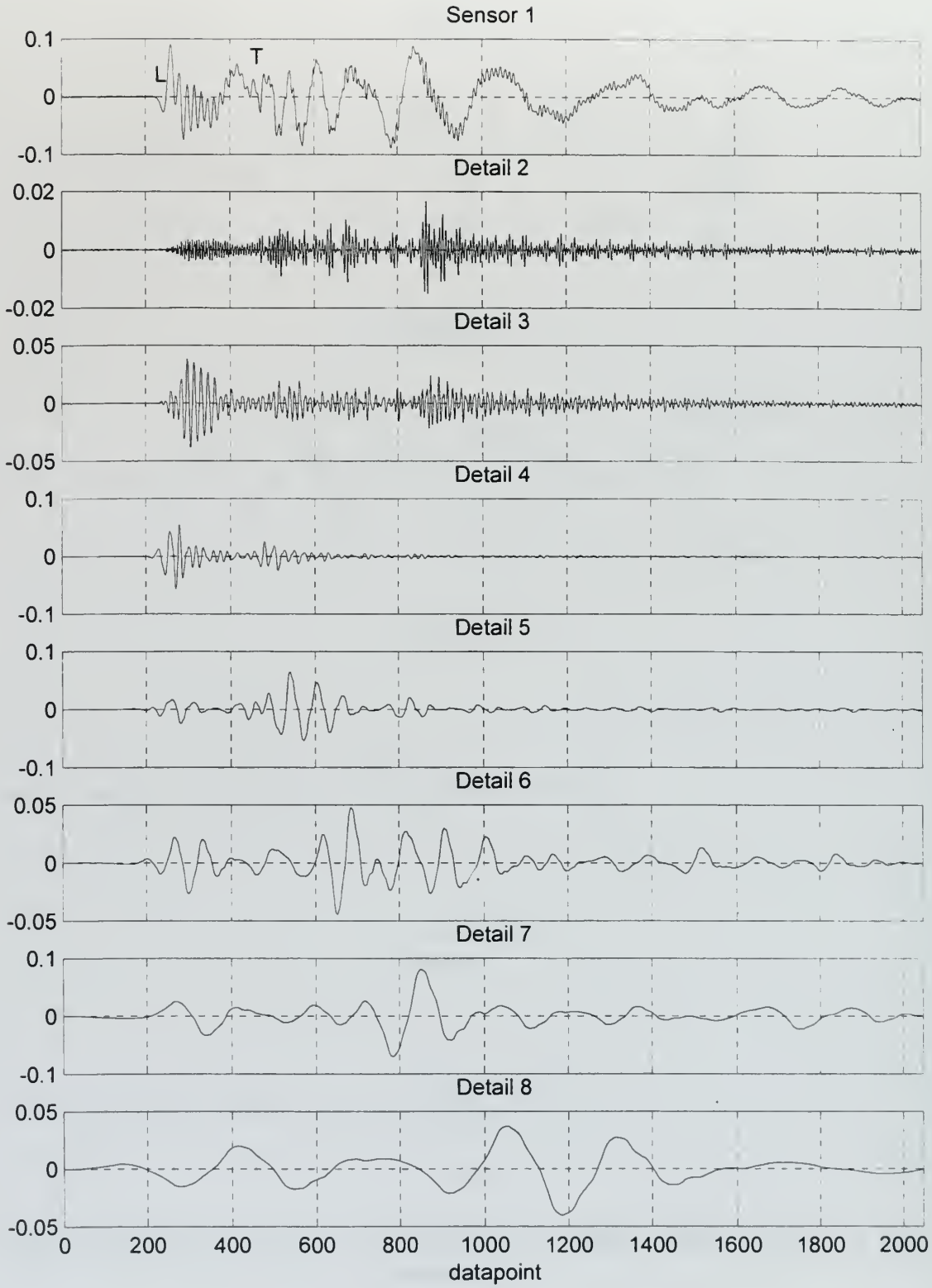

Figure A.10. Small Steel Rod Signal no. 61 Sensor #1 with Wavelet Details 2 through 8

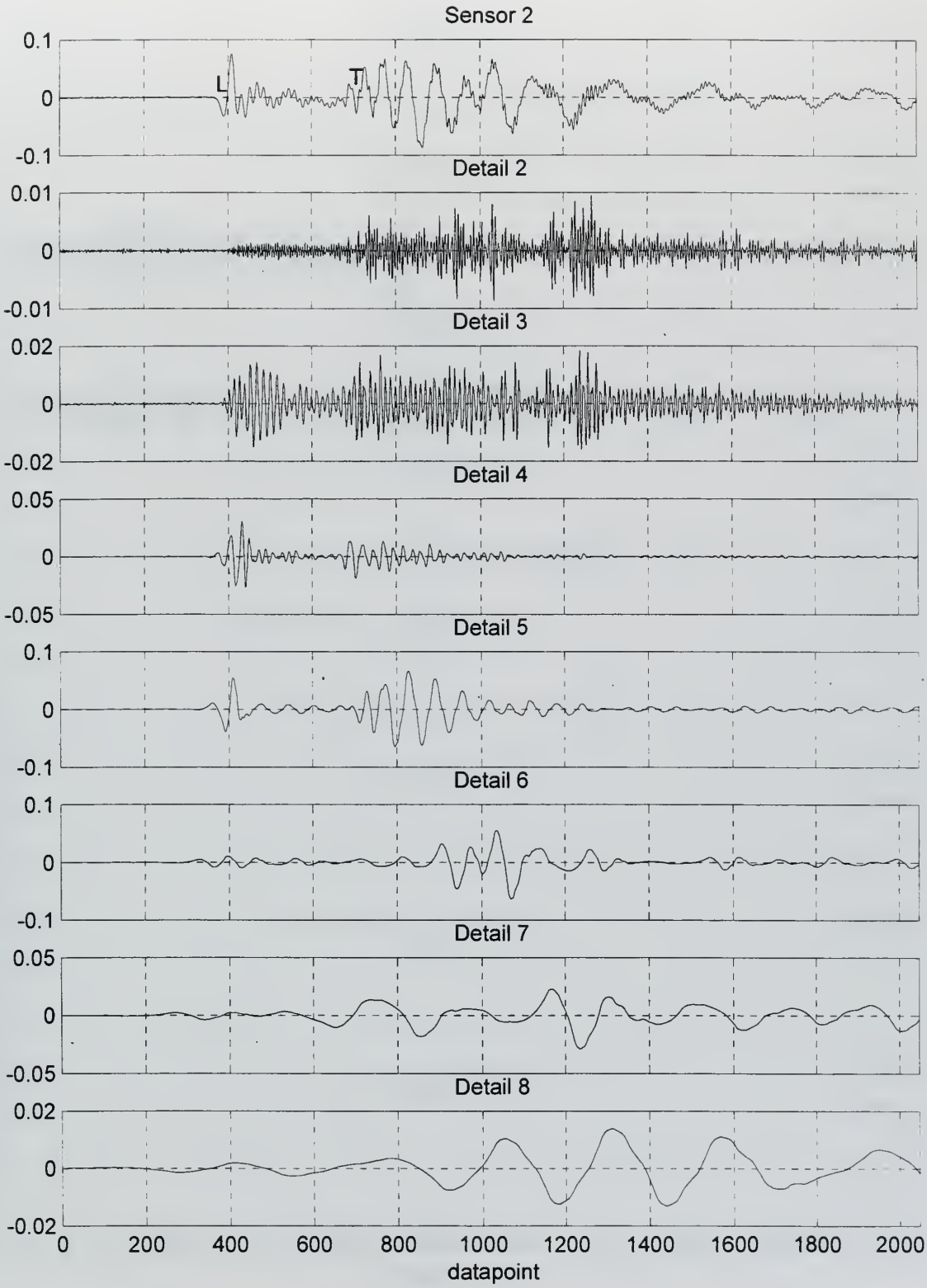

Figure A.11. Small Steel Rod Signal no. 61 Sensor #2 with Wavelet Details 2 through 8

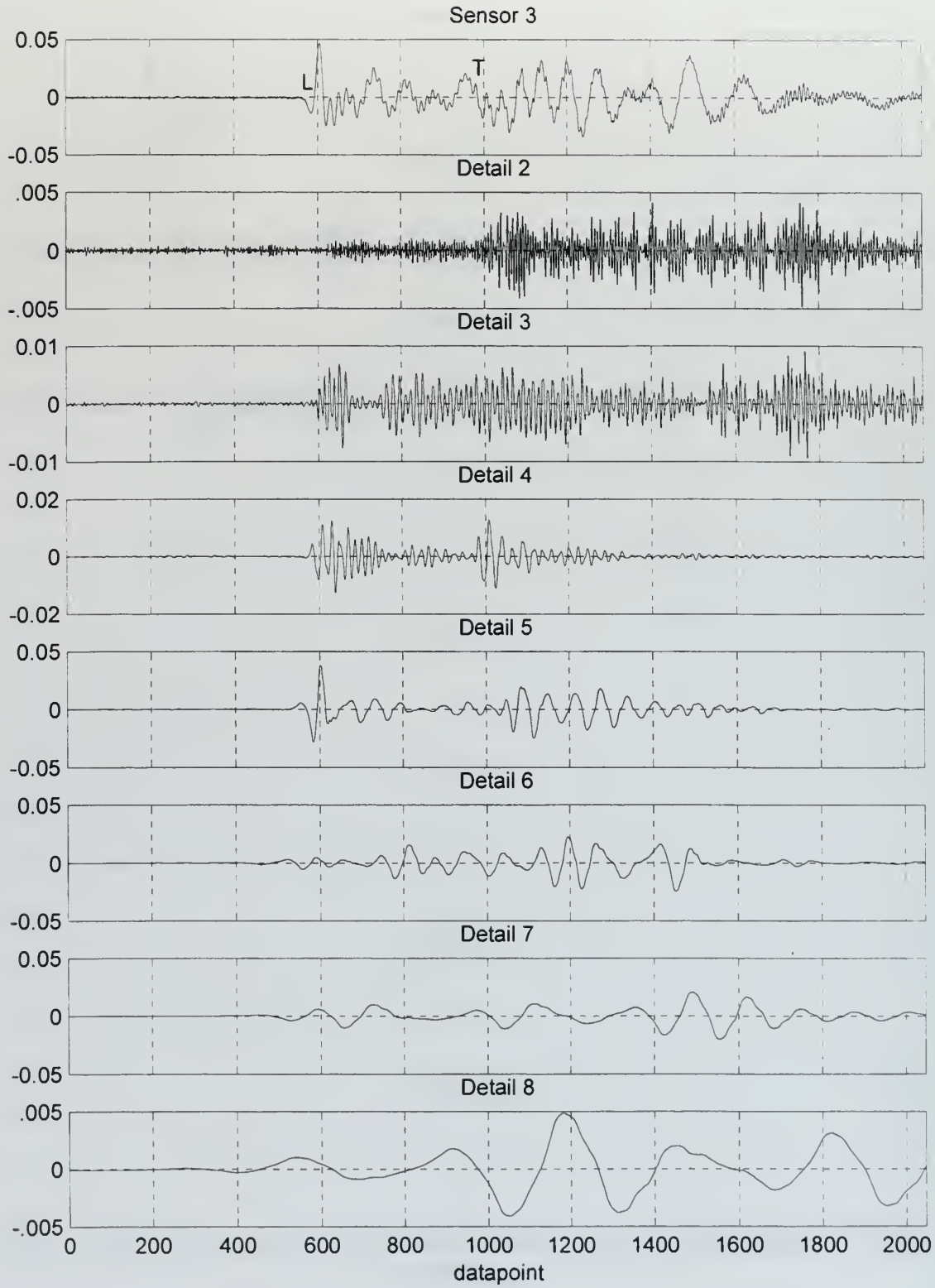

Figure A.12. Small Steel Rod Signal no. 61 Sensor #3 with Wavelet Details 2 through 8

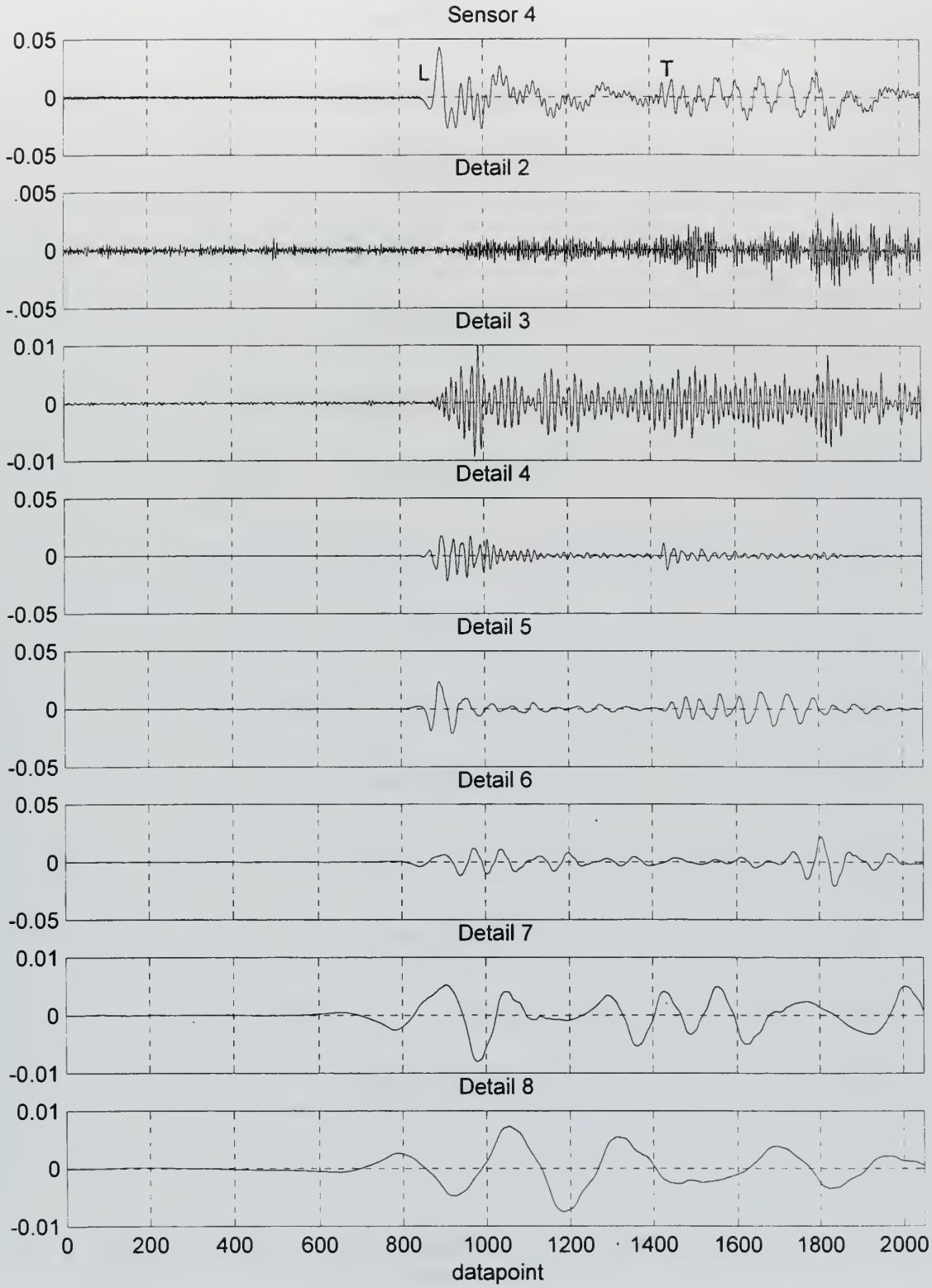

Figure A.13. Small Steel Rod Signal no. 61 Sensor #4 with Wavelet Details 2 through 8

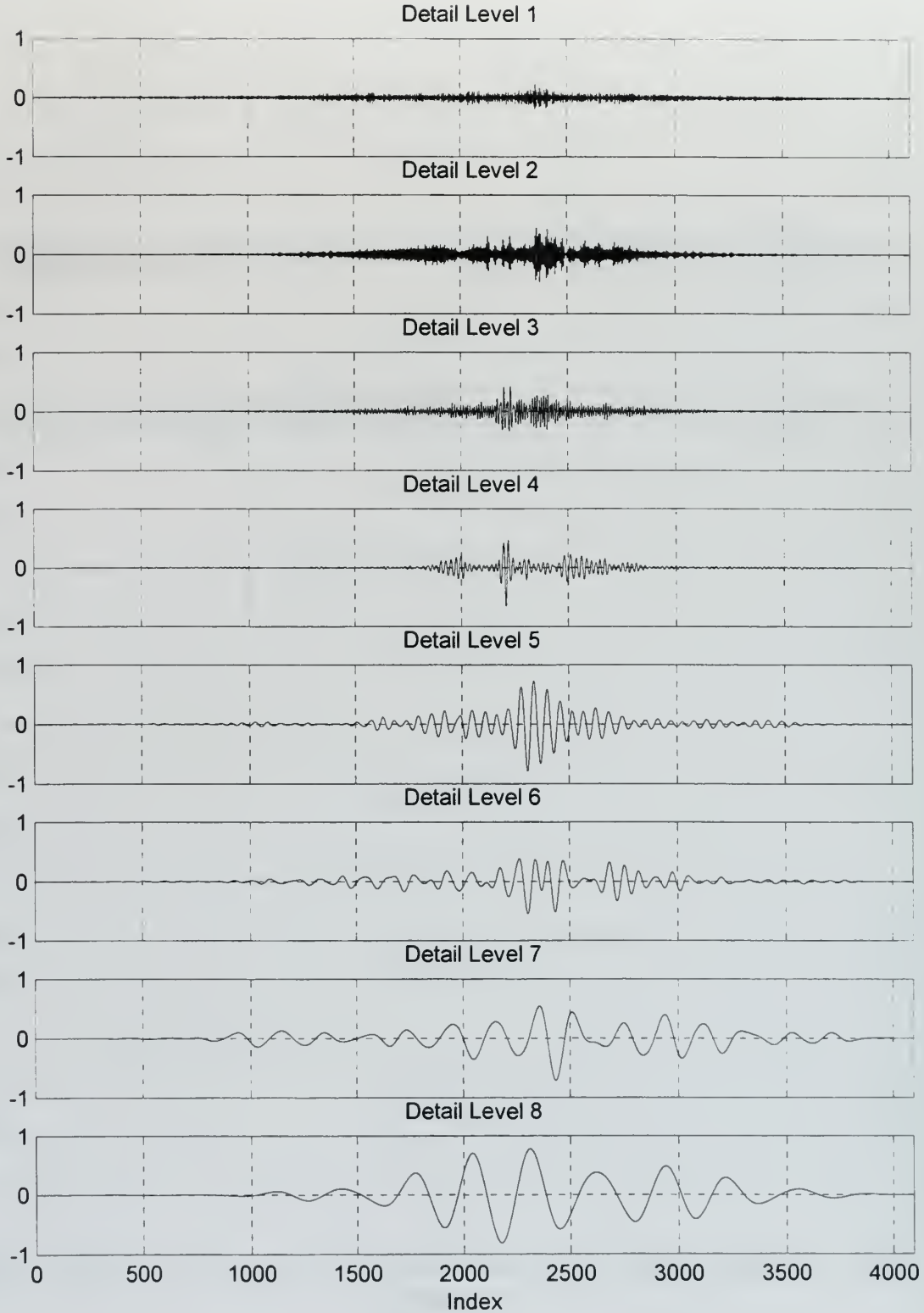

Figure A.14. Small Steel Rod Signal no. 61 Crosscorrelation of Details for Sensor #1 to #2

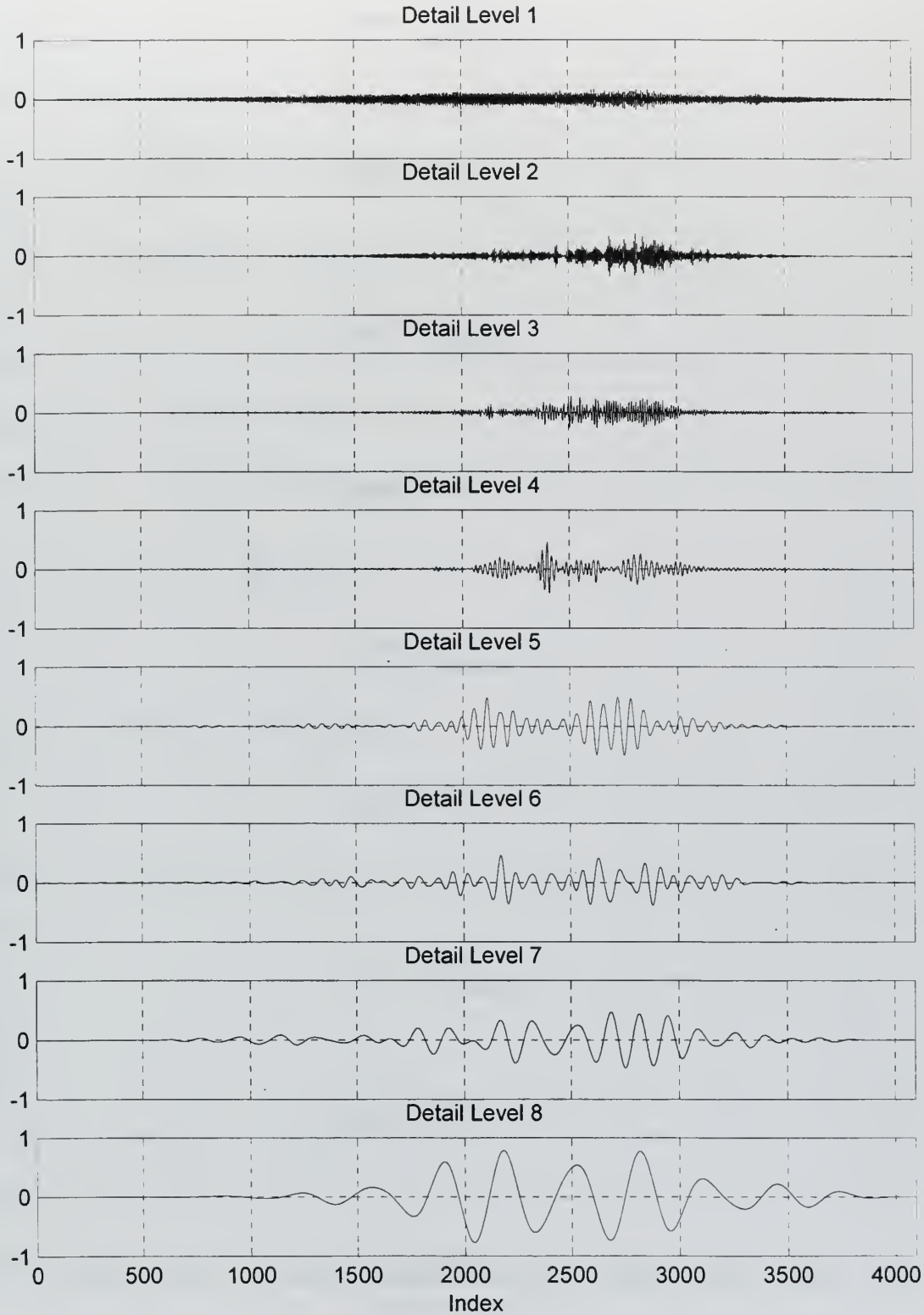

Figure A.15. Small Steel Rod Signal no. 61 Crosscorrelation of Details for Sensor #1 to #3

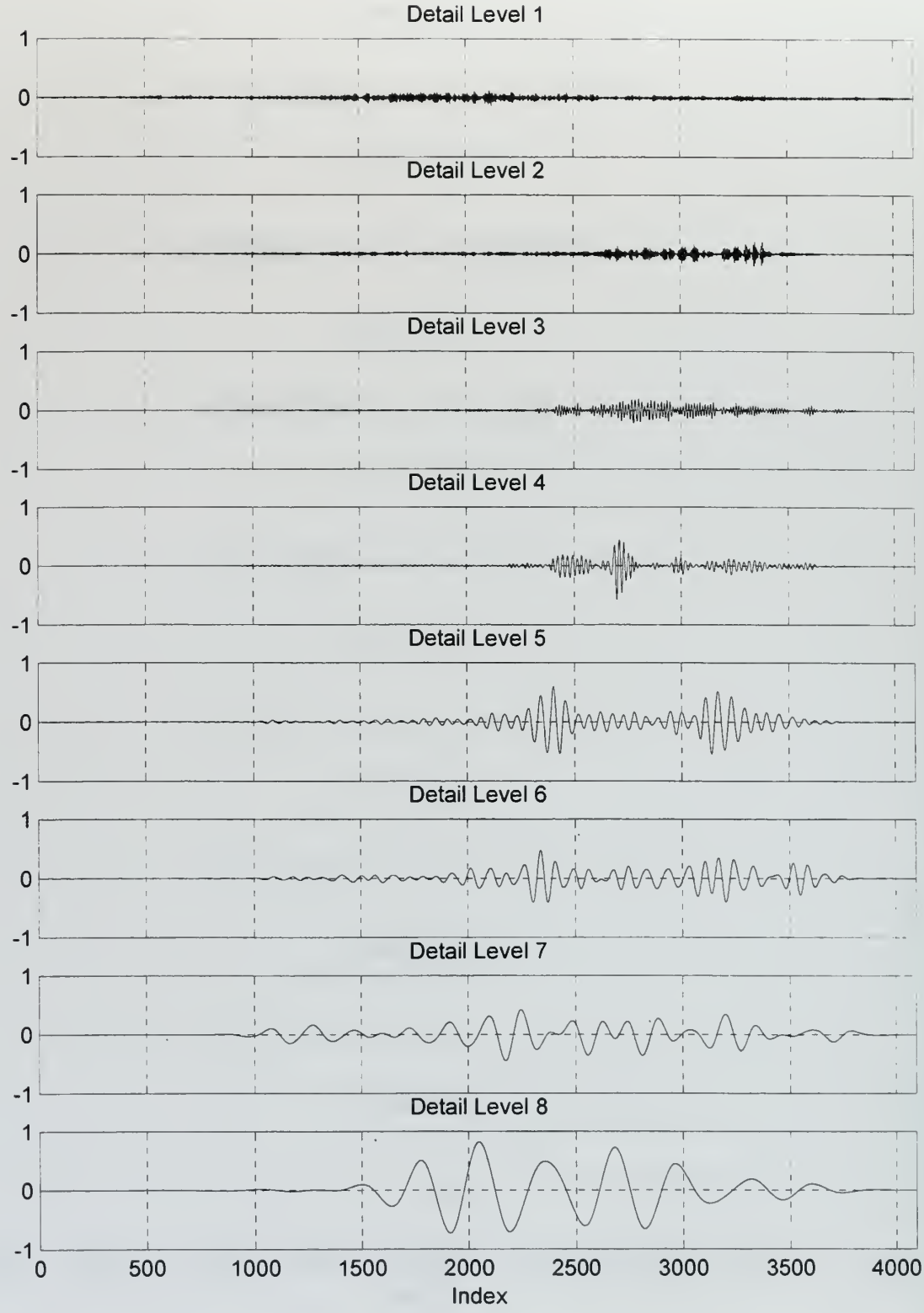

Figure A.16. Small Steel Rod Signal no. 61 Crosscorrelation of Details for Sensor #1 to #4

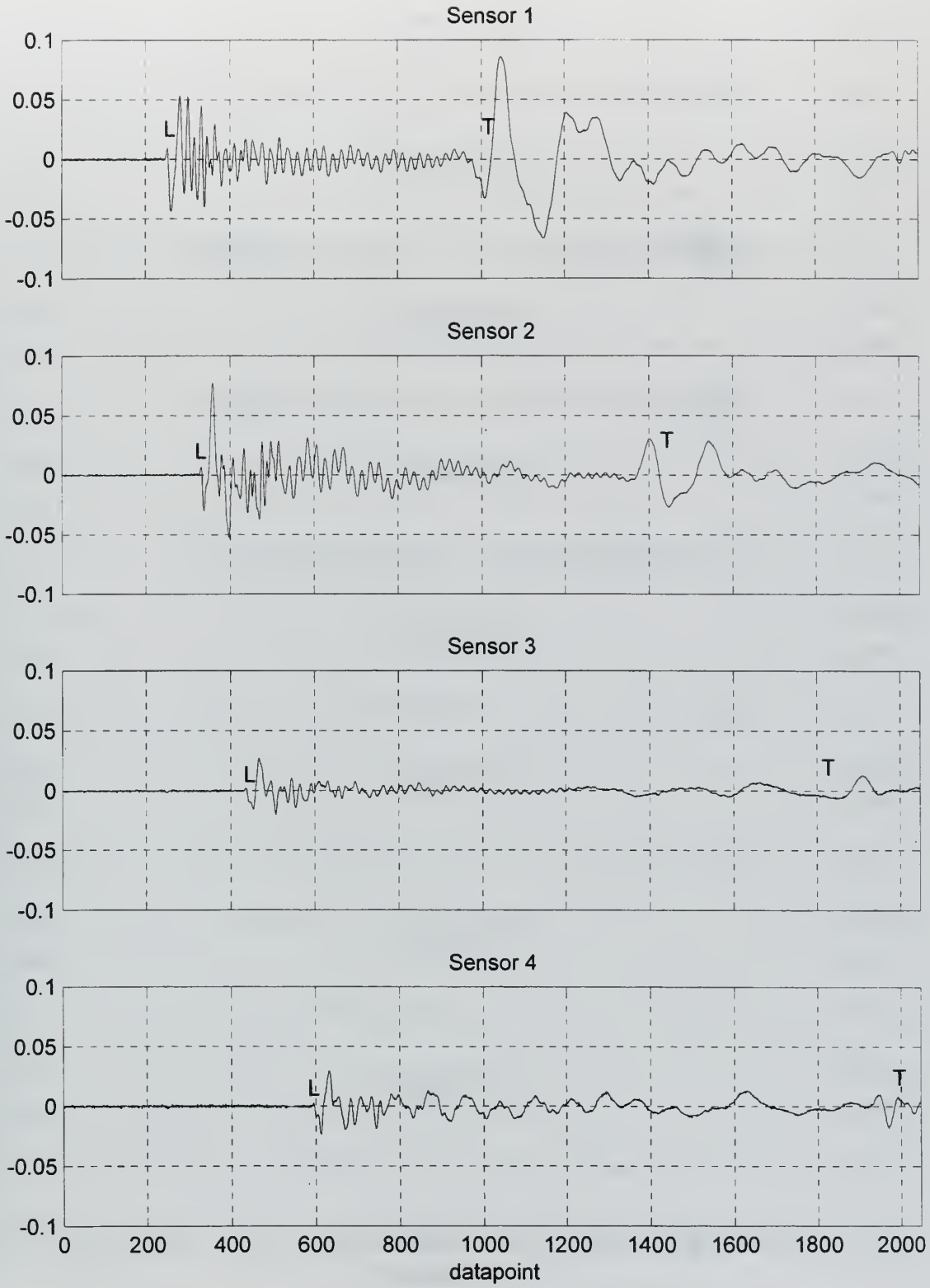

Figure A.17. Carbon Fiber Rod Signal no. 38 Sensors #1 through #4

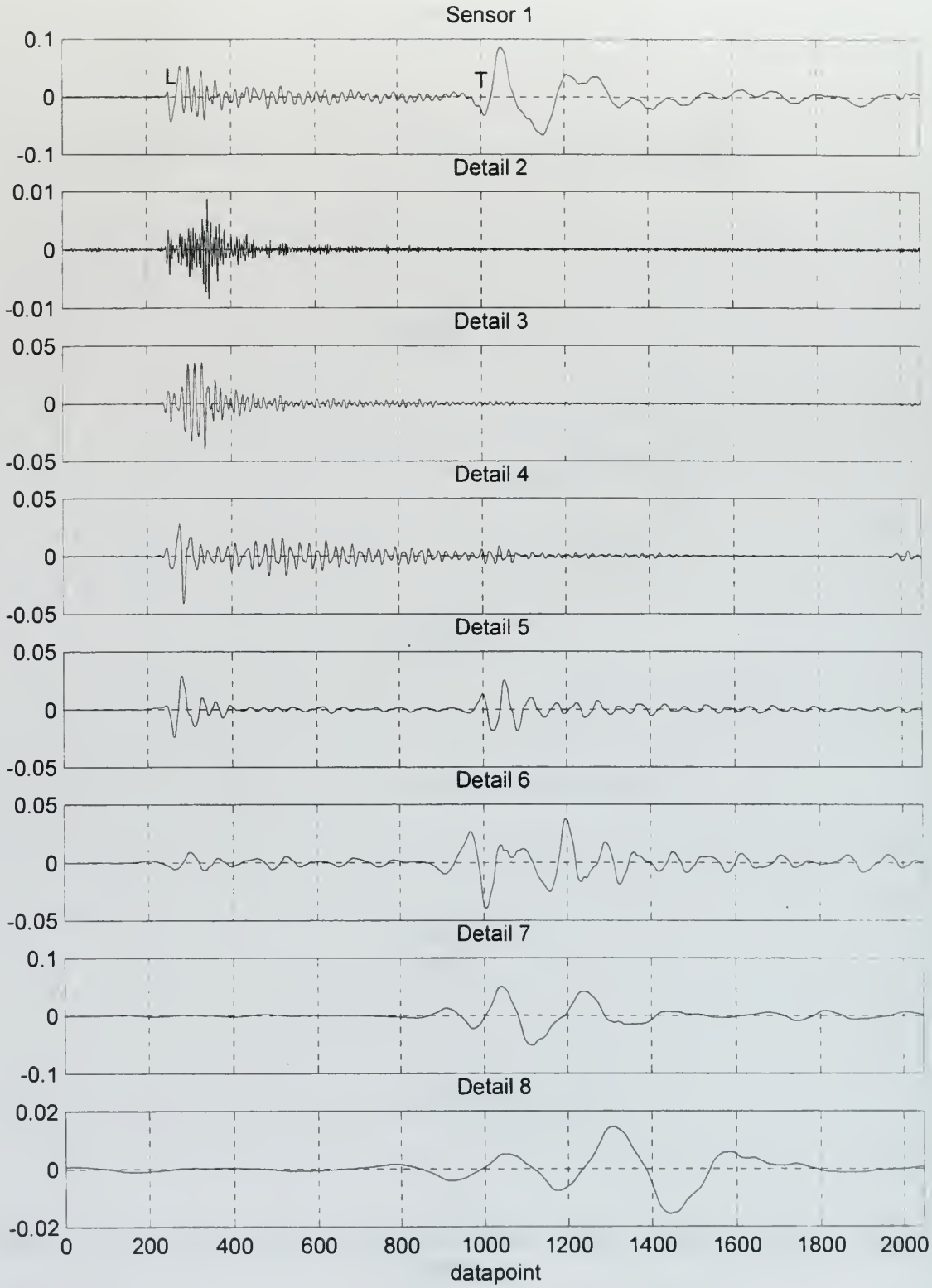

Figure A.18. Carbon Fiber Rod Signal no. 38 Sensor #1 with Wavelet Details 2 through 8

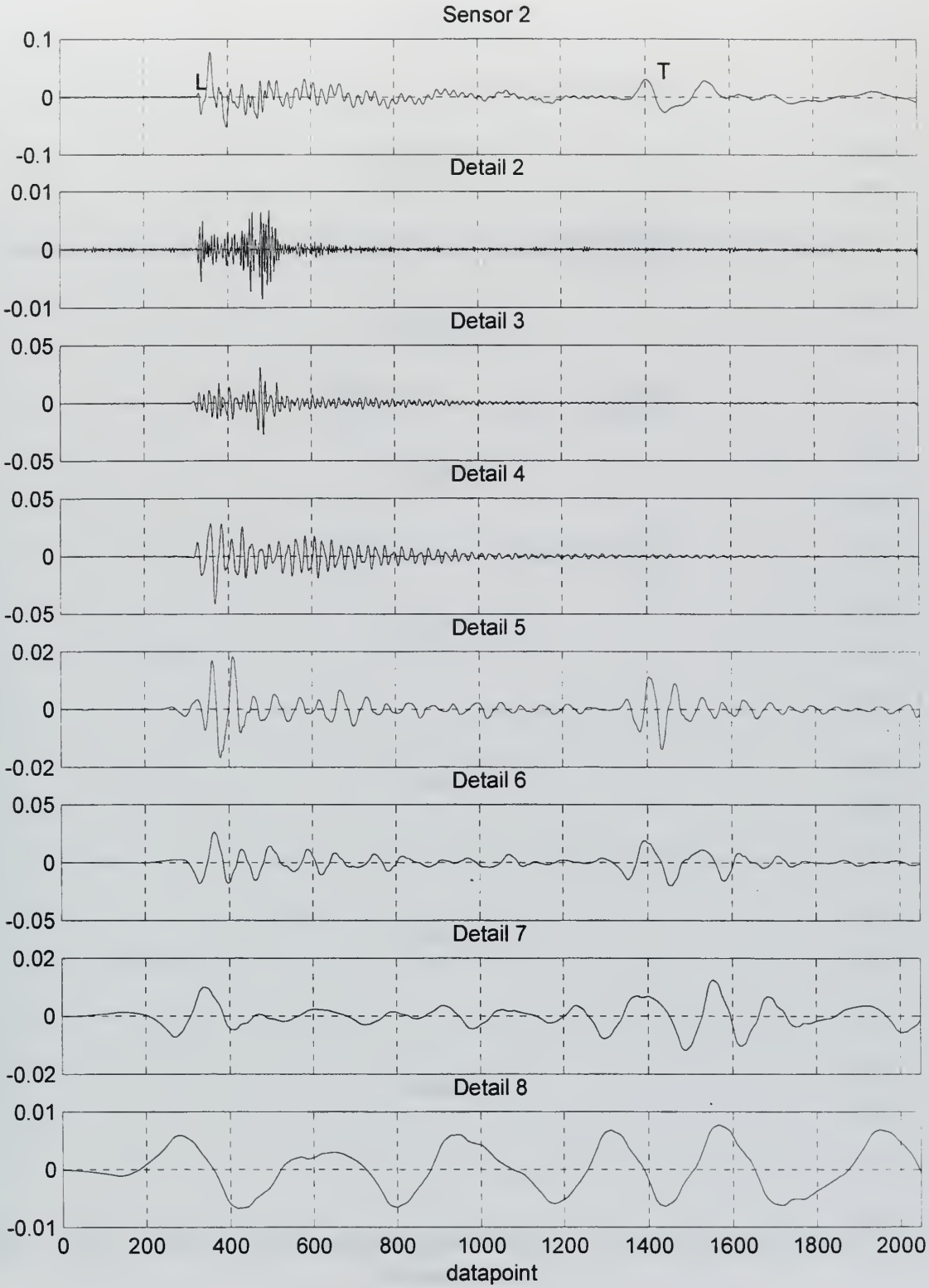

Figure A.19. Carbon Fiber Rod Signal no. 38 Sensor #2 with Wavelet Details 2 through 8

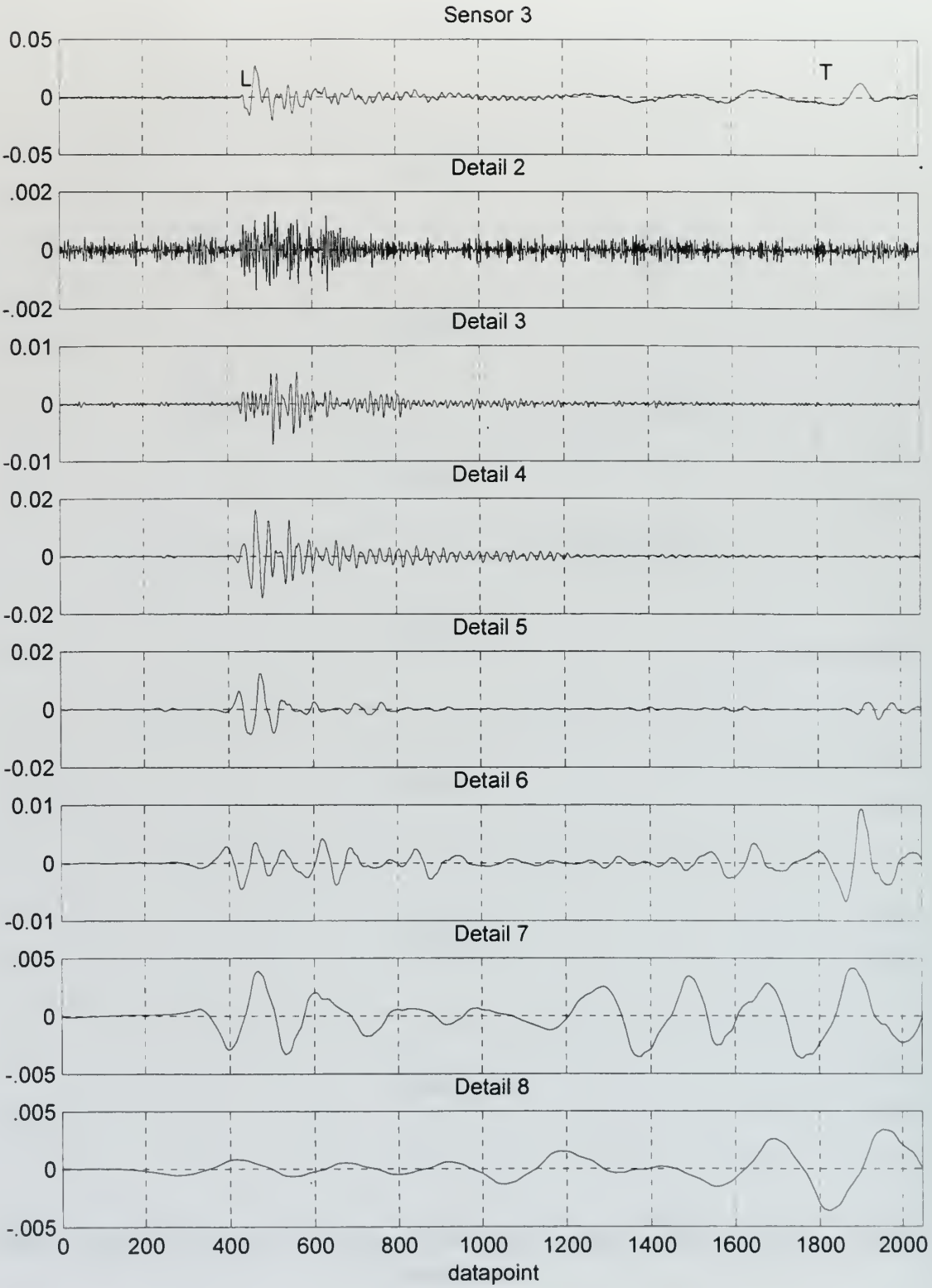

Figure A.20. Carbon Fiber Rod Signal no. 38 Sensor #3 with Wavelet Details 2 through 8

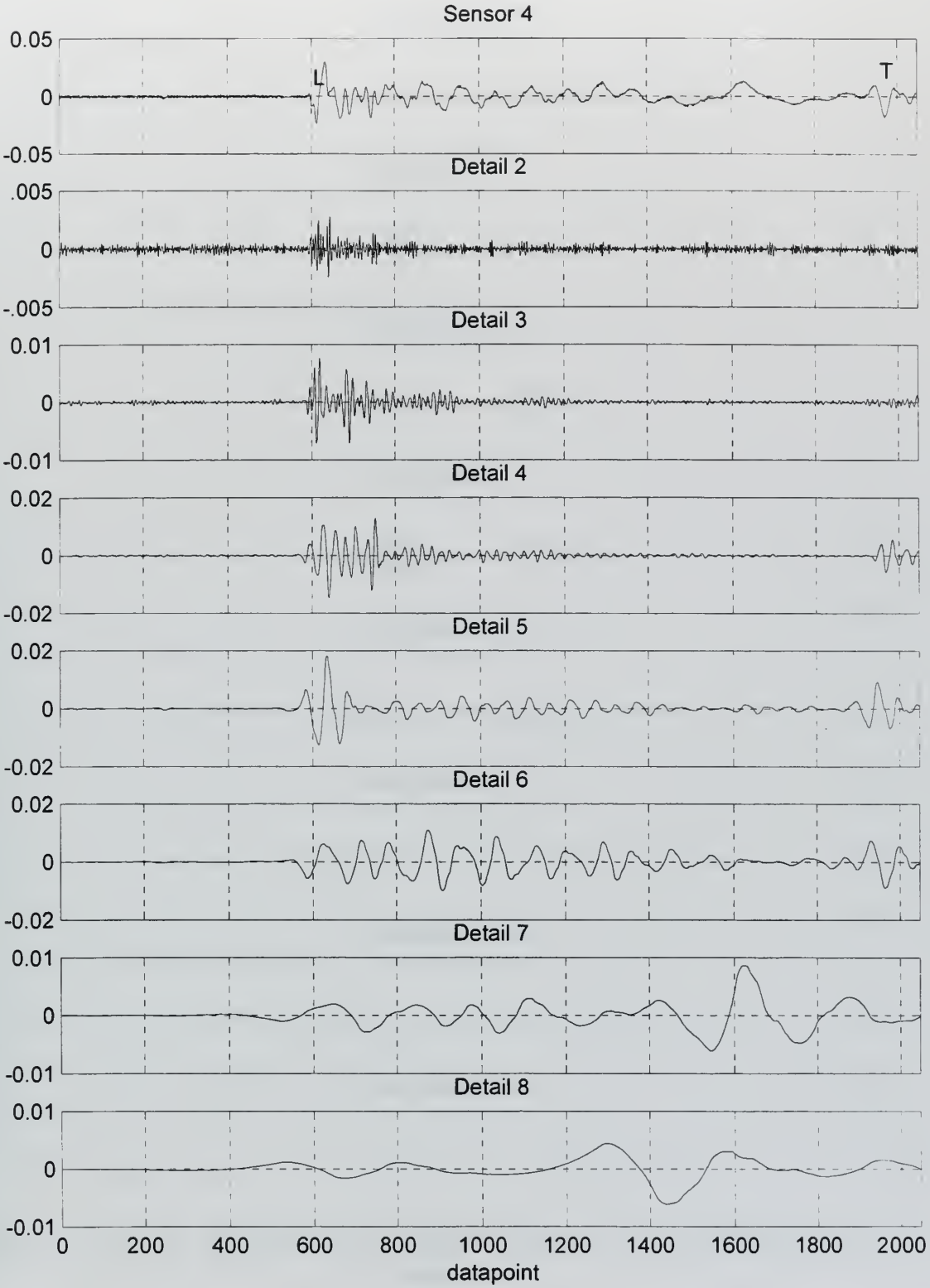

Figure A.21. Carbon Fiber Rod Signal no. 38 Sensor #4 with Wavelet Details 2 through 8

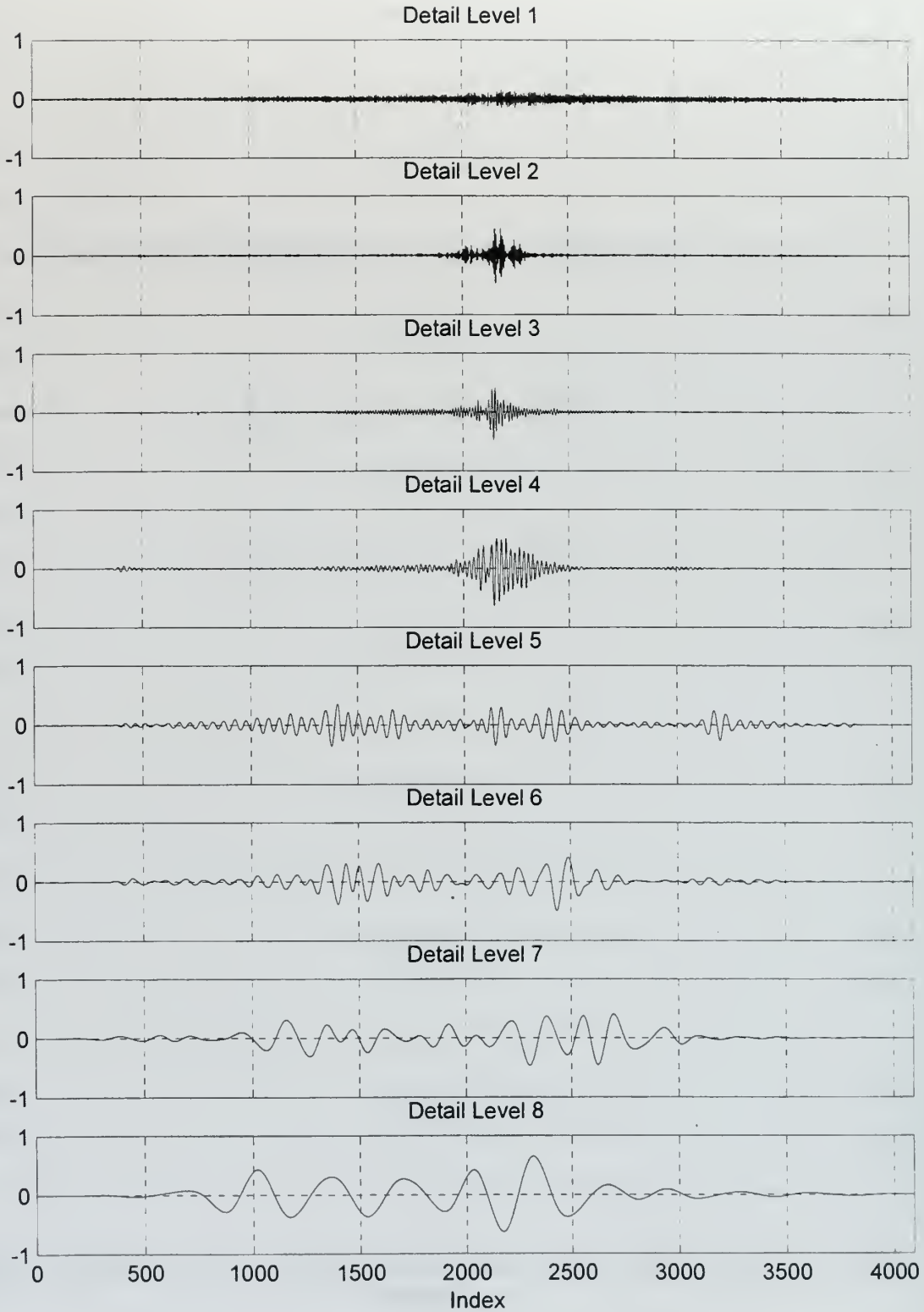

Figure A.22. Carbon Fiber Rod Signal no. 38 Crosscorrelation of Details for Sensor #1 to #2

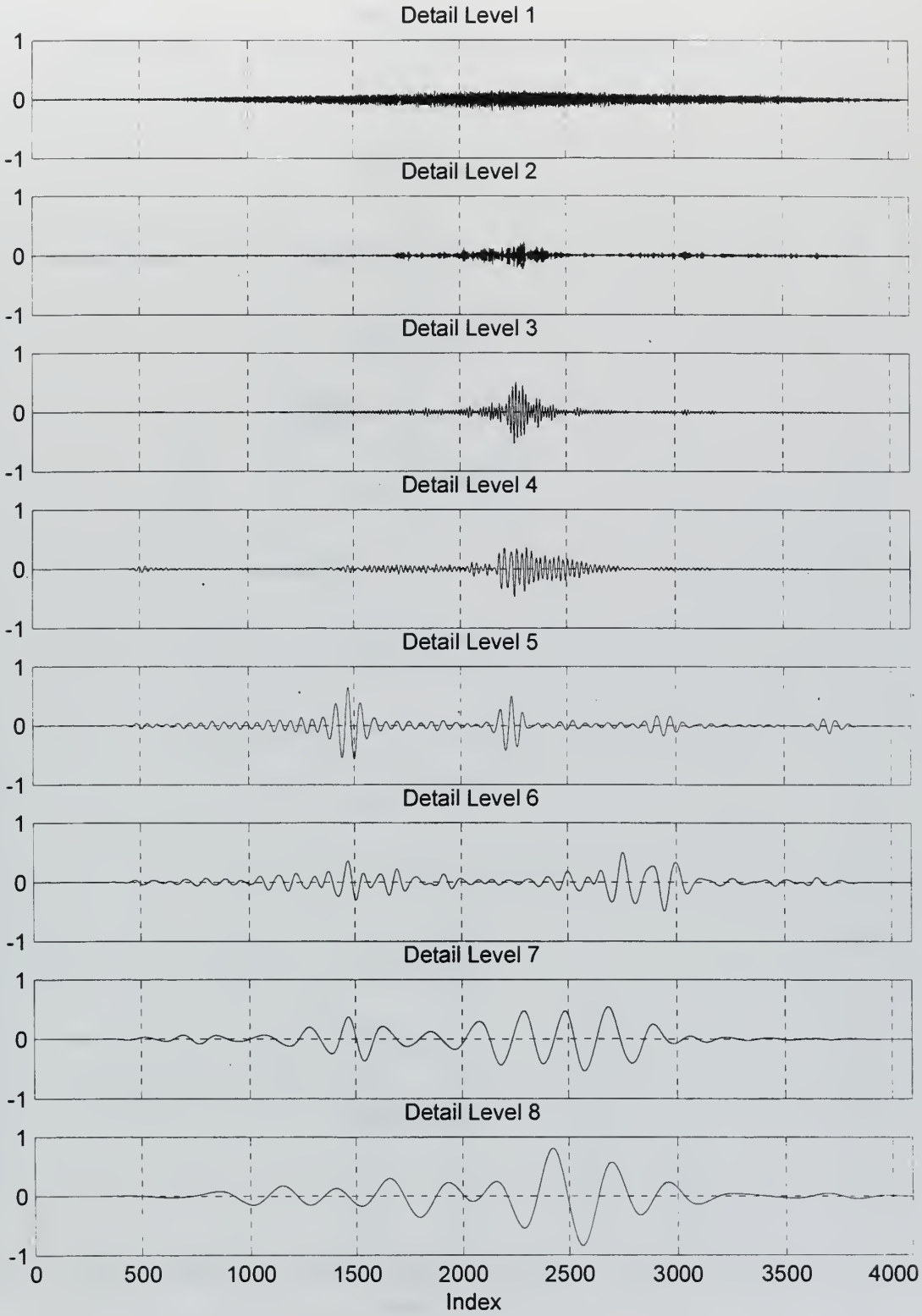

Figure A.23. Carbon Fiber Rod Signal no. 38 Crosscorrelation of Details for Sensor #1 to #3

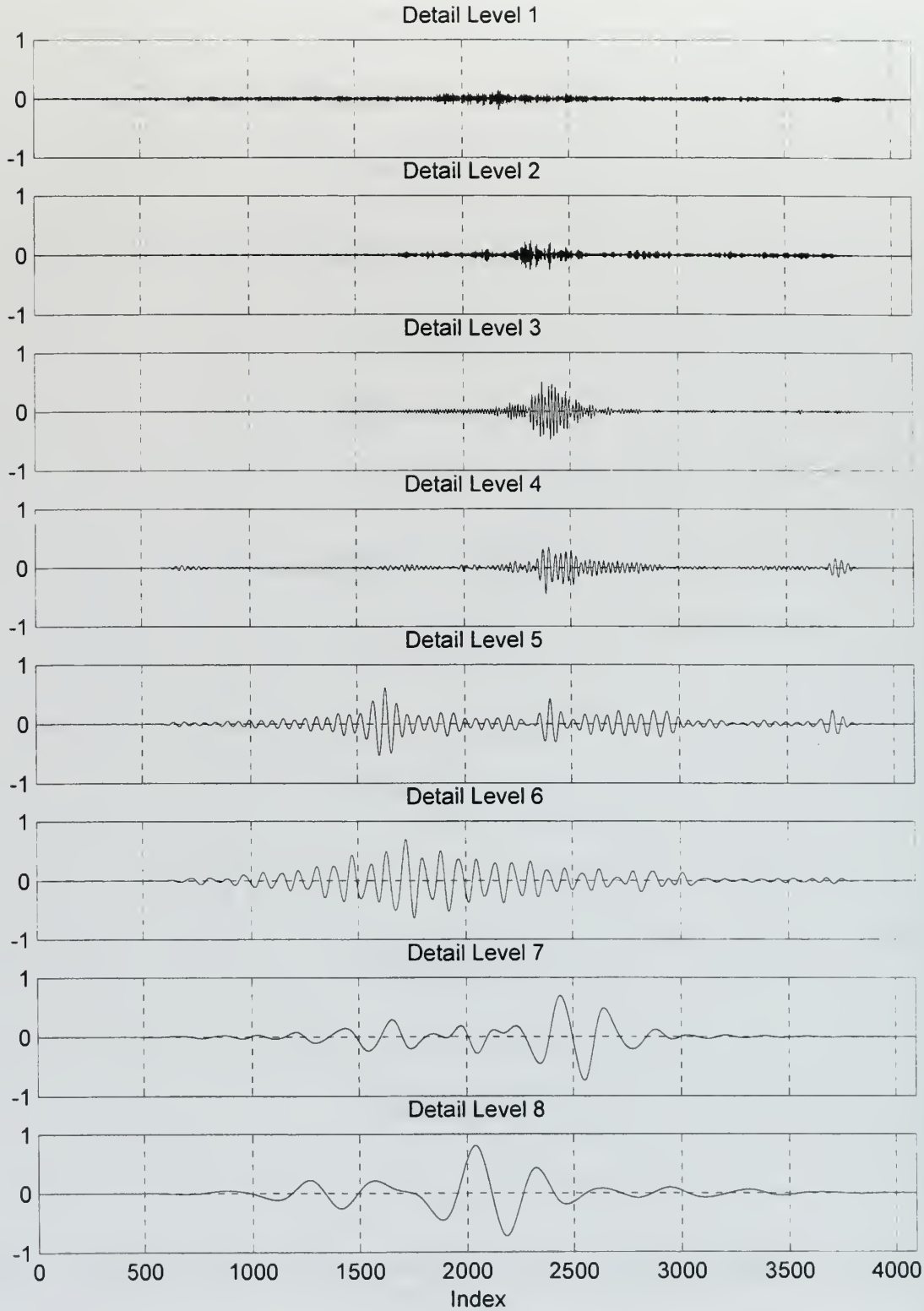

Figure A.24. Carbon Fiber Rod Signal no. 38 Crosscorrelation of Details for Sensor #1 to #4

APPENDIX B. LOCATION AND BEST CORRELATION LEVEL HISTOGRAMS

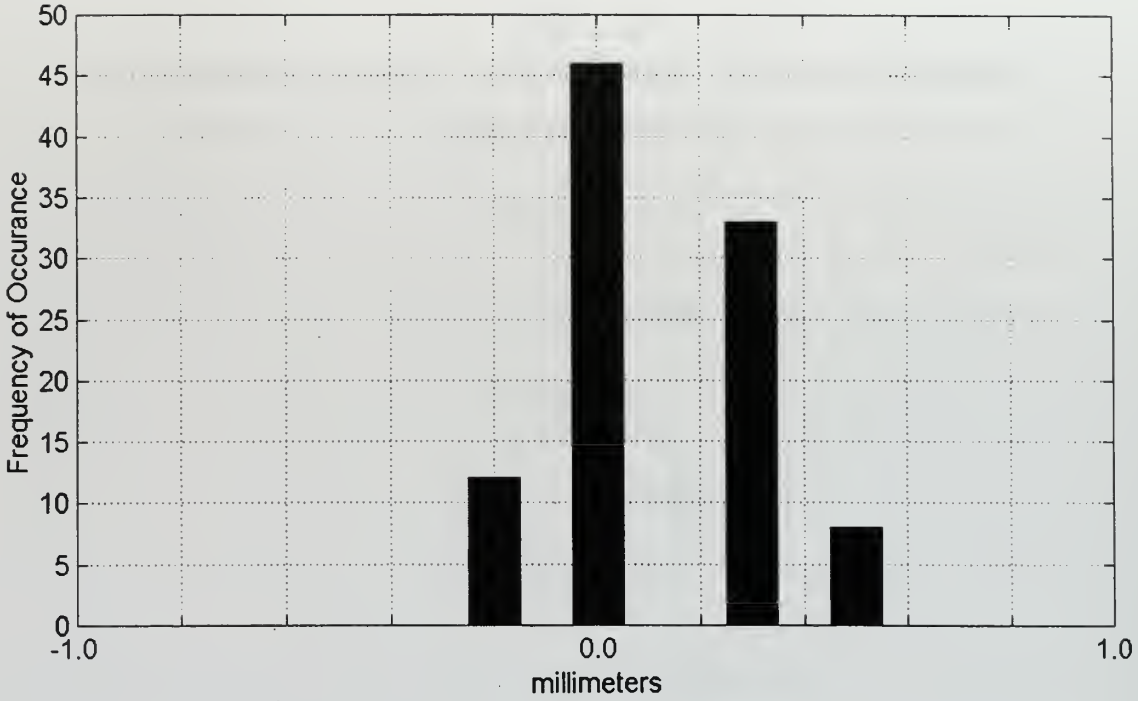

Figure B.1. Threshold Crossing Location Histogram for Large Steel Rod Sensors #1 and #2 Mean = 0.116 mm, Std Dev. = 0.205 mm, Transducer Diameter = 9.525 mm.

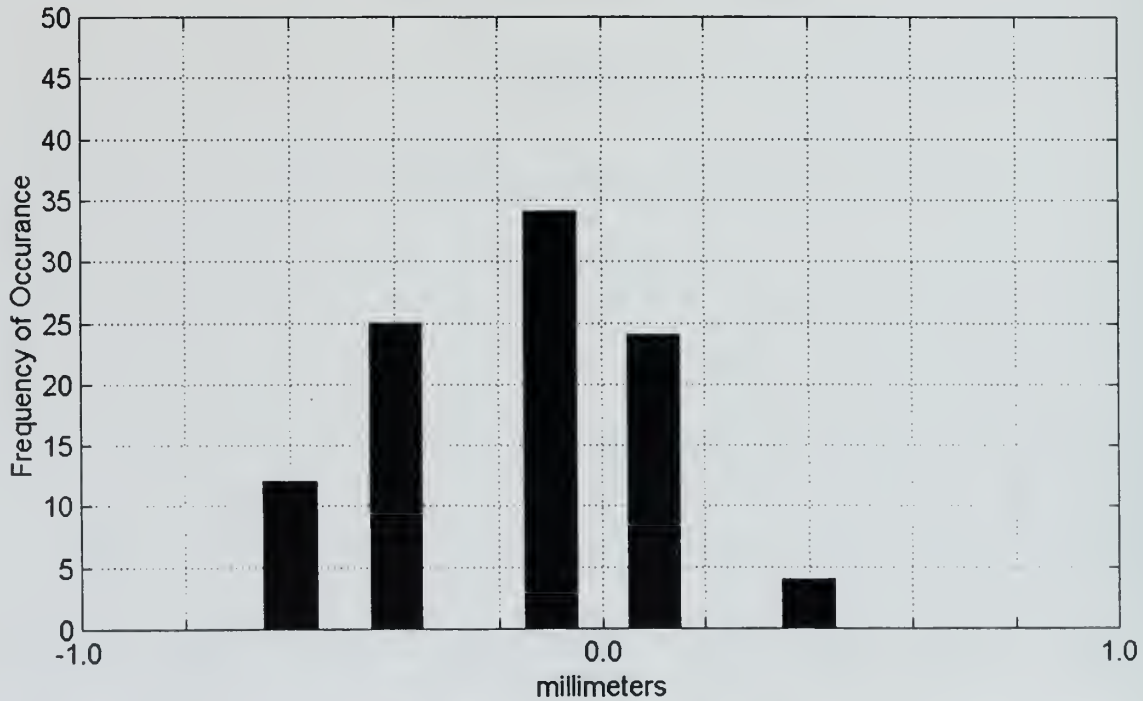

Figure B.2. Threshold Crossing Location Histogram for Large Steel Rod Sensors #1 and #3 Mean = -0.168 mm, Std Dev. = 0.263 mm, Transducer Diameter = 9.525 mm.

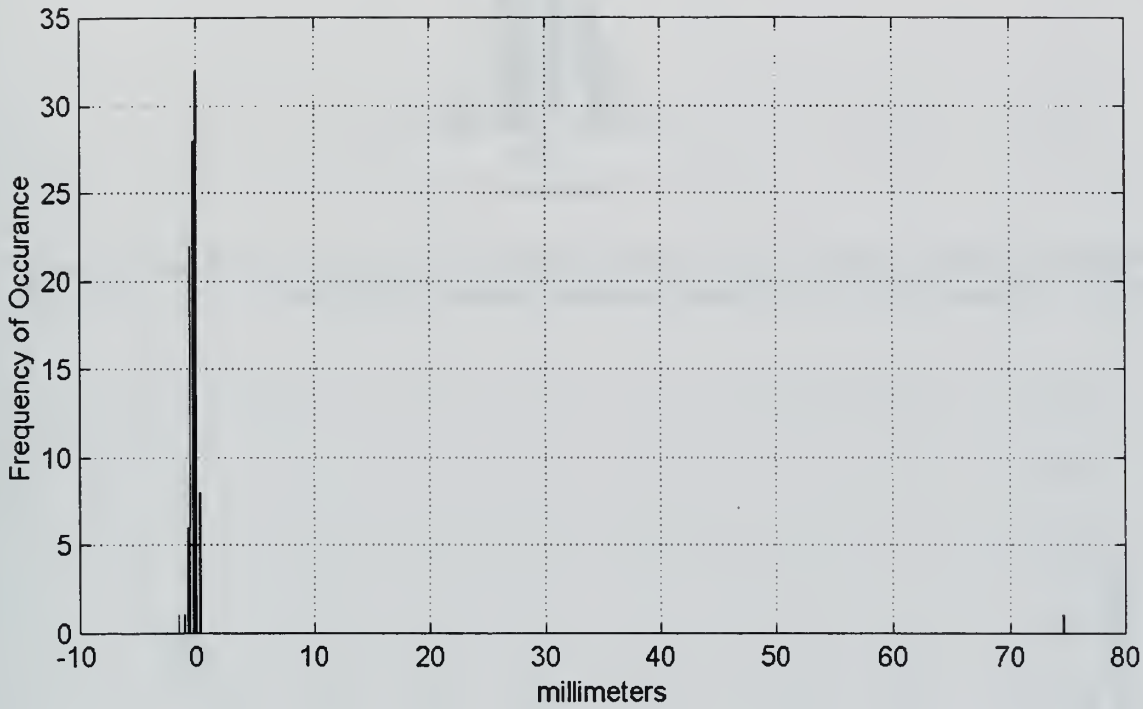

Figure B.3. Threshold Crossing Location Histogram for Large Steel Rod Sensors #1 and #4 Mean = 0.443 mm, Std Dev. = 7.535 mm, Transducer Diameter = 9.525 mm.

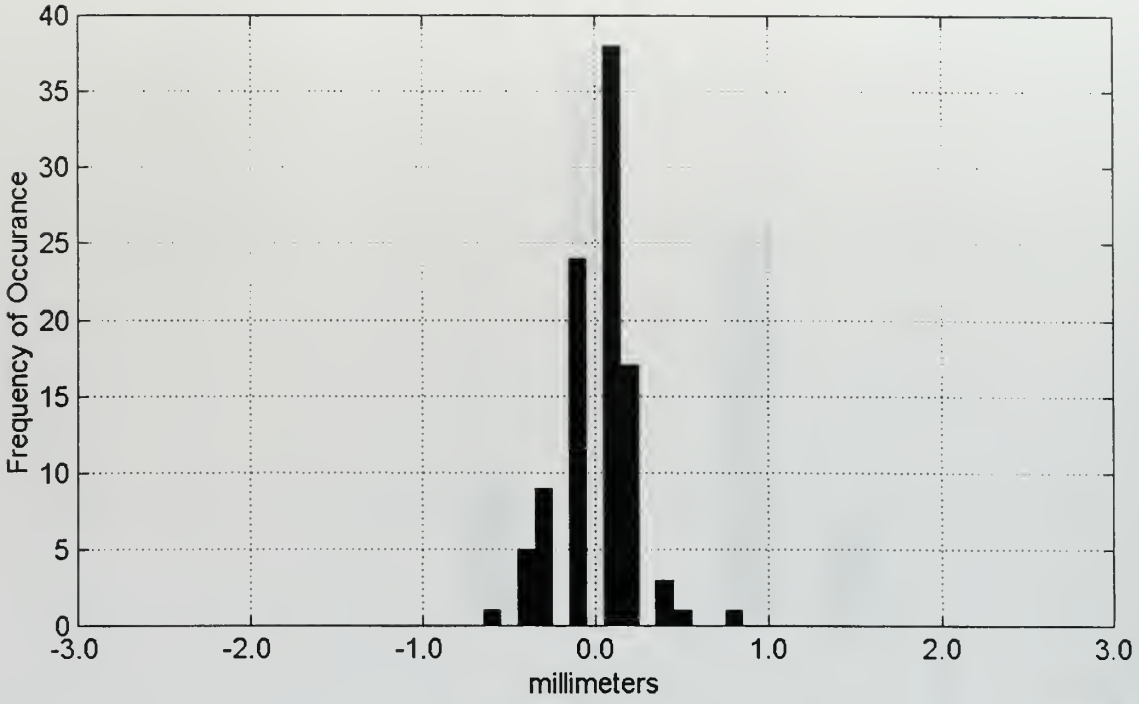

Figure B.4. Gaussian Crosscorrelation Location Histogram for Large Steel Rod Sensors #1 and #2 Mean = 0.020 mm, Std Dev. = 0.217 mm, Transducer Diameter = 9.525 mm.

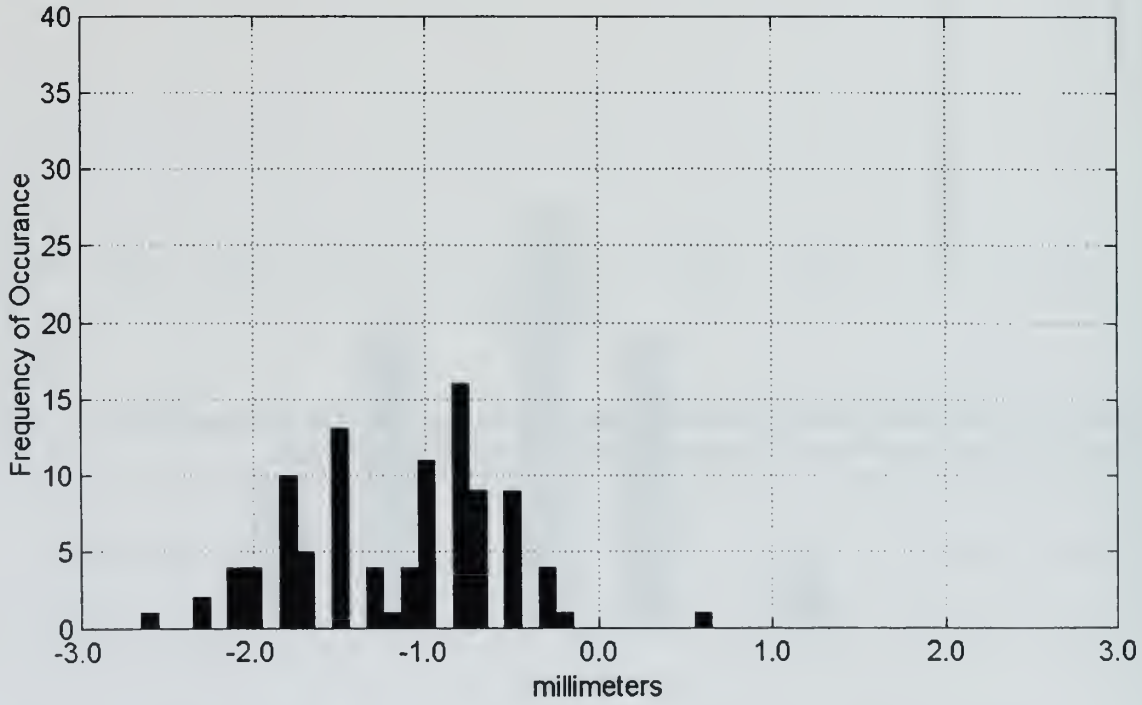

Figure B.5. Gaussian Crosscorrelation Location Histogram for Large Steel Rod Sensors #1 and #3 Mean = -1.170 mm, Std Dev. = 0.058 mm, Transducer Diameter = 9.525 mm.

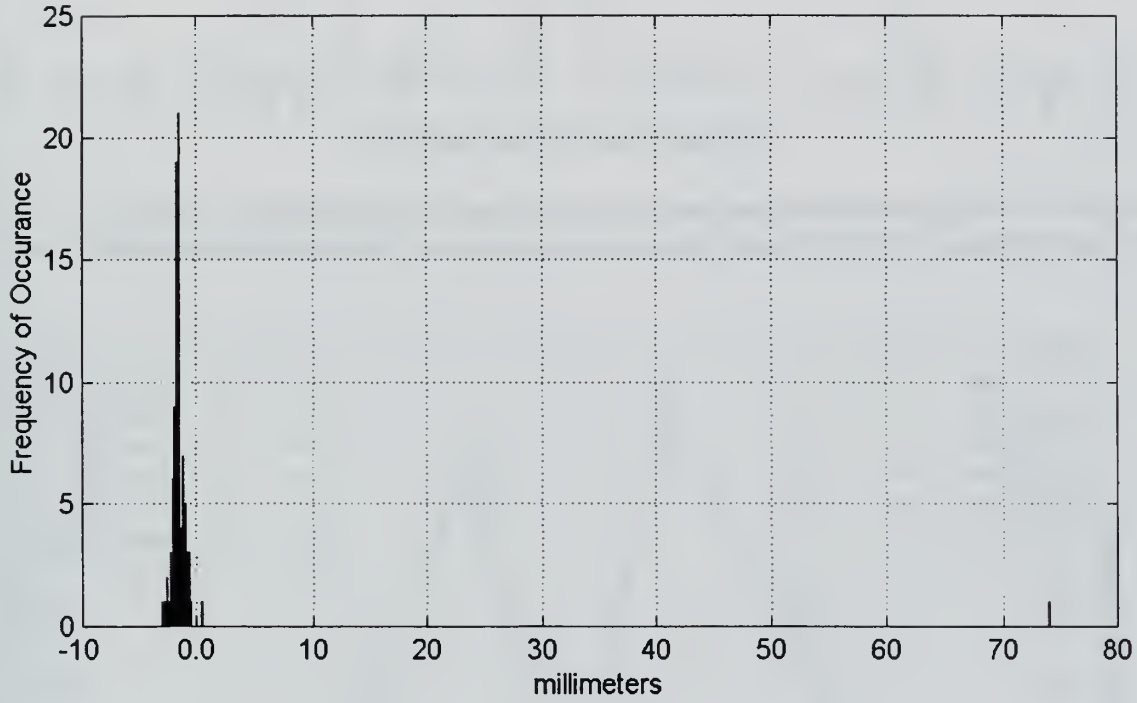

Figure B.6. Gaussian Crosscorrelation Location Histogram for Large Steel Rod Sensors #1 and #4 Mean = -0.848 mm, Std Dev. = 7.617 mm, Transducer Diameter = 9.525 mm.

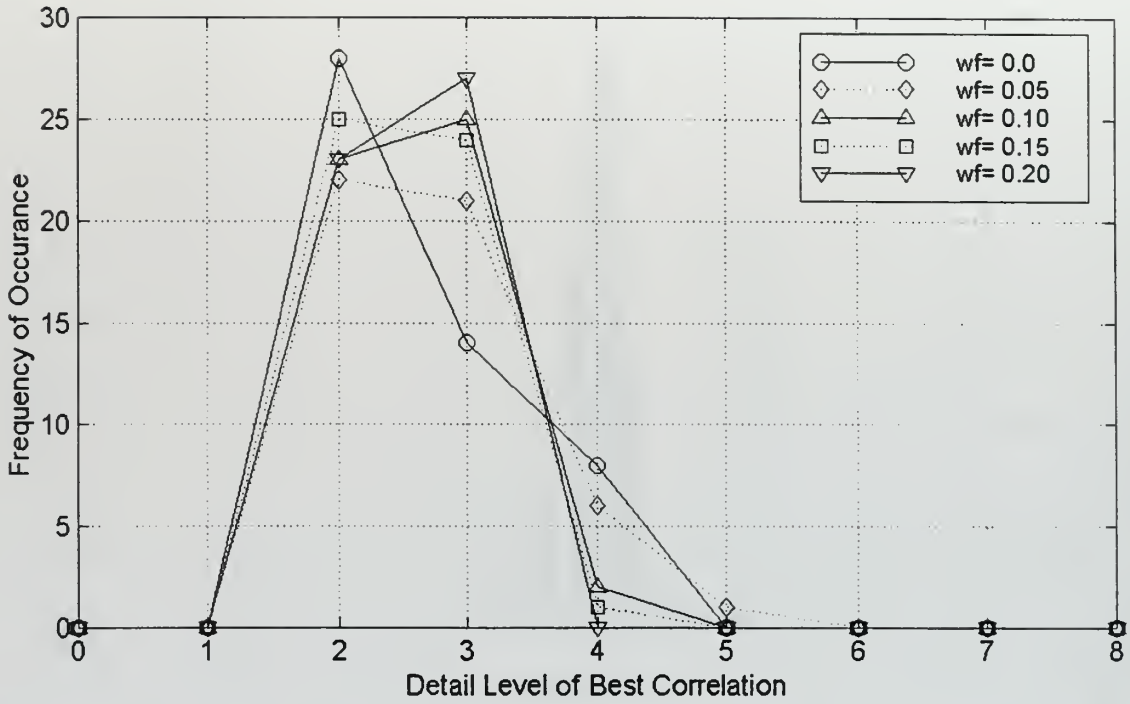

Figure B.7. Histogram of Detail Level of Best Crosscorrelation, Large Steel Rod Signals 01 through 50, Sensors #1 and #2 ,min. variance, weighting factor = [0.0, 0.05, 0.10, 0.15, 0.20]

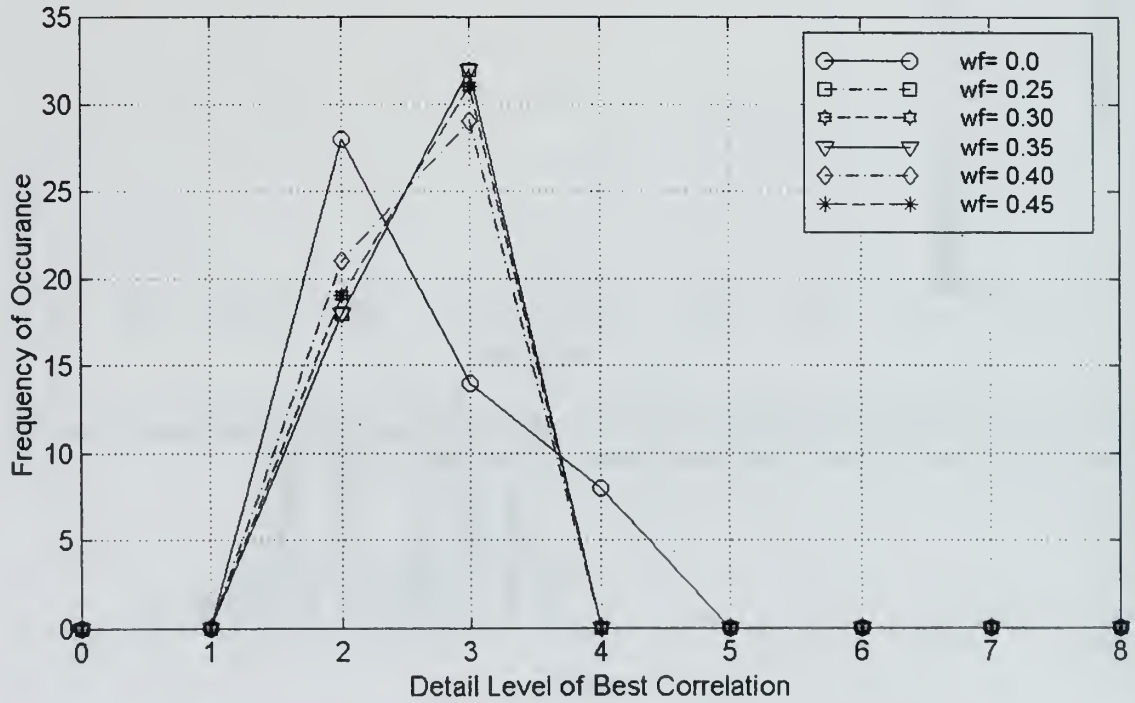

Figure B.8. Histogram of Detail Level of Best Crosscorrelation Large Steel Rod Signals 01 through 50, Sensors #1 and #2, min. variance, weighting factor = [0.0, 0.25, 0.30, 0.35, 0.40, 0.45]

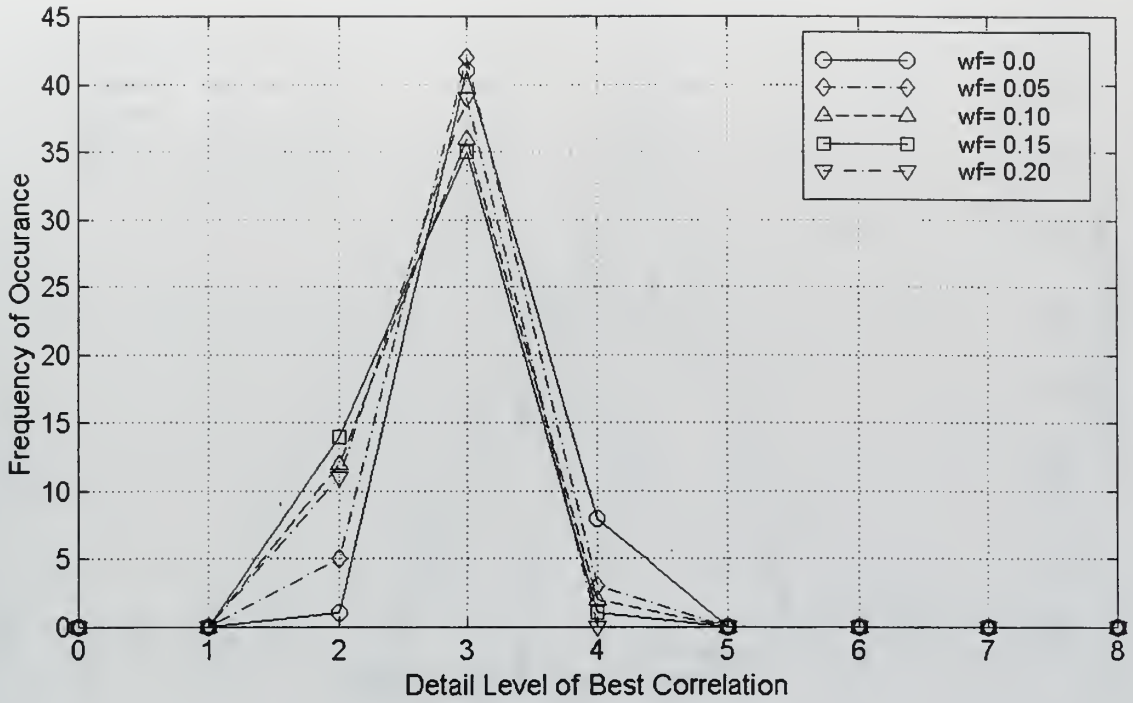

Figure B.9. Histogram of Detail Level of Best Crosscorrelation Large Steel Rod Signals 01 through 50, Sensors #1 and #3, min. variance, weighting factor = [0.0, 0.05, 0.10, 0.15, 0.20]

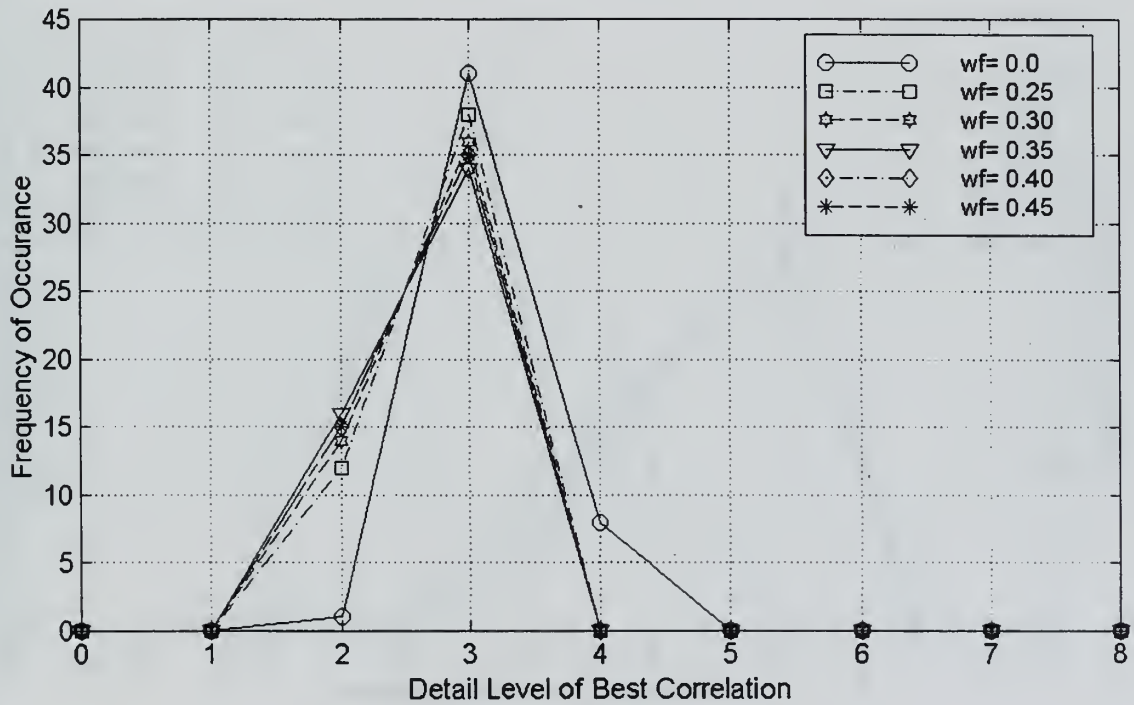

Figure B.10. Histogram of Detail Level of Best Crosscorrelation Large Steel Rod Signals 01 through 50, Sensors #1 and #3, min. variance, weighting factor = [0.0, 0.25, 0.30, 0.35, 0.40, 0.45]

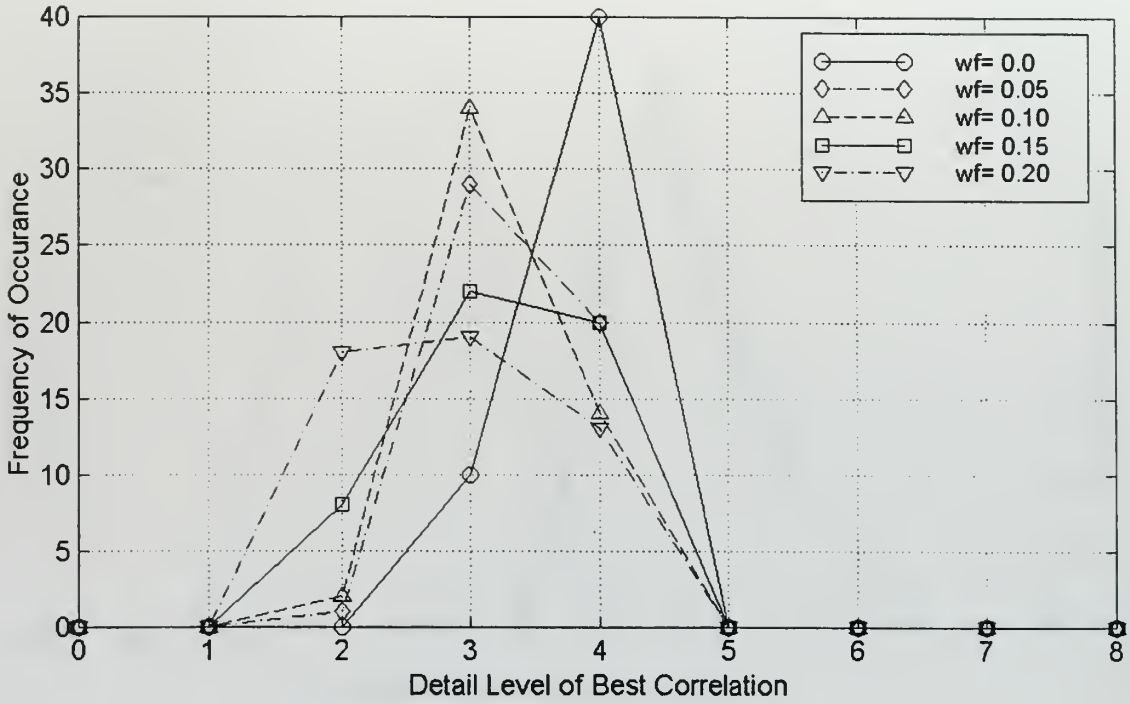

Figure B.11. Histogram of Detail Level of Best Crosscorrelation Large Steel Rod Signals 01 through 50, Sensors #1 and #4 ,min. variance, weighting factor = [0.0, 0.05, 0.10, 0.15, 0.20]

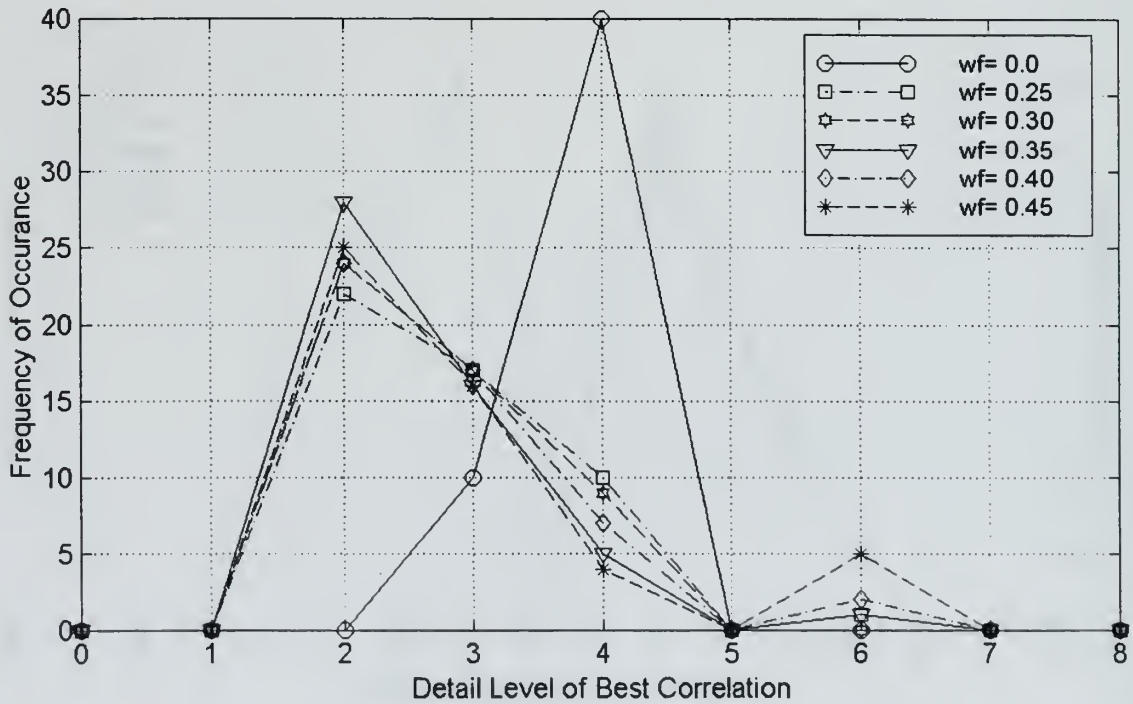

Figure B.12. Histogram of Detail Level of Best Crosscorrelation Large Steel Rod Signals 01 through 50, Sensors #1 and #4, min. variance, weighting factor = [0.0, 0.25, 0.30, 0.35, 0.40, 0.45]

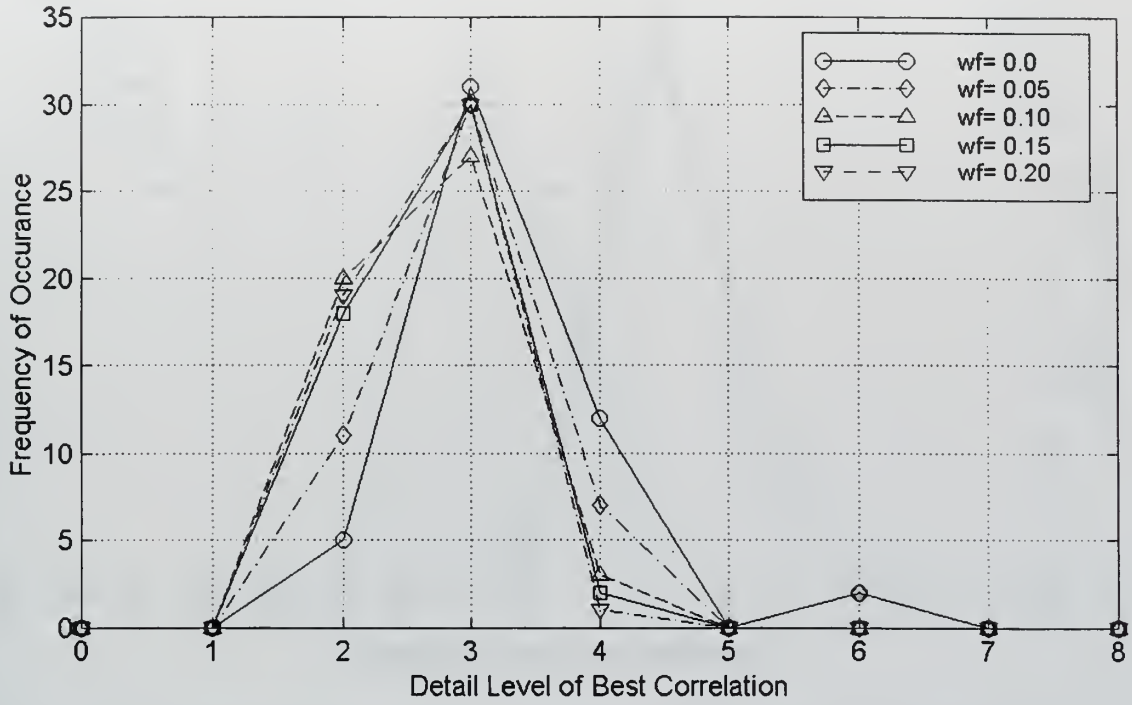

Figure B.13. Histogram of Detail Level of Best Crosscorrelation Large Steel Rod Signals 01 through 50, Sensors #1 and #2, min.(variance/max.), weighting factor = [0.0, 0.05, 0.10, 0.15, 0.20]

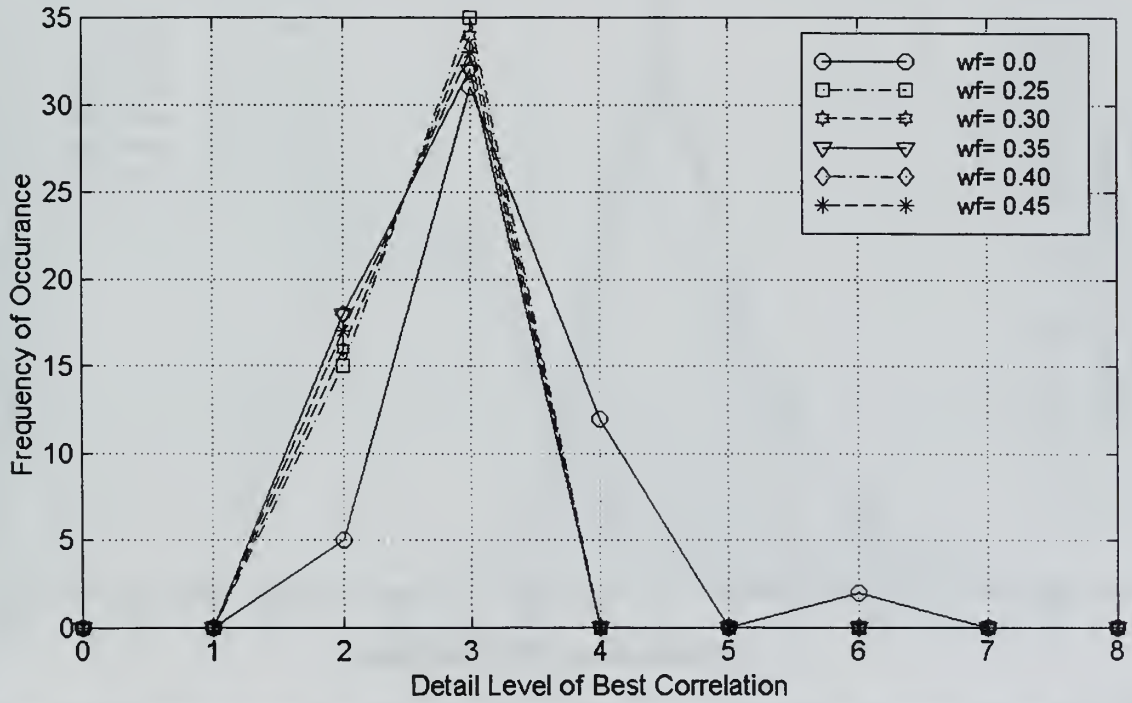

Figure B.14. Histogram of Detail Level of Best Crosscorrelation Large Steel Rod Signals 01 through 50, Sensors #1 and #2, min.(variance/max.), weighting factor = [0.0, 0.25, 0.30, 0.35, 0.40, 0.45]

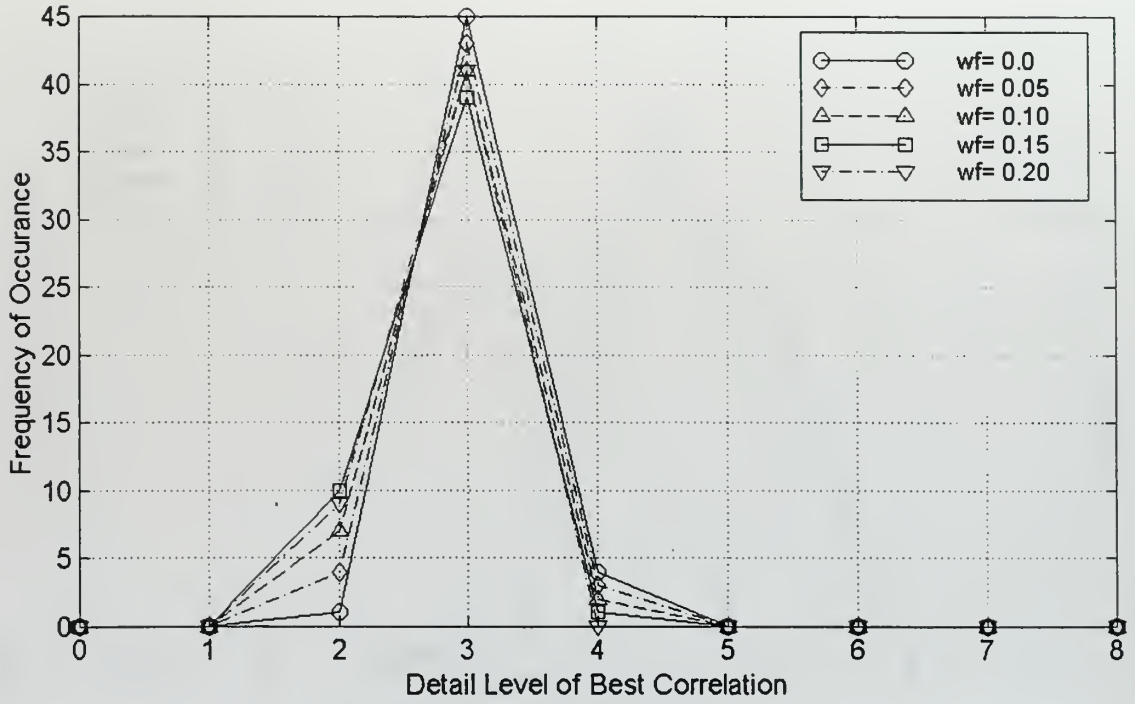

Figure B.15. Histogram of Detail Level of Best Crosscorrelation Large Steel Rod Signals 01 through 50, Sensors #1 and #3, min.(variance/max.), weighting factor = [0.0, 0.05, 0.10, 0.15, 0.20]

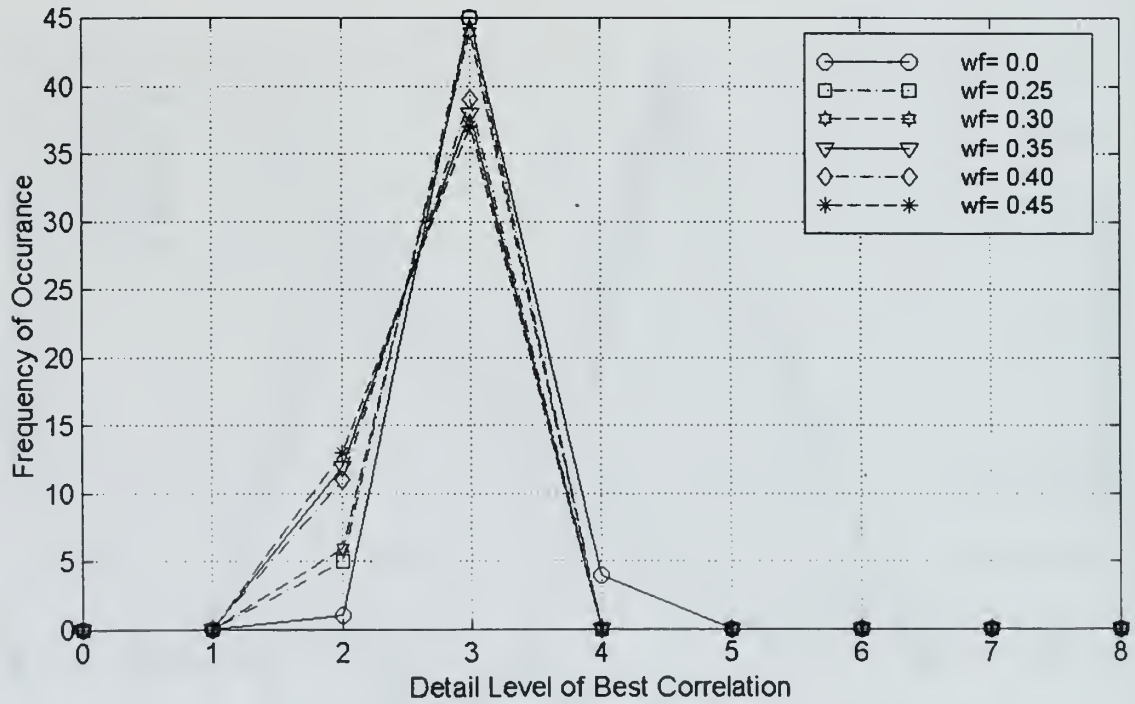

Figure B.16. Histogram of Detail Level of Best Crosscorrelation Large Steel Rod Signals 01 through 50, Sensors #1 and #3, min.(variance/max.), weighting factor = [0.0, 0.25, 0.30, 0.35, 0.40, 0.45]

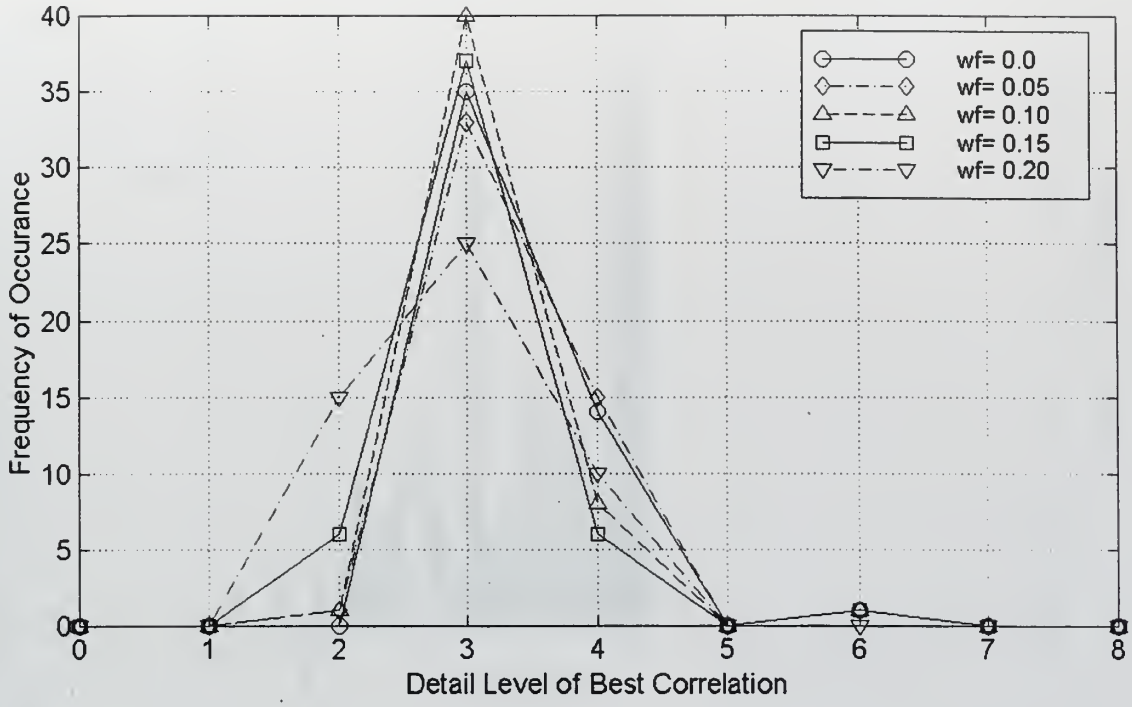

Figure B.17. Histogram of Detail Level of Best Crosscorrelation Large Steel Rod Signals 01 through 50, Sensors #1 and #4, min.(variance/max.), weighting factor = [0.0, 0.05, 0.10, 0.15, 0.20]

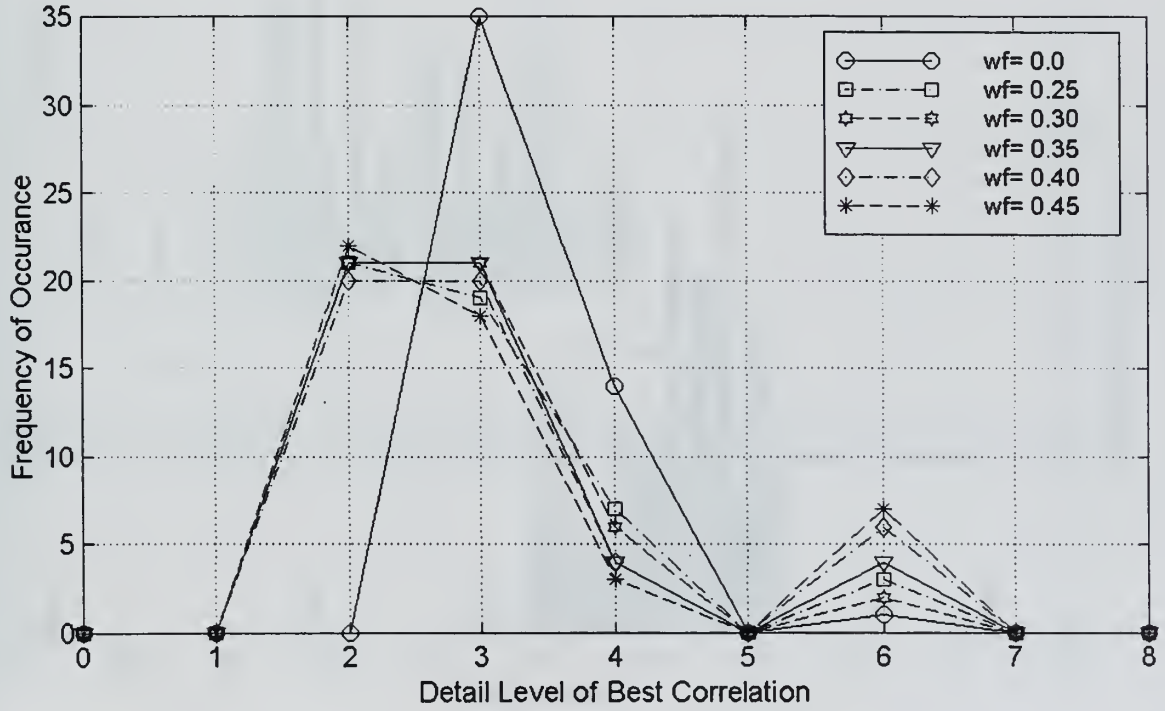

Figure B.18. Histogram of Detail Level of Best Crosscorrelation Large Steel Rod Signals 01 through 50, Sensors #1 and #4, min.(variance/max.), weighting factor = [0.0, 0.25, 0.30, 0.35, 0.40, 0.45]

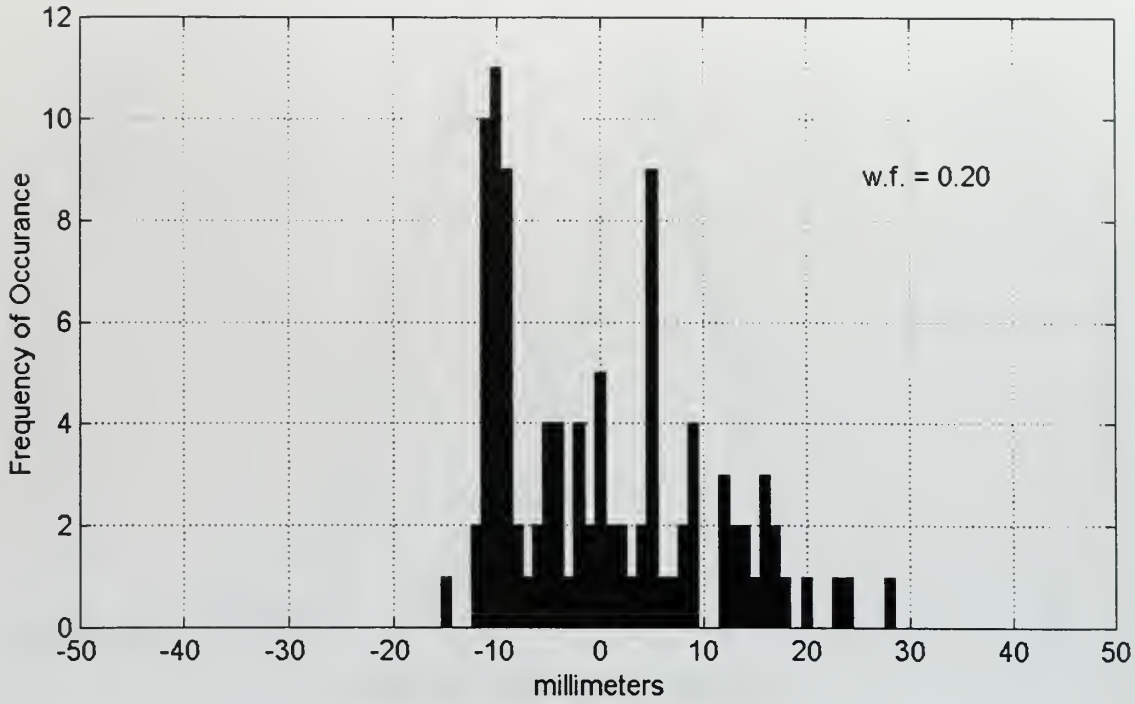

Figure B.19. Wavelet Detail Crosscorrelation Location Histogram for Large Steel Rod Sensors #1 and #2, Mean = -0.002 mm, Std Dev. = 10.115 mm, Transducer Diameter = 9.525 mm.

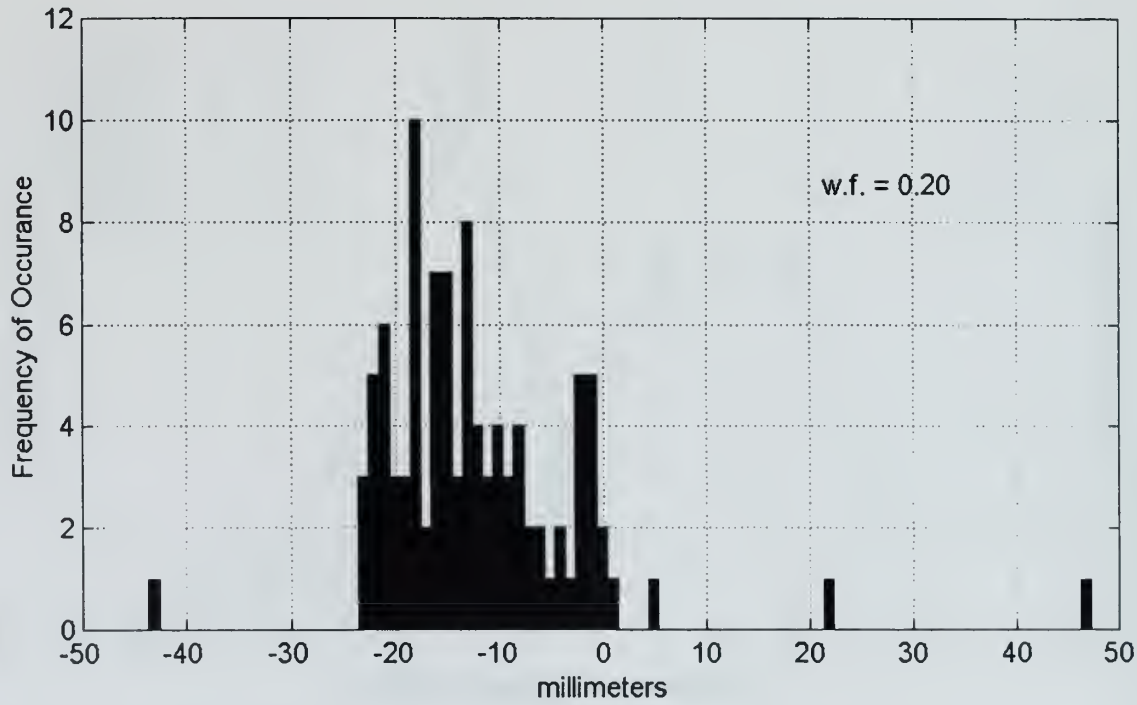

Figure B.20. Wavelet Detail Crosscorrelation Location Histogram for Large Steel Rod Sensors #1 and #3, Mean = -12.154 mm, Std Dev. = 10.206 mm, Transducer Diameter = 9.525 mm.

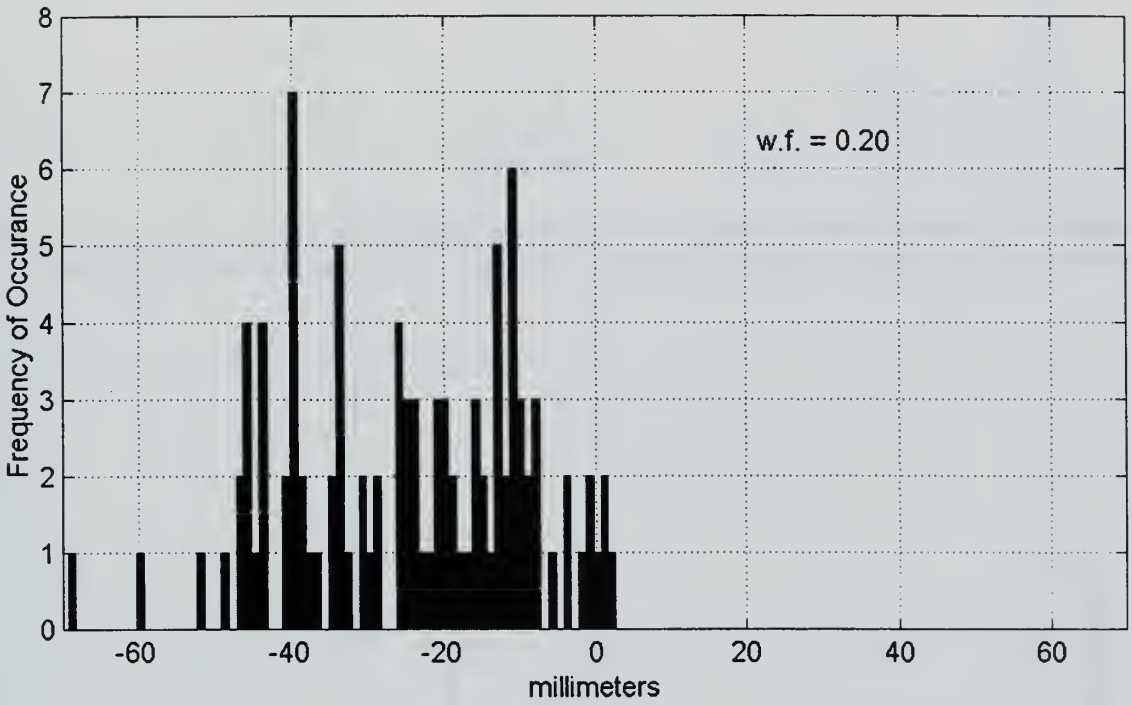

Figure B.21. Wavelet Detail Crosscorrelation Location Histogram for Large Steel Rod Sensors #1 and #4, Mean = -24.762 mm, Std Dev. = 15.405 mm, Transducer Diameter = 9.525 mm.

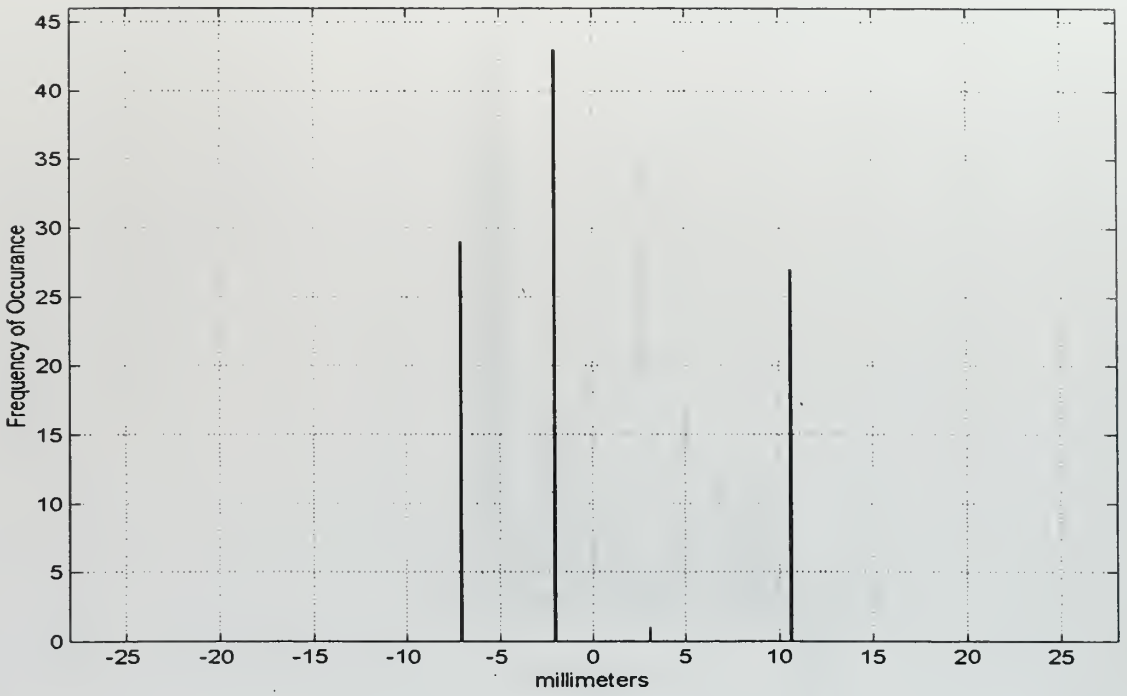

Figure B.22. Wavelet Detail Crosscorrelation Location Histogram for Large Steel Rod, Detail 3 max, Sensors #1 and #2, Mean = 0.006 mm, Std Dev. = 6.849 mm, Transducer Diameter = 9.525 mm.

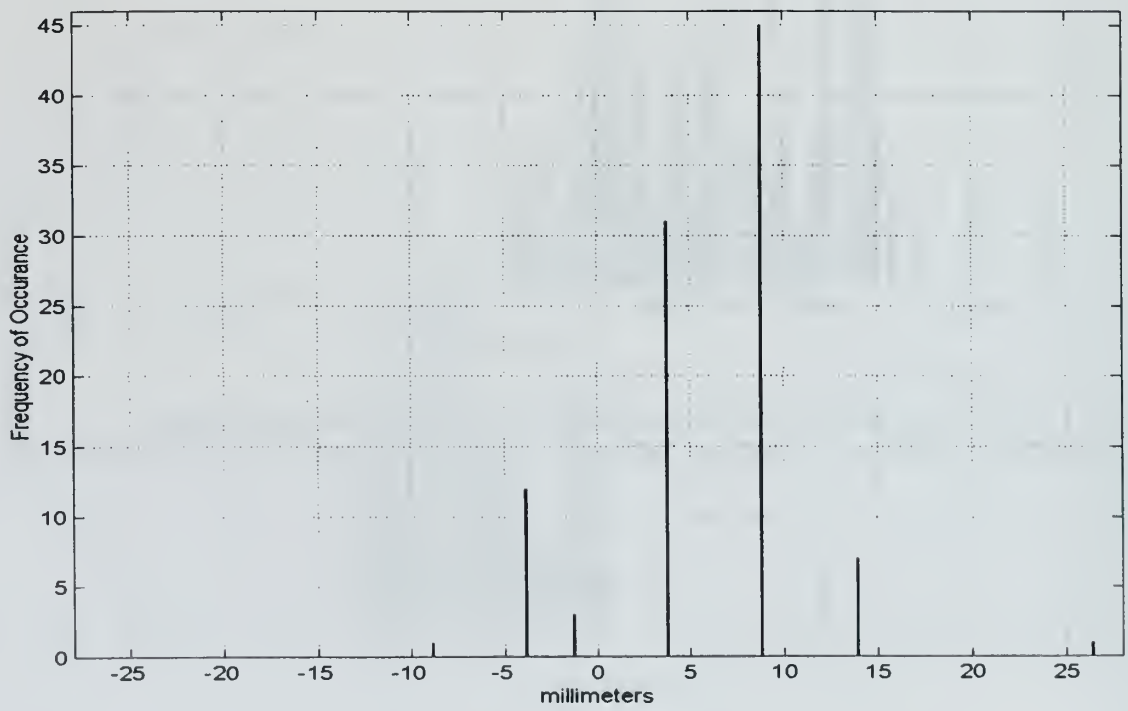

Figure B.23. Wavelet Detail Crosscorrelation Location Histogram for Large Steel Rod, Detail 3 max, Sensors #1 and #3, Mean = 5.780 mm, Std Dev. = 5.392 mm, Transducer Diameter = 9.525 mm.

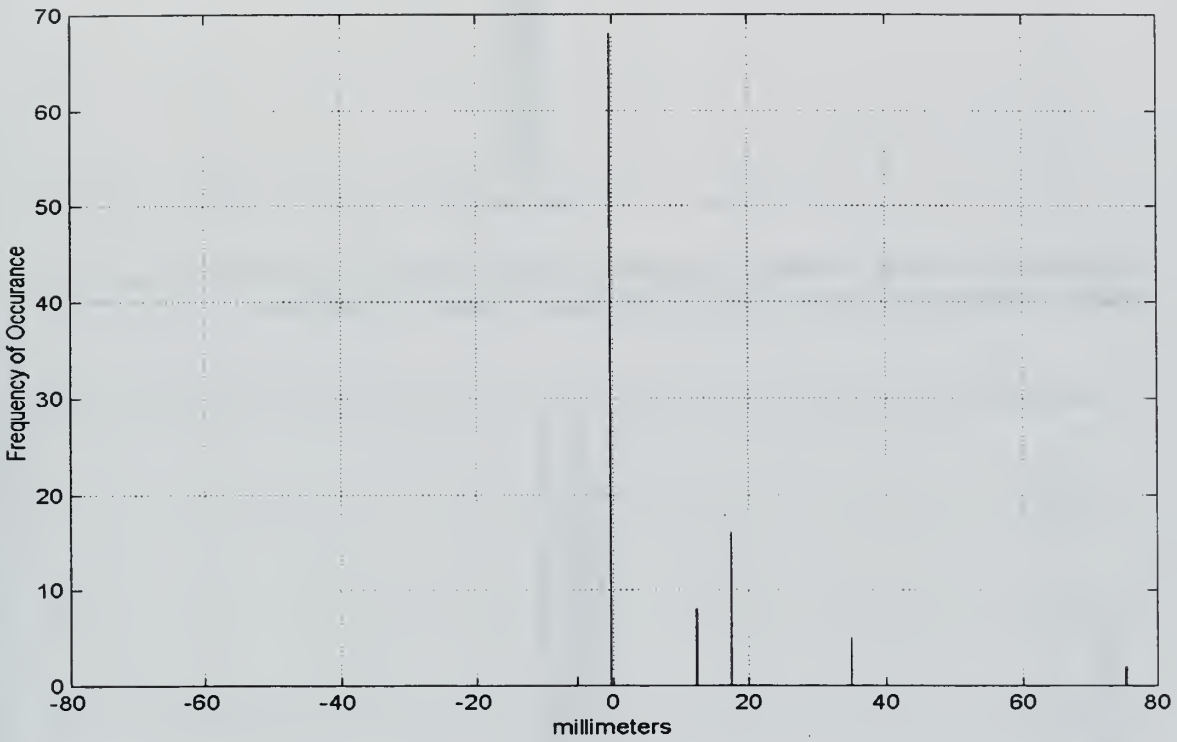

Figure B.24. Wavelet Detail Crosscorrelation Location Histogram for Large Steel Rod Detail 3 max, Sensors #1 and #4, Mean = 6.850 mm, Std Dev. = 13.823 mm, Transducer Diameter = 9.525 mm.

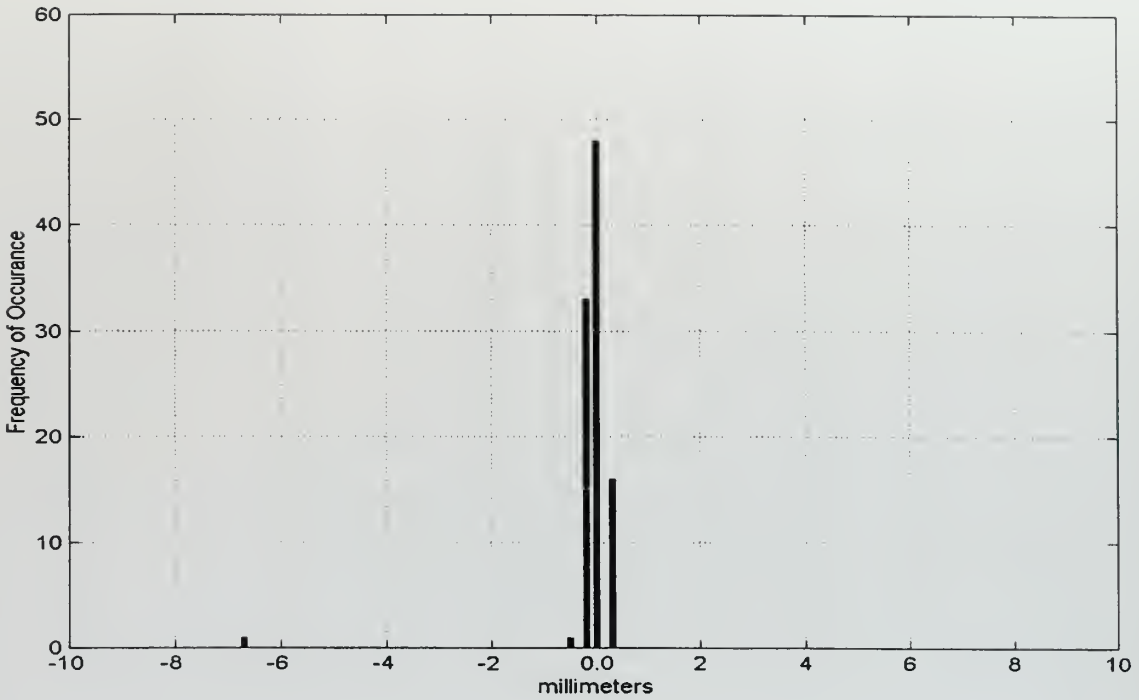

Figure B.25. Threshold Crossing Location Histogram for Small Steel Rod Sensors #1 and 2 Mean = -0.091 mm, Std Dev. = 0.693 mm, Transducer Diameter = 5.080 mm.

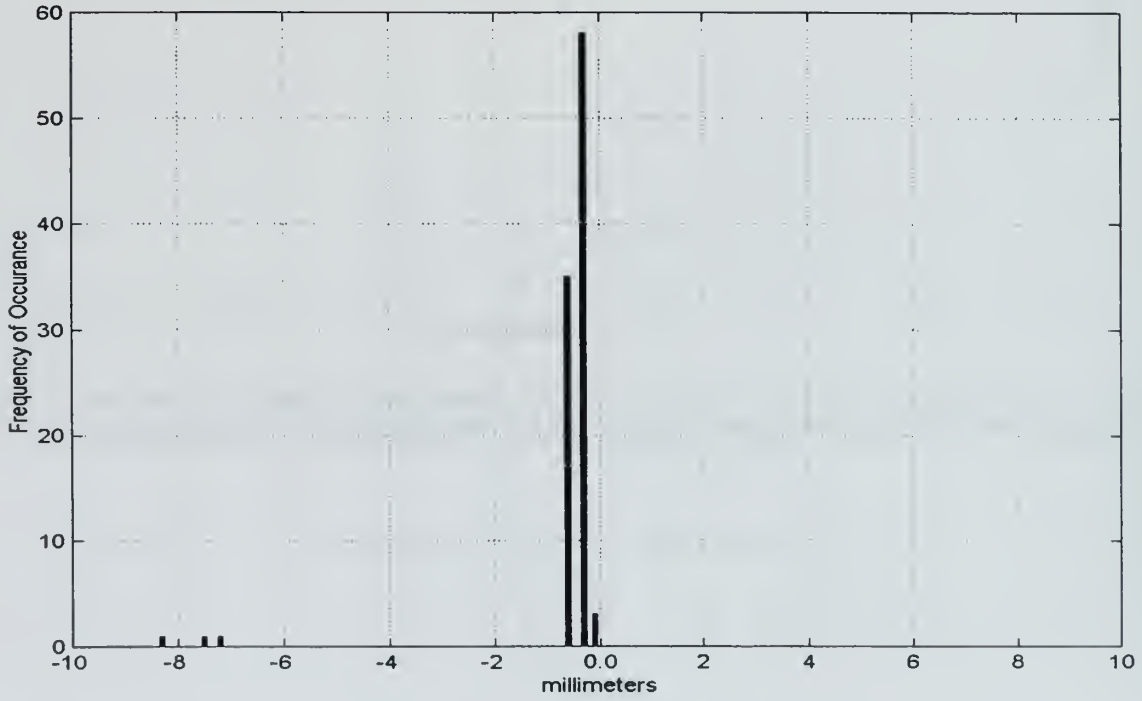

Figure B.26. Threshold Crossing Location Histogram for Small Steel Rod Sensors #1 and #3 Mean = -0.623 mm, Std Dev. = 1.263 mm, Transducer Diameter = 5.080 mm.

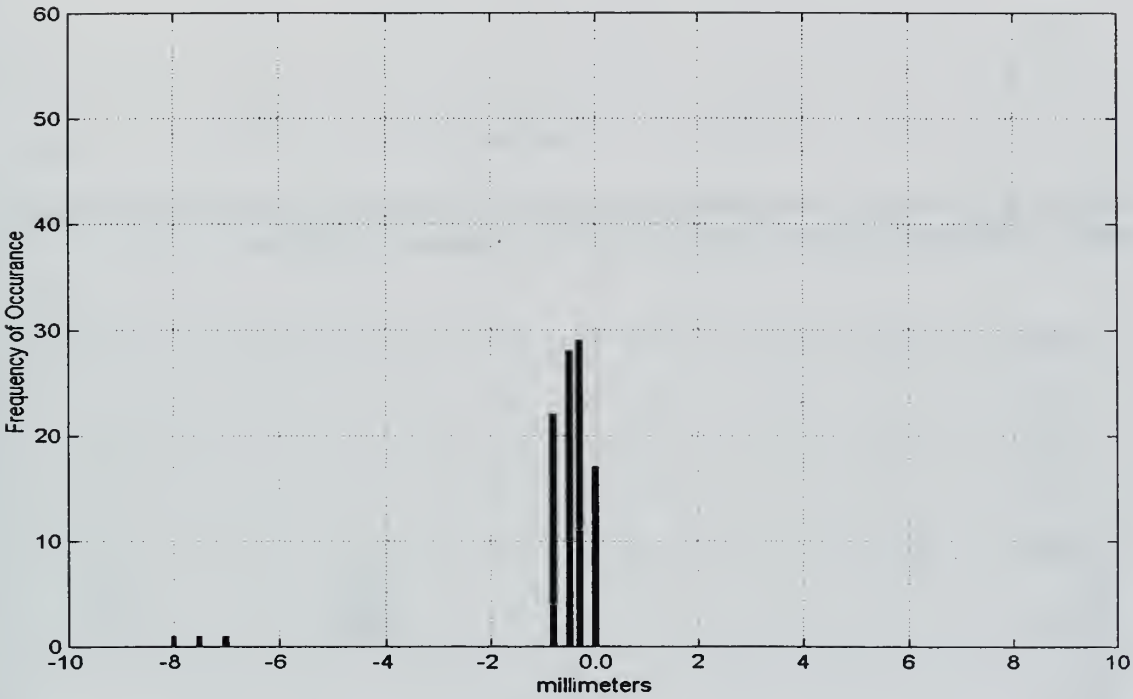

Figure B.27. Threshold Crossing Location Histogram for Small Steel Rod Sensors #1 and #4 Mean = -0.634 mm, Std Dev. = 1.250 mm, Transducer Diameter = 5.080 mm.

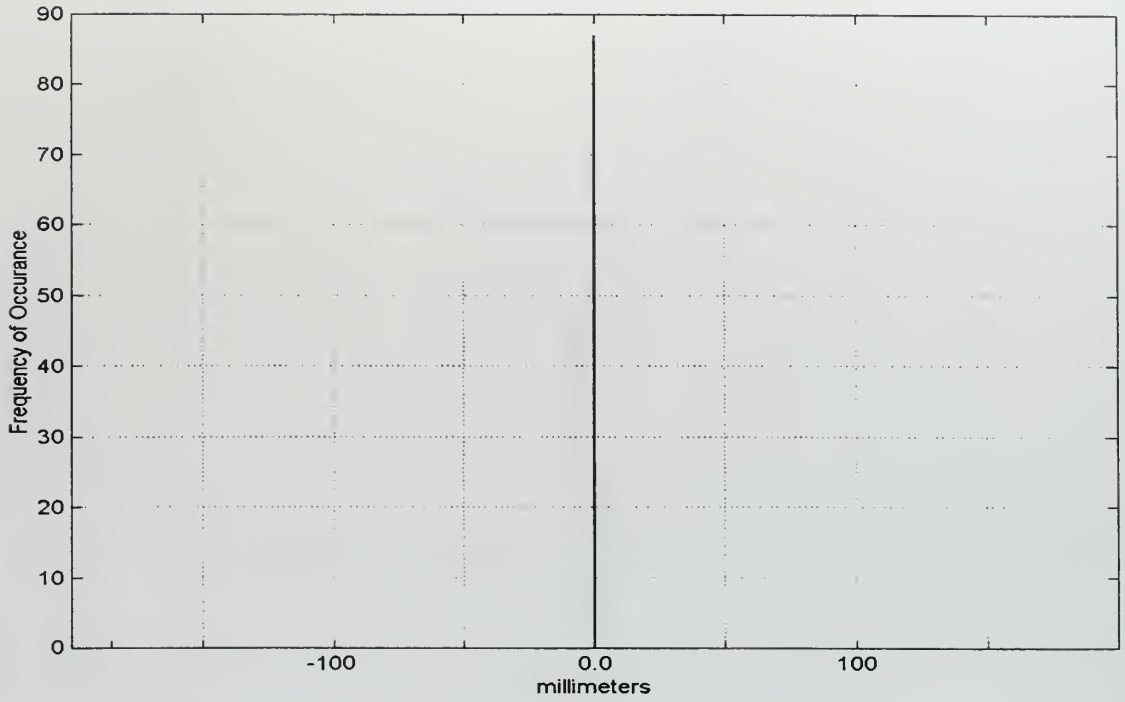

Figure B.28. Gaussian Crosscorrelation Location Histogram for Small Steel Rod Sensors #1 and #2 Mean = -1.869 mm, Std Dev. = 18.573 mm, Transducer Diameter = 5.080 mm.

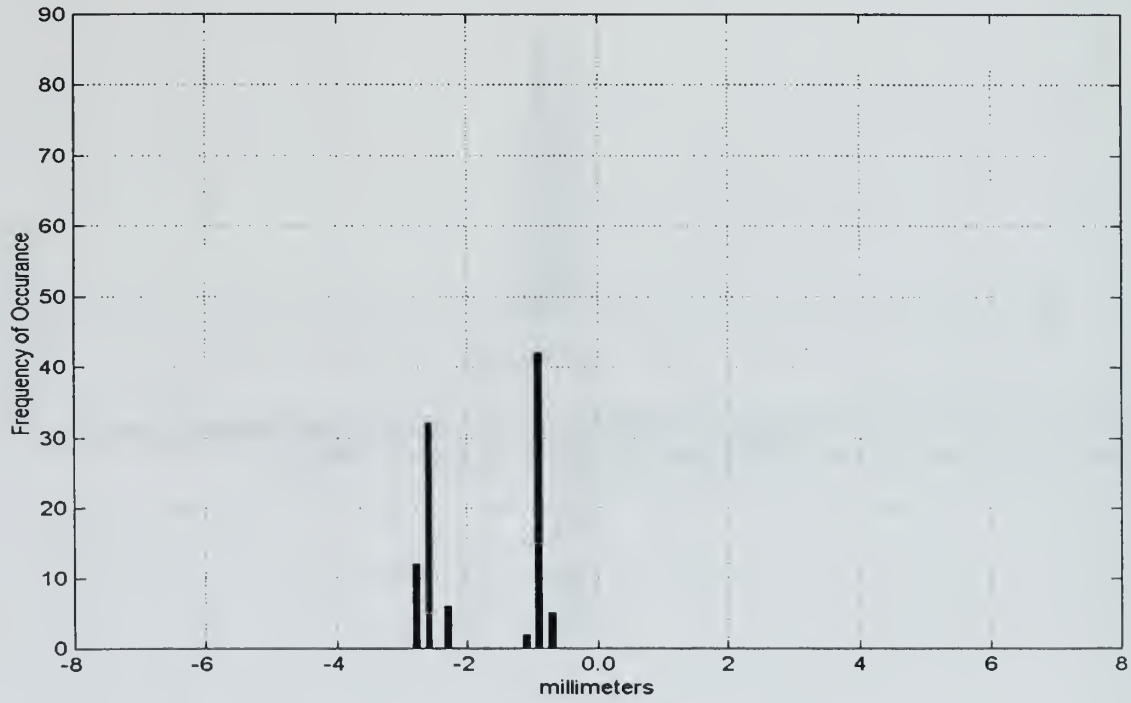

Figure B.29. Gaussian Crosscorrelation Location Histogram for Small Steel Rod Sensors #1 and #3 Mean = -1.759 mm, Std Dev. = 0.874 mm, Transducer Diameter =5.080 mm.

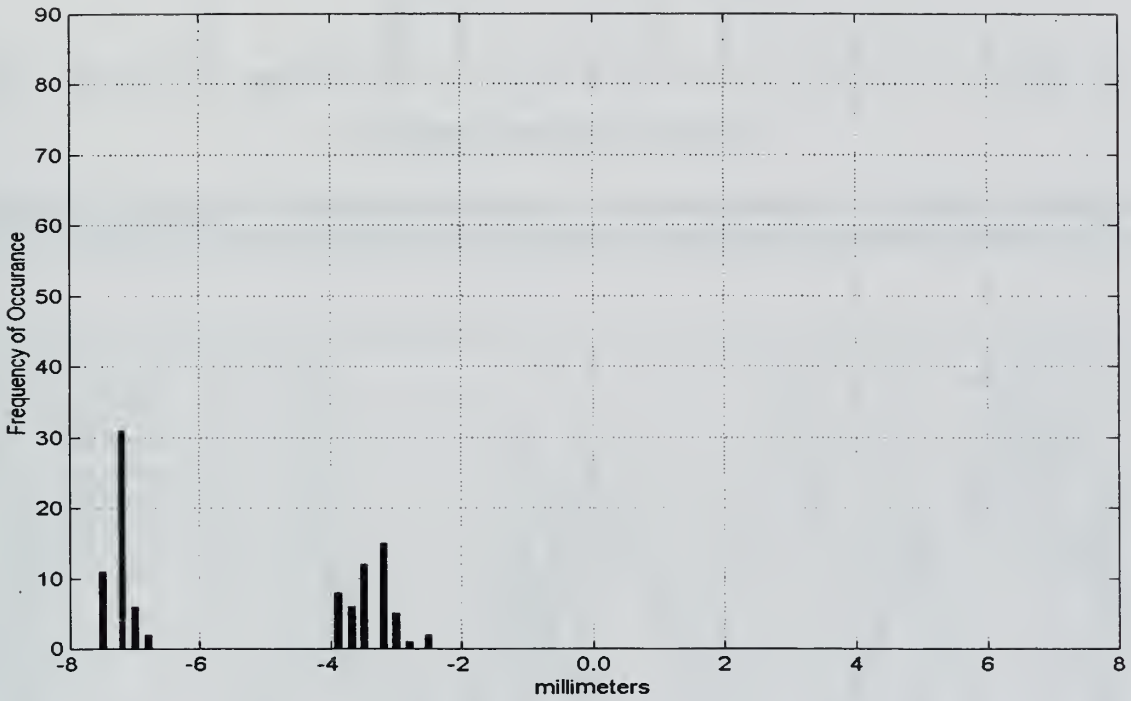

Figure B.30. Gaussian Crosscorrelation Location Histogram for Small Steel Rod Sensors #1 and #4 Mean =-5.328 mm, Std Dev. = 1.947 mm, Transducer Diameter = 5.080 mm.

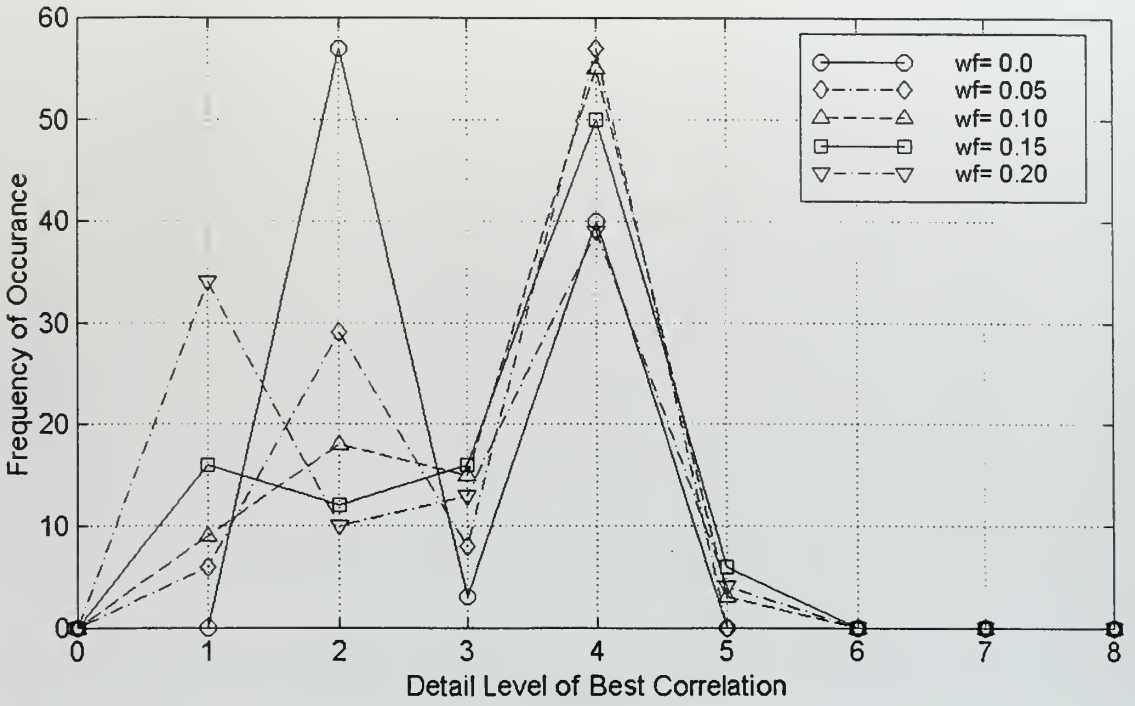

Figure B.31. Histogram of Detail Level of Best Crosscorrelation Small Steel Rod Signals 01 through 100, Sensors #1 and #2, min.(variance/max.), weighting factor = [0.0, 0.05, 0.10, 0.15, 0.20]

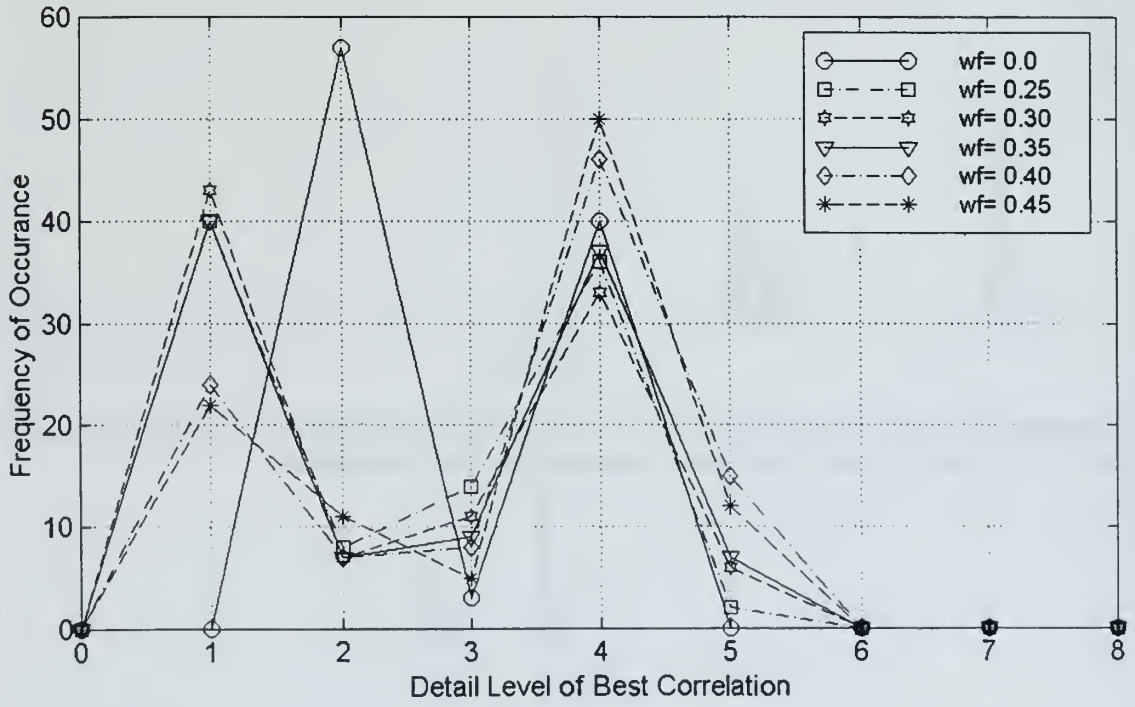

Figure B.32. Histogram of Detail Level of Best Crosscorrelation Small Steel Rod Signals 01 through 100, Sensors #1 and #2, min.(variance/max.), weighting factor = [0.0, 0.25, 0.30, 0.35, 0.40, 0.45]

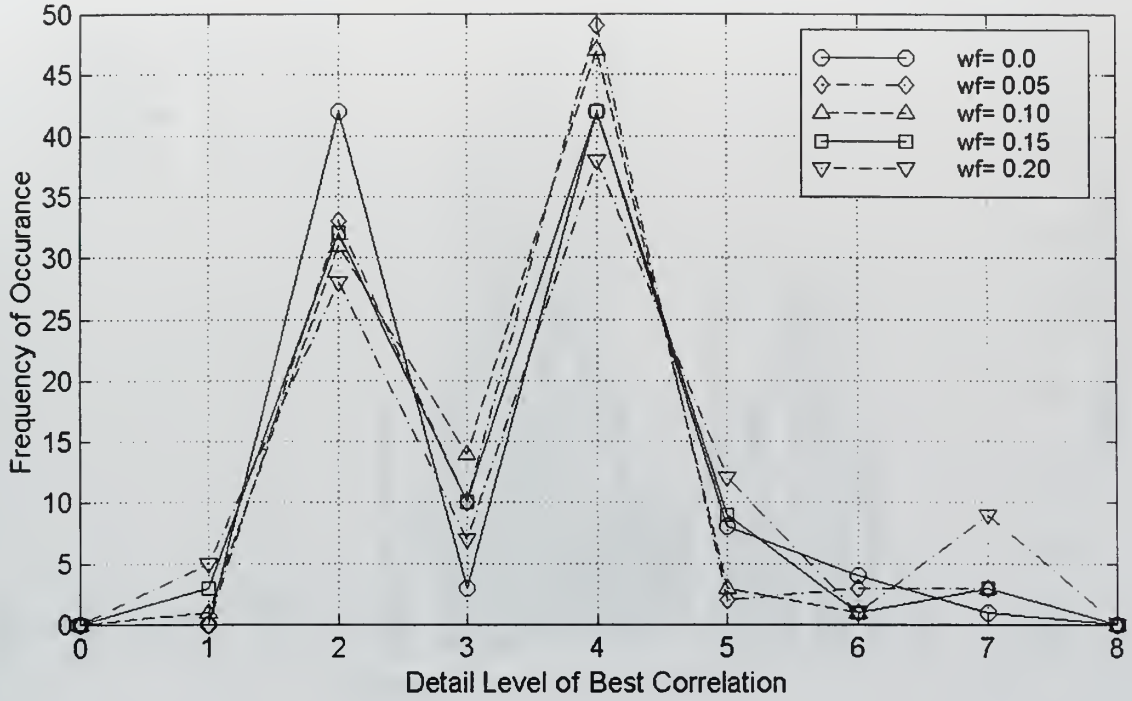

Figure B.33. Histogram of Detail Level of Best Crosscorrelation Small Steel Rod Signals 01through 100, Sensors #1 and #3, min.(variance/max.), weighting factor = [0.0, 0.05, 0.10, 0.15, 0.20]

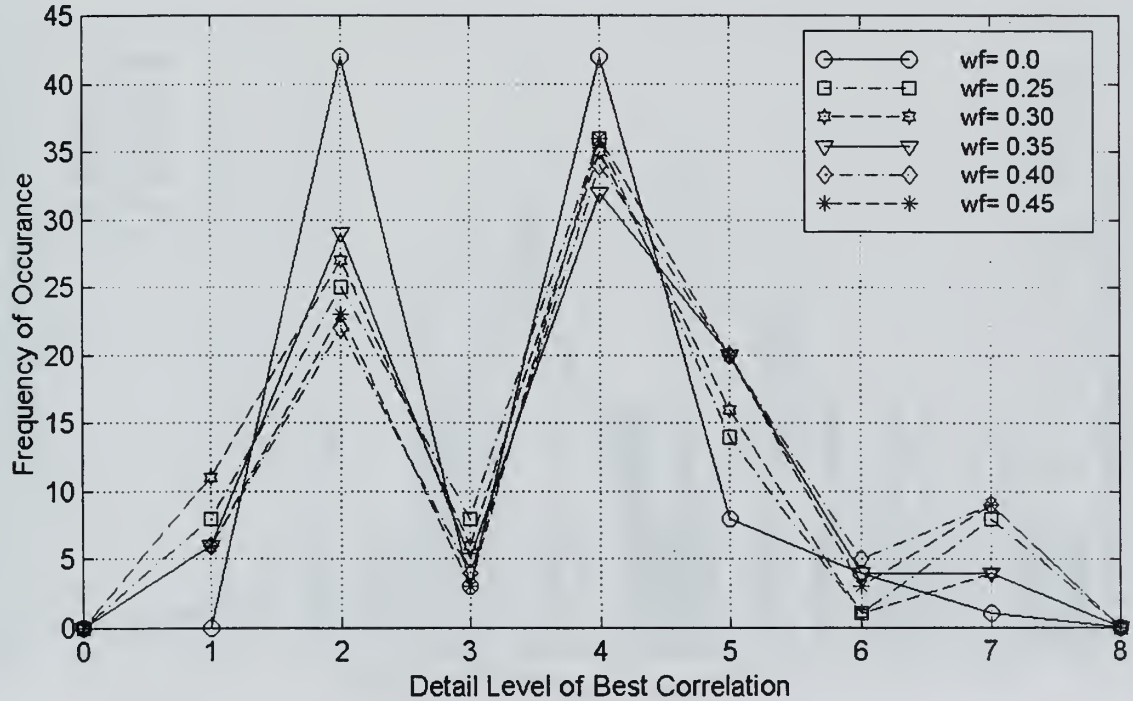

Figure B.34. Histogram of Detail Level of Best Crosscorrelation Small Steel Rod Signals 01 through 100, Sensors #1 and #3, min.(variance/max.), weighting factor = [0.0, 0.25, 0.30, 0.35, 0.40, 0.45]

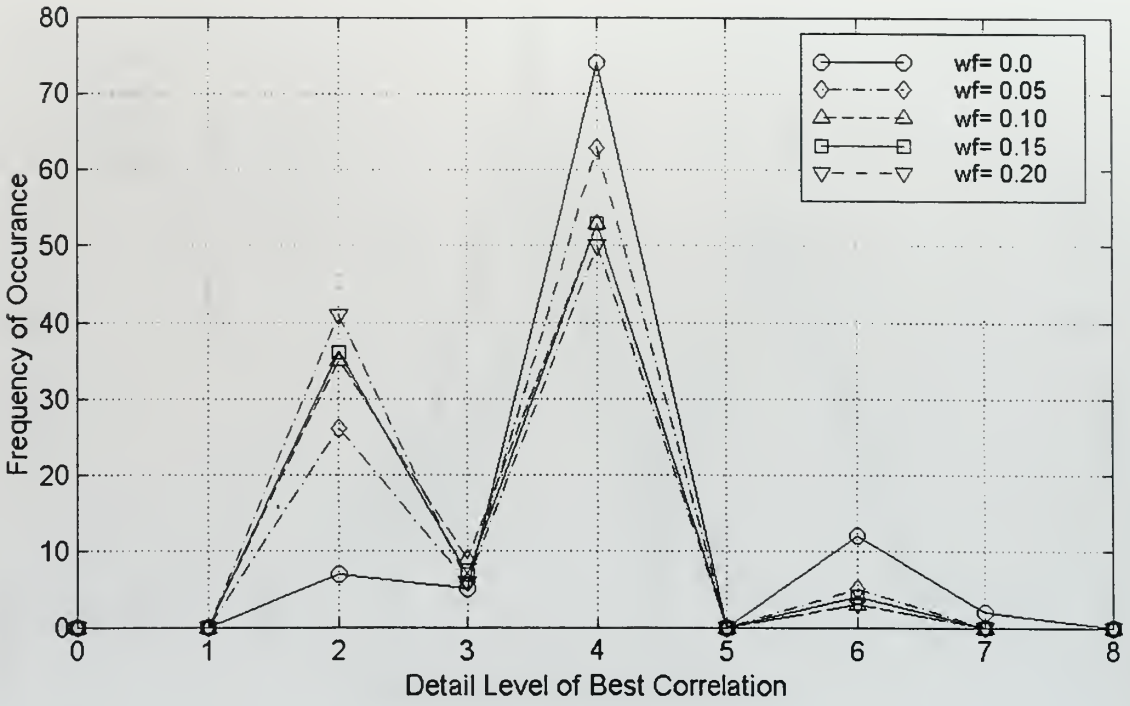

Figure B.35. Histogram of Detail Level of Best Crosscorrelation Small Steel Rod Signals 01through 100, Sensors #1 and #4, min.(variance/max.), weighting factor = [0.0, 0.05, 0.10, 0.15, 0.20]

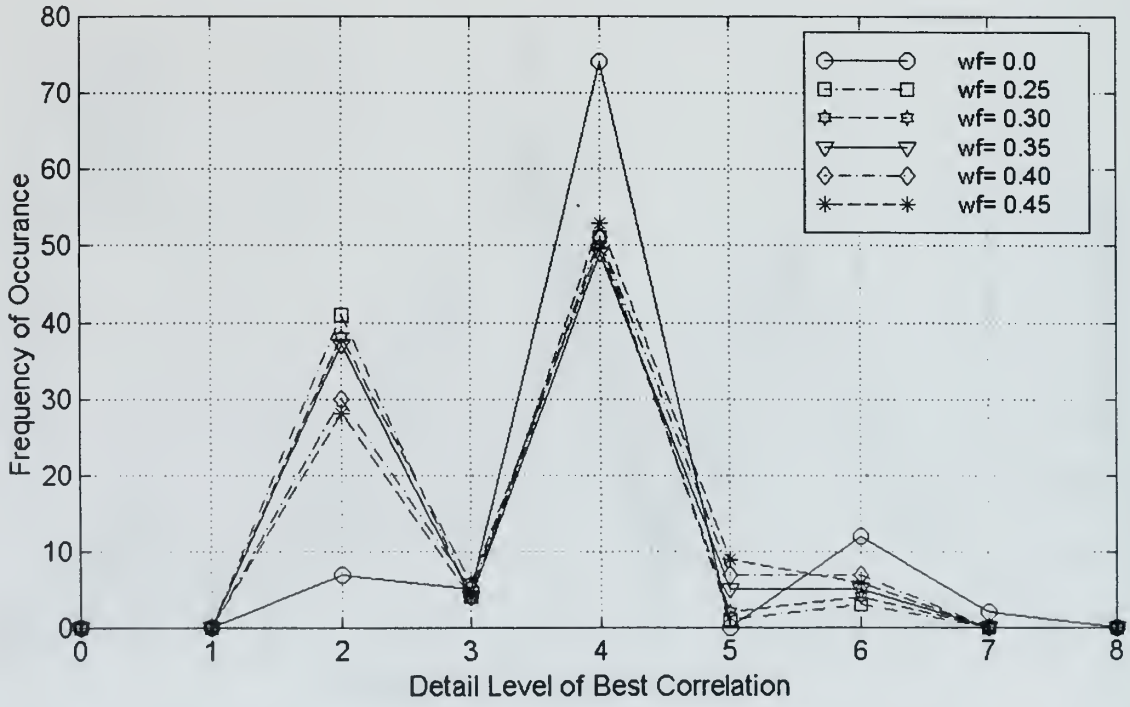

Figure B.36. Histogram of Detail Level of Best Crosscorrelation Small Steel Rod Signals 01 through 100, Sensors #1 and #4, min.(variance/max.), weighting factor = [0.0, 0.25, 0.30, 0.35, 0.40, 0.45]

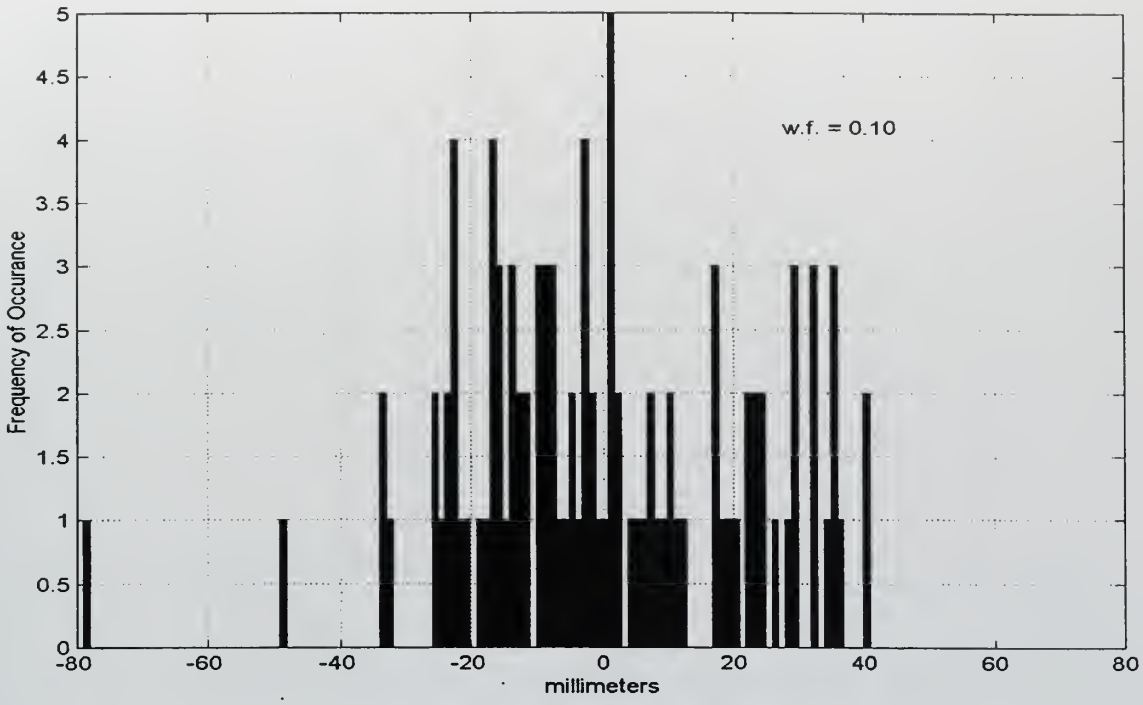

Figure B.37. Wavelet Detail Crosscorrelation Location Histogram for Small Steel Rod Sensors #1 and #2, Mean = -0.008 mm, Std Dev. = 21.470 mm, Transducer Diameter = 5.080 mm.

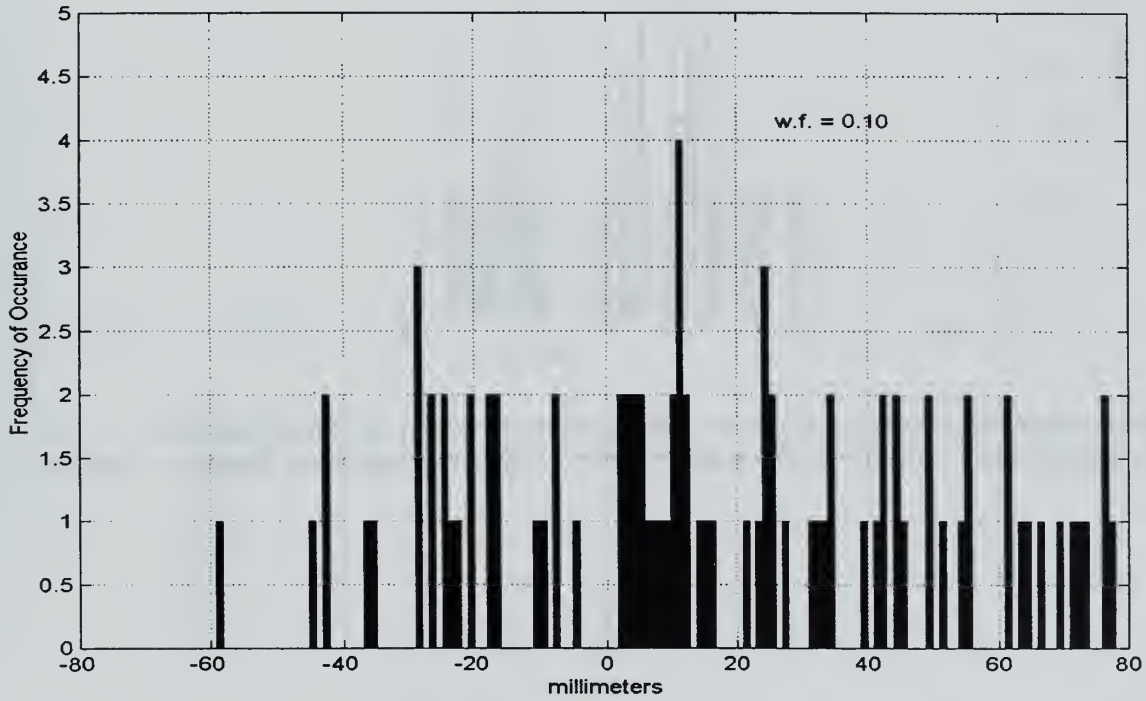

Figure B.38. Wavelet Detail Crosscorrelation Location Histogram for Small Steel Rod Sensors #1 and #3, Mean = 23.281 mm, Std Dev. = 43.284 mm, Transducer Diameter = 5.080 mm.

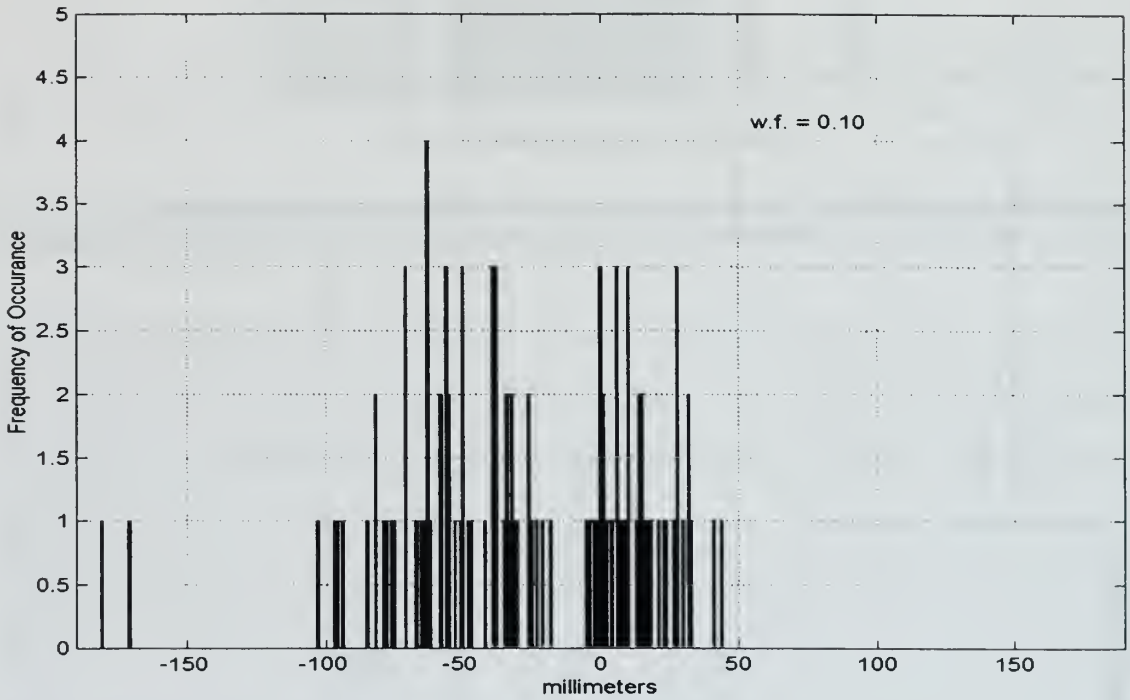

Figure B.39. Wavelet Detail Crosscorrelation Location Histogram for Small Steel Rod Sensors #1 and #4, Mean = -28.541 mm, Std Dev. = 43.473 mm, Transducer Diameter = 5.080 mm.

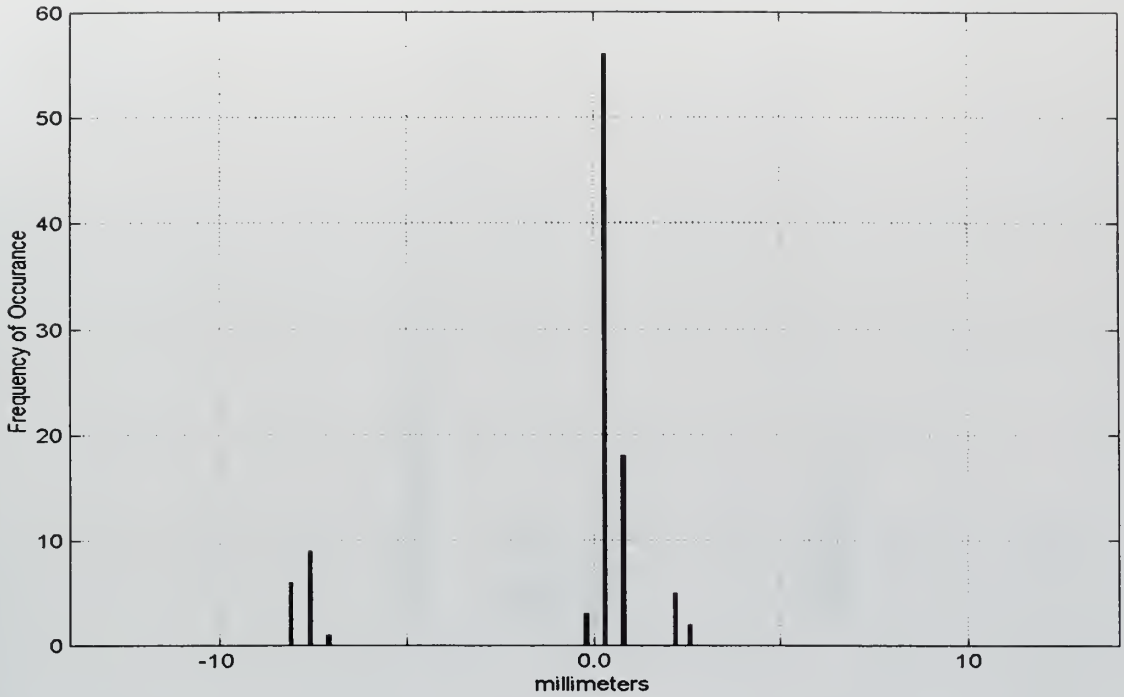

Figure B.40. Threshold Crossing Location Histogram for Carbon Fiber Rod Sensors #1 and #2 Mean = -0.773 mm, Std Dev. = 3.112 mm, Transducer Diameter = 5.080 mm.

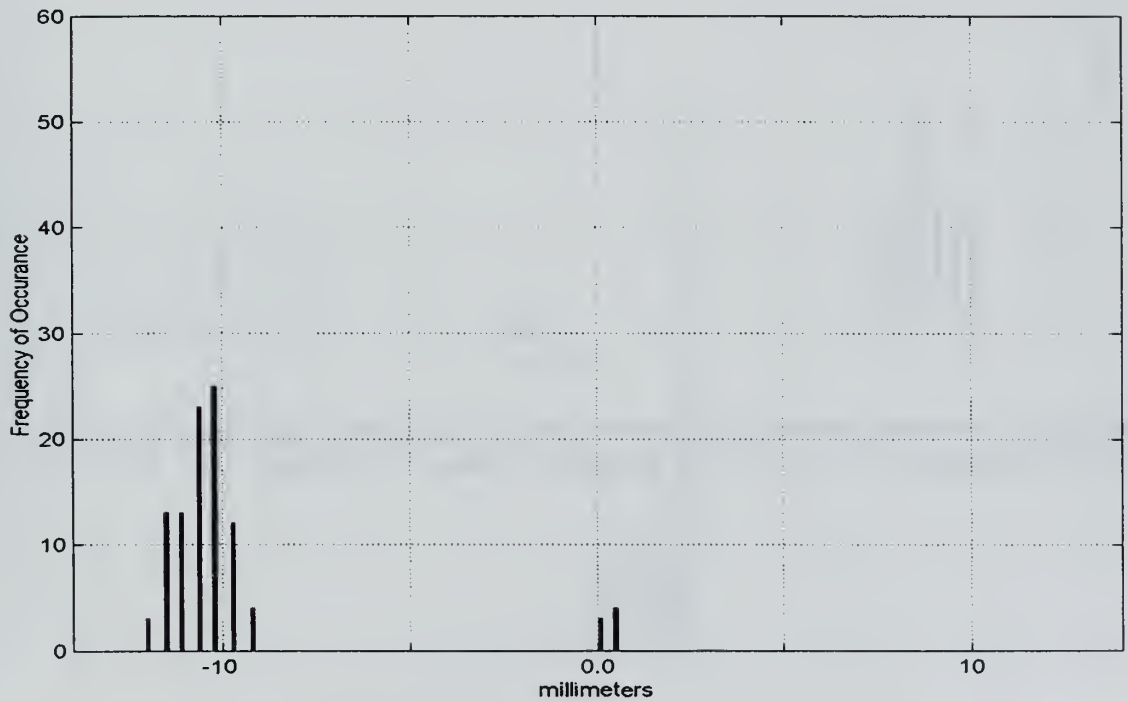

Figure B.41. Threshold Crossing Location Histogram for Carbon Fiber Rod Sensors #1 and #3 Mean = -9.795 mm, Std Dev. = 2.865 mm, Transducer Diameter = 5.080 mm.

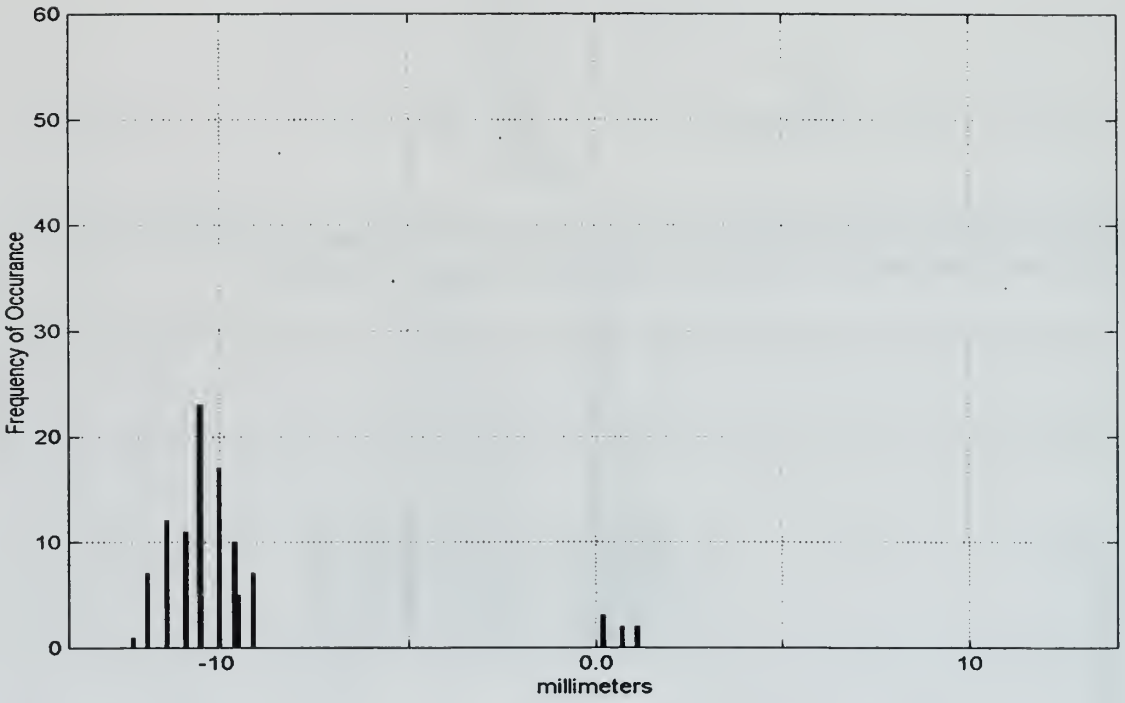

Figure B.42. Threshold Crossing Location Histogram for Carbon Fiber Rod Sensors #1 and #4 Mean = -9.668 mm, Std Dev. = 2.937 mm, Transducer Diameter = 5.080 mm.

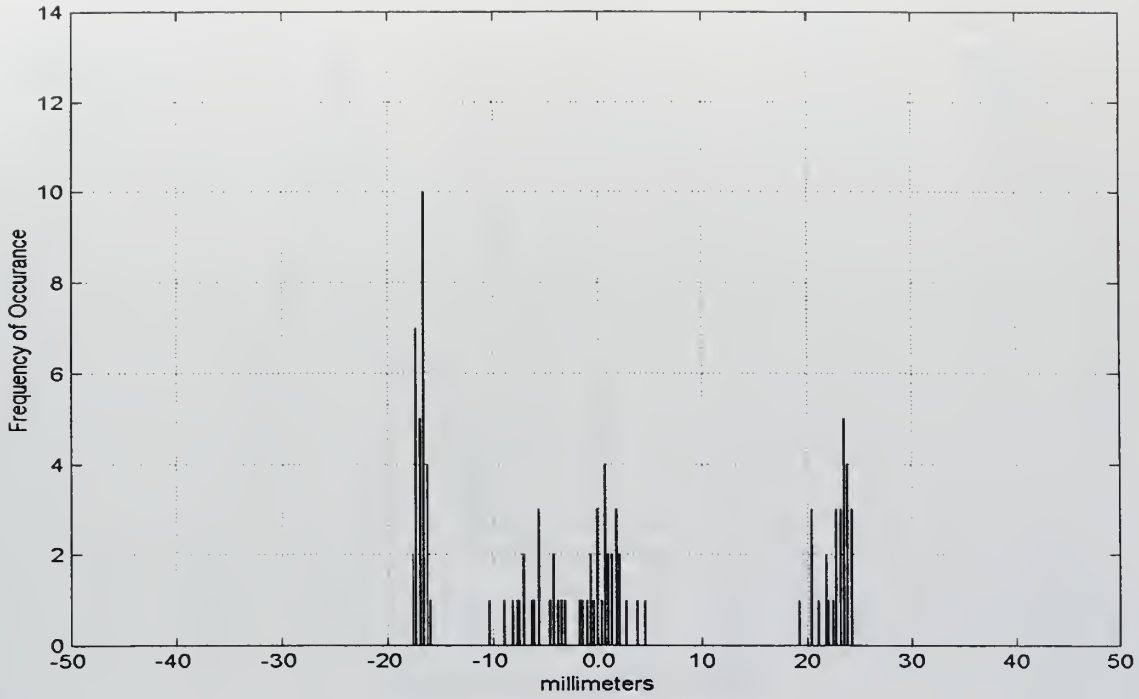

Figure B.43. Gaussian Crosscorrelation Location Histogram for Carbon Fiber Rod Sensors #1 and #2 Mean = 0.344 mm, Std Dev. = 15.212 mm, Transducer Diameter = 5.080 mm.

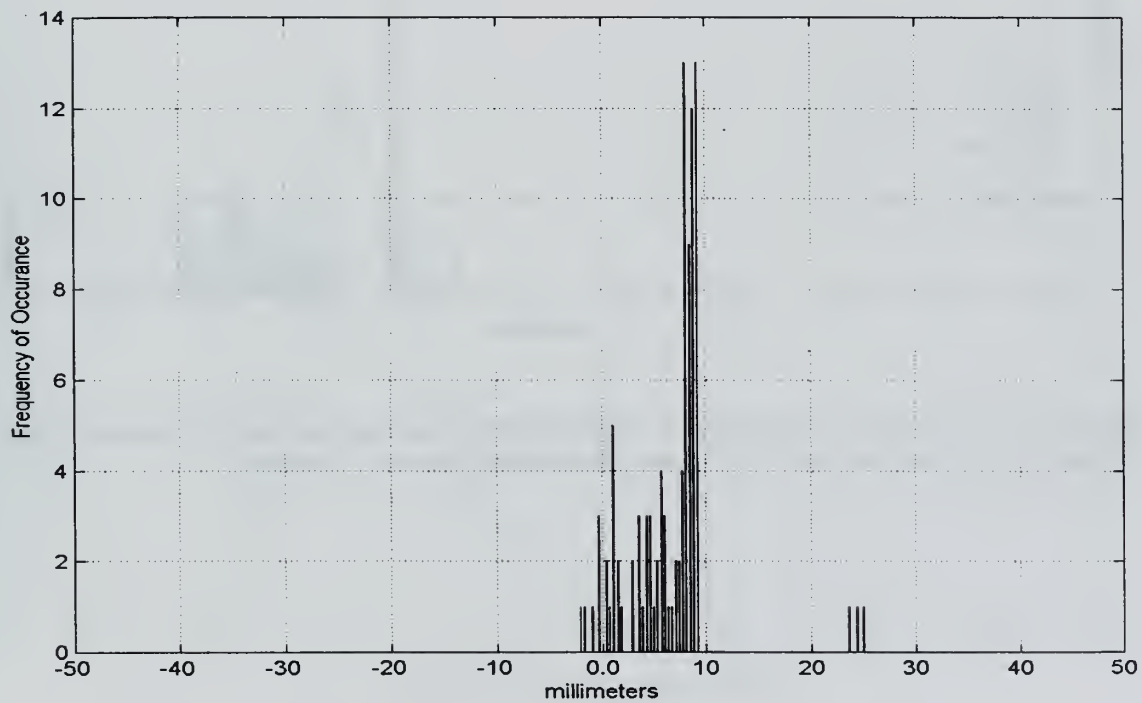

Figure B.44. Gaussian Crosscorrelation Location Histogram for Carbon Fiber Rod Sensors #1 and #3 Mean = 7.174 mm, Std Dev. = 6.514 mm, Transducer Diameter =5.080 mm.

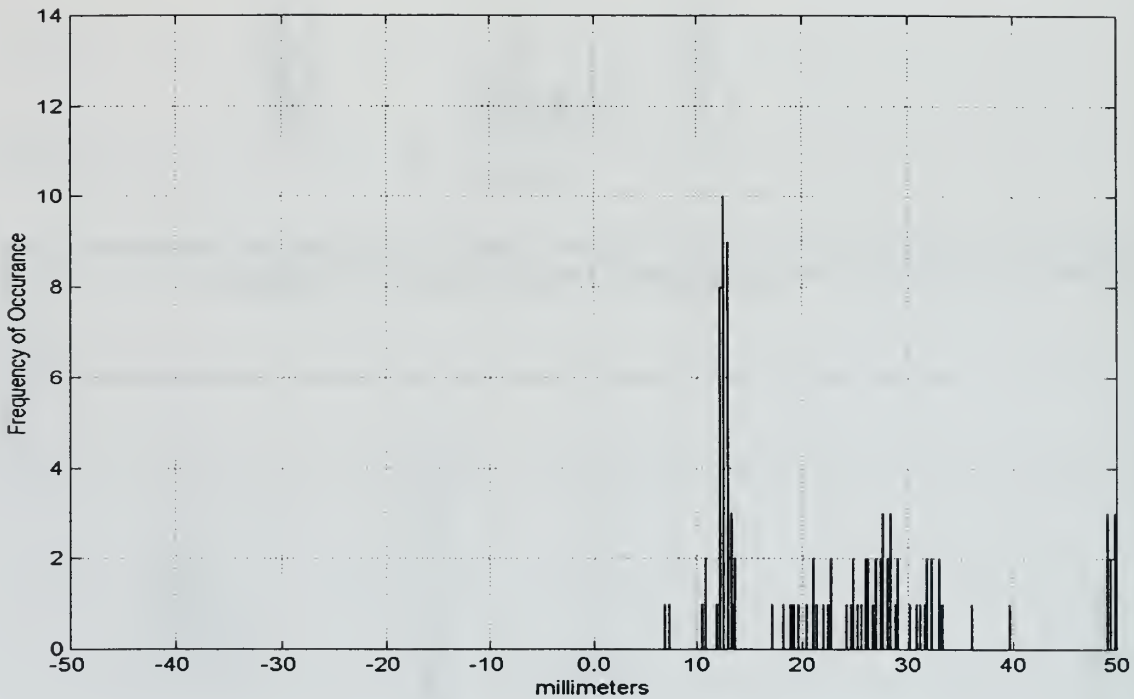

Figure B.45. Gaussian Crosscorrelation Location Histogram for Carbon Fiber Rod Sensors #1 and #4 Mean =22.825 mm, Std Dev. = 11.505 mm, Transducer Diameter = 5.080 mm.

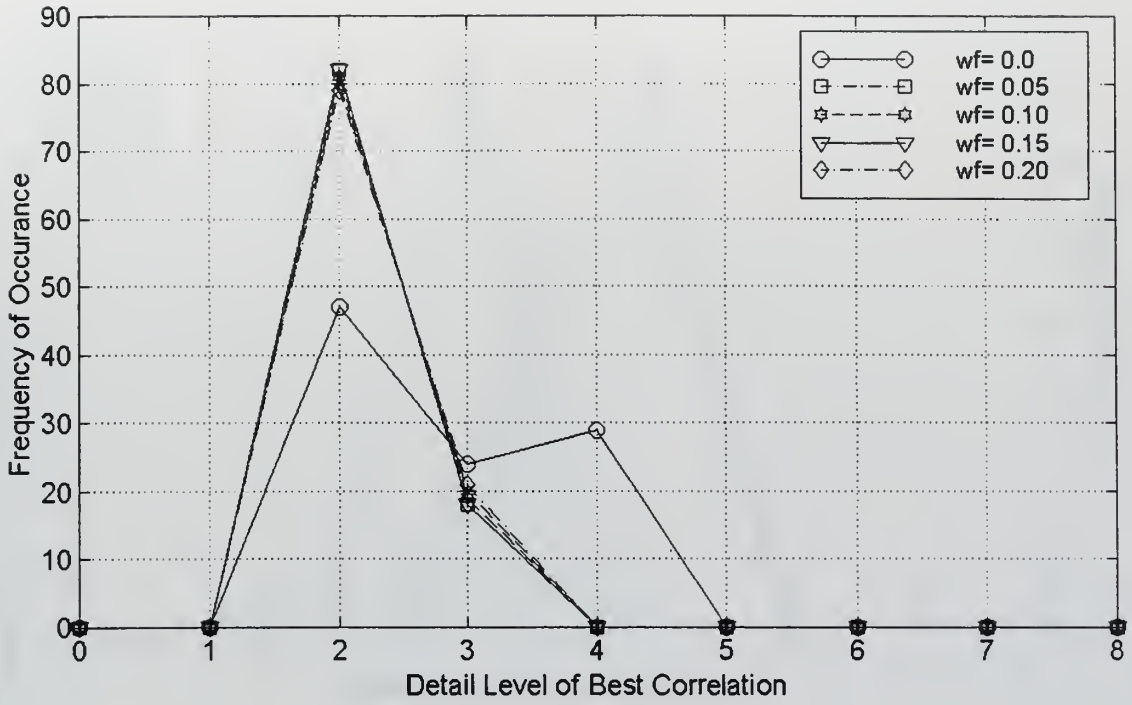

Figure B.46. Histogram of Detail Level of Best Crosscorrelation Carbon Fiber Rod Signals 01 through 100, Sensors #1 and #2, min.(variance/max.), weighting factor = [0.0, 0.05, 0.10, 0.15, 0.20]

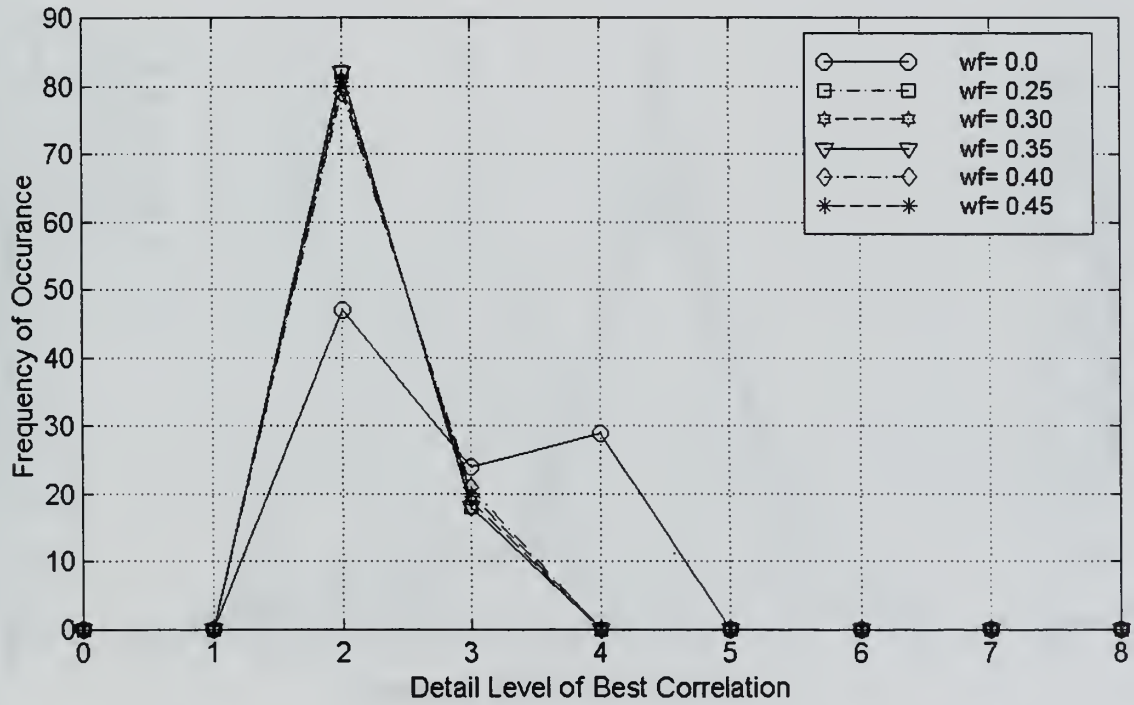

Figure B.47. Histogram of Detail Level of Best Crosscorrelation Carbon Fiber Rod Signals 01 - 100, Sensors #1 and #2, min.(variance/max.), weighting factor =[0.0, 0.25, 0.30, 0.35, 0.40, 0.45]

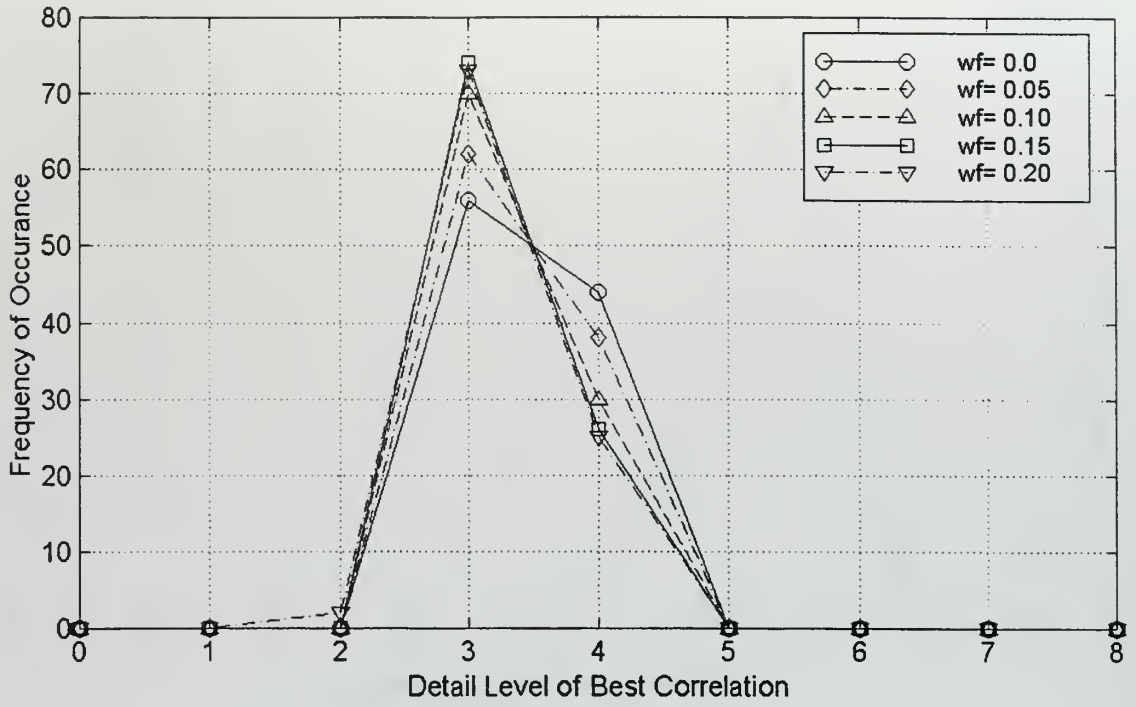

Figure B.48. Histogram of Detail Level of Best Crosscorrelation Carbon Fiber Rod Signals 01 - 100, Sensors #1 and 33, min.(variance/max.), weighting factor = [0.0, 0.05, 0.10, 0.15, 0.20]

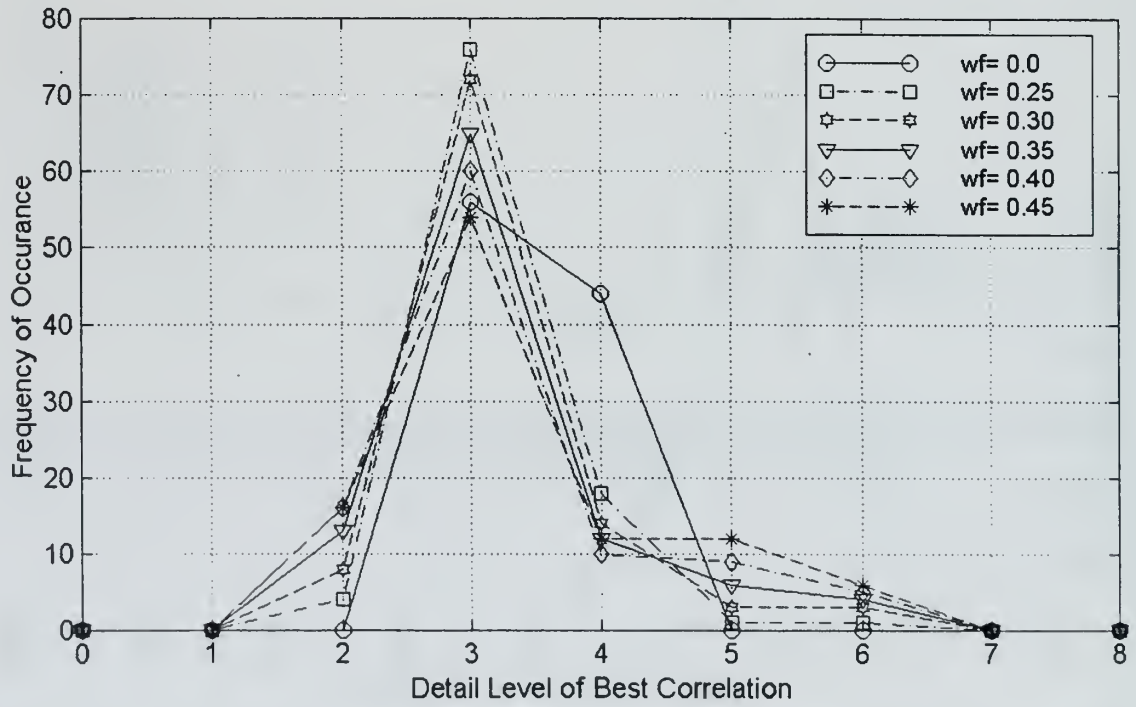

Figure B.49. Histogram of Detail Level of Best Crosscorrelation Carbon Fiber Rod Signals 01 - 100, Sensors #1 and 33, min.(variance/max.), weighting factor =[0.0, 0.25, 0.30, 0.35, 0.40, 0.45]

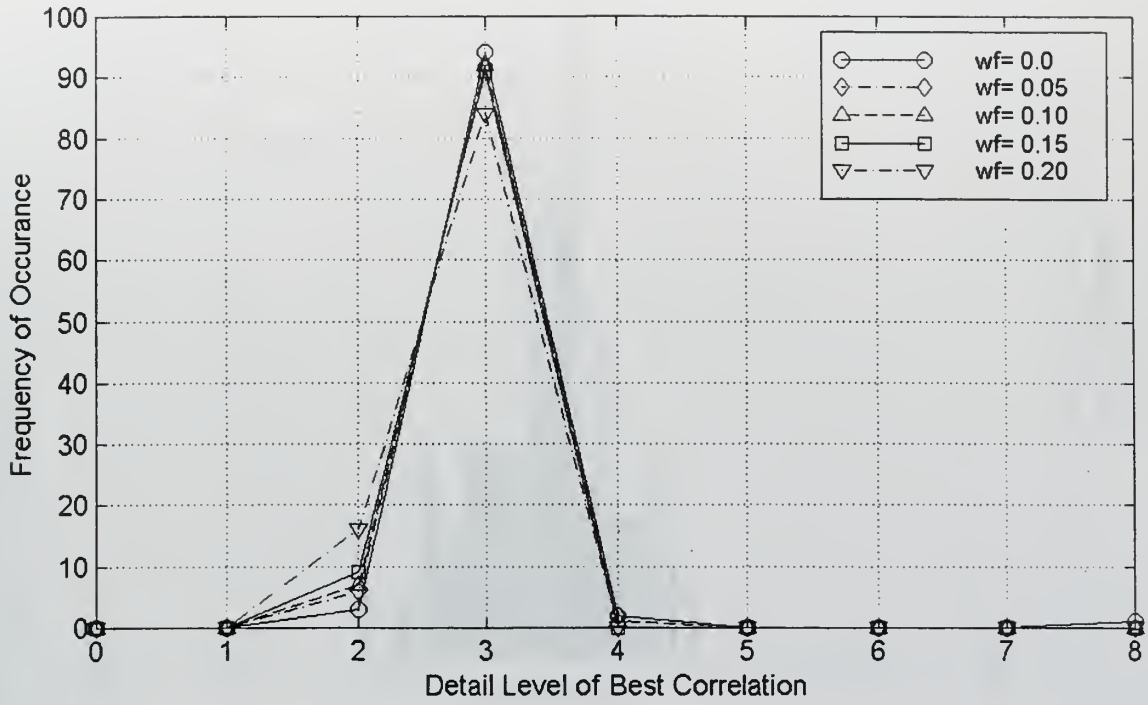

Figure B.50. Histogram of Detail Level of Best Crosscorrelation Carbon Fiber Rod Signals 01 - 100, Sensors #1 and #4, min.(variance/max.), weighting factor = [0.0, 0.05, 0.10, 0.15, 0.20]

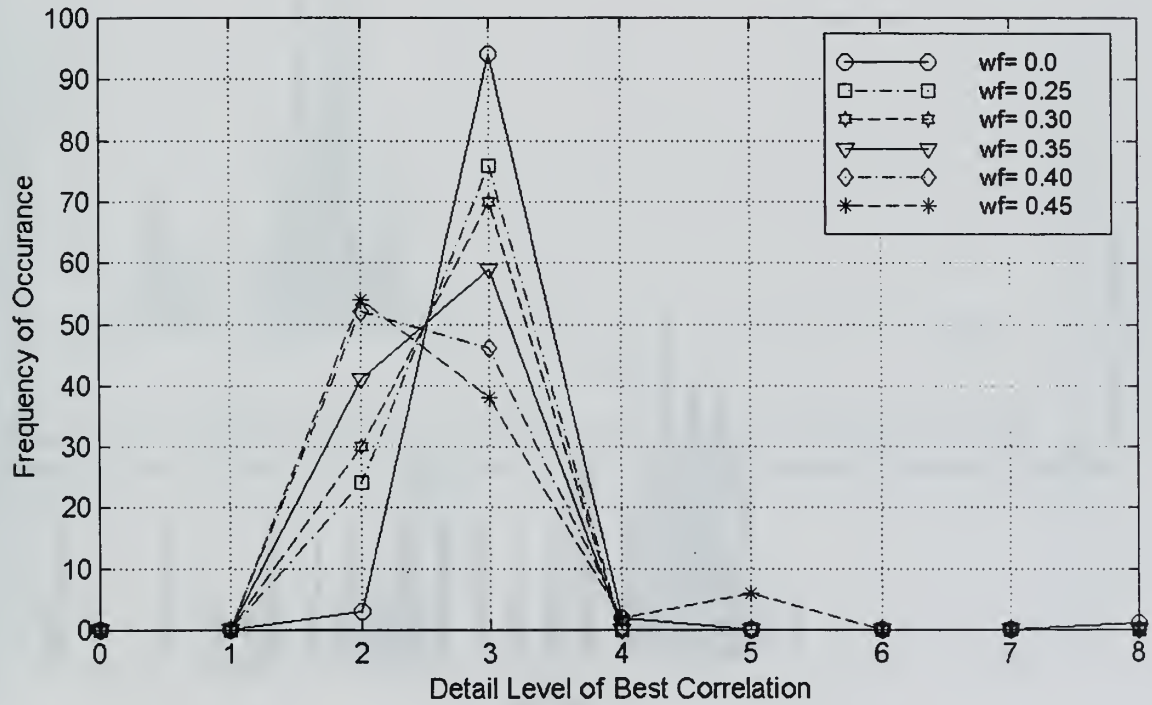

Figure B.51. Histogram of Detail Level of Best Crosscorrelation Carbon Fiber Rod Signals 01 - 100, Sensors #1 and 34, min.(variance/max.), weighting factor =[0.0, 0.25, 0.30, 0.35, 0.40, 0.45]

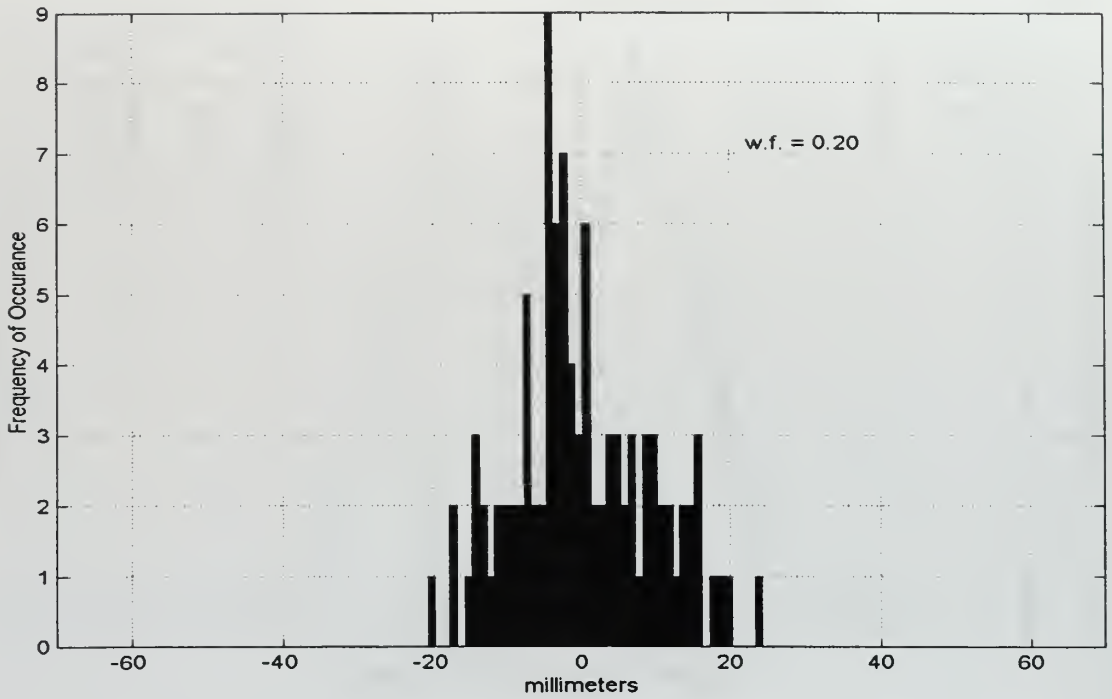

Figure B.52. Wavelet Detail Crosscorrelation Location Histogram for Carbon Fiber Rod Sensors #1 and #2, Mean = 0.000 mm, Std Dev. = 9.281 mm, Transducer Diameter = 5.080 mm.

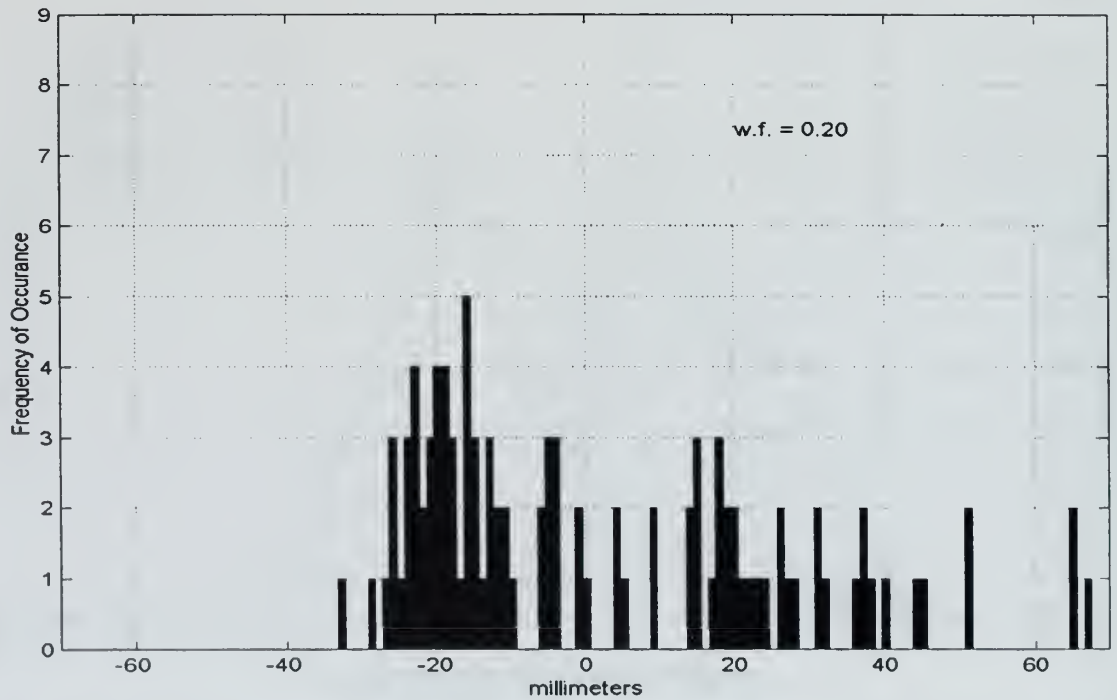

Figure B.53. Wavelet Detail Crosscorrelation Location Histogram for Carbon Fiber Rod Sensors #1 and #3, Mean = 1.726 mm, Std Dev. = 24.617 mm, Transducer Diameter = 5.080 mm.

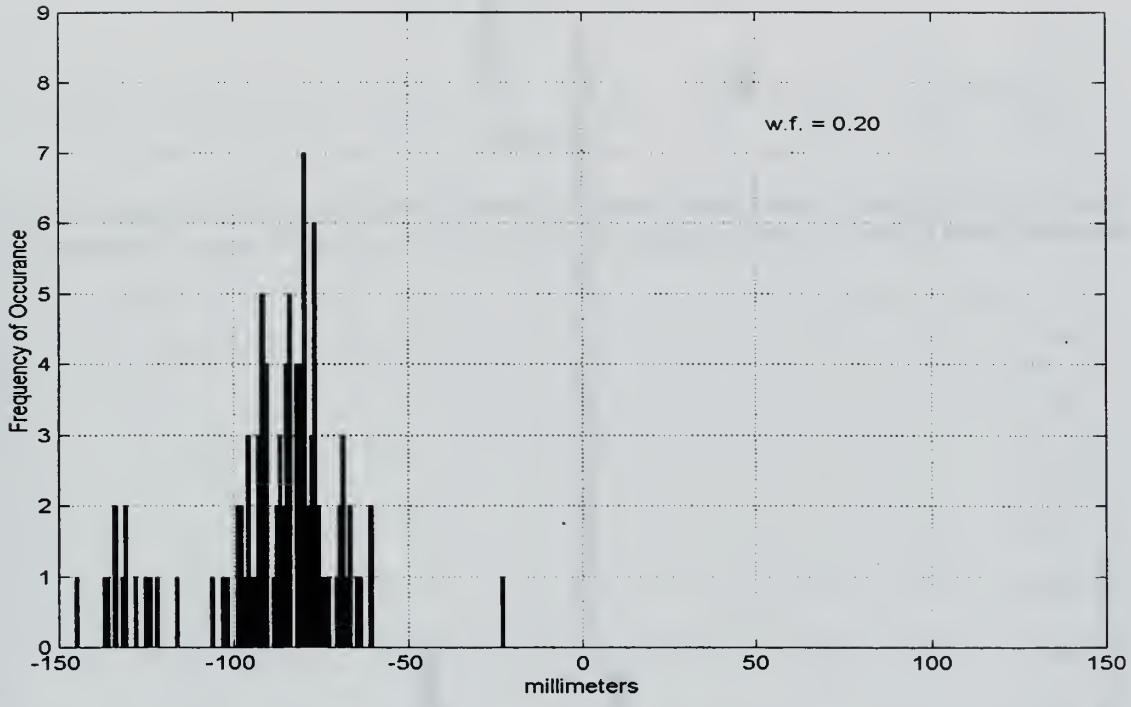

Figure B.54. Wavelet Detail Crosscorrelation Location Histogram for Carbon Fiber Rod Sensors #1 and #4, Mean = -88.572 mm, Std Dev. = 19.861 mm, Transducer Diameter = 5.080 mm.

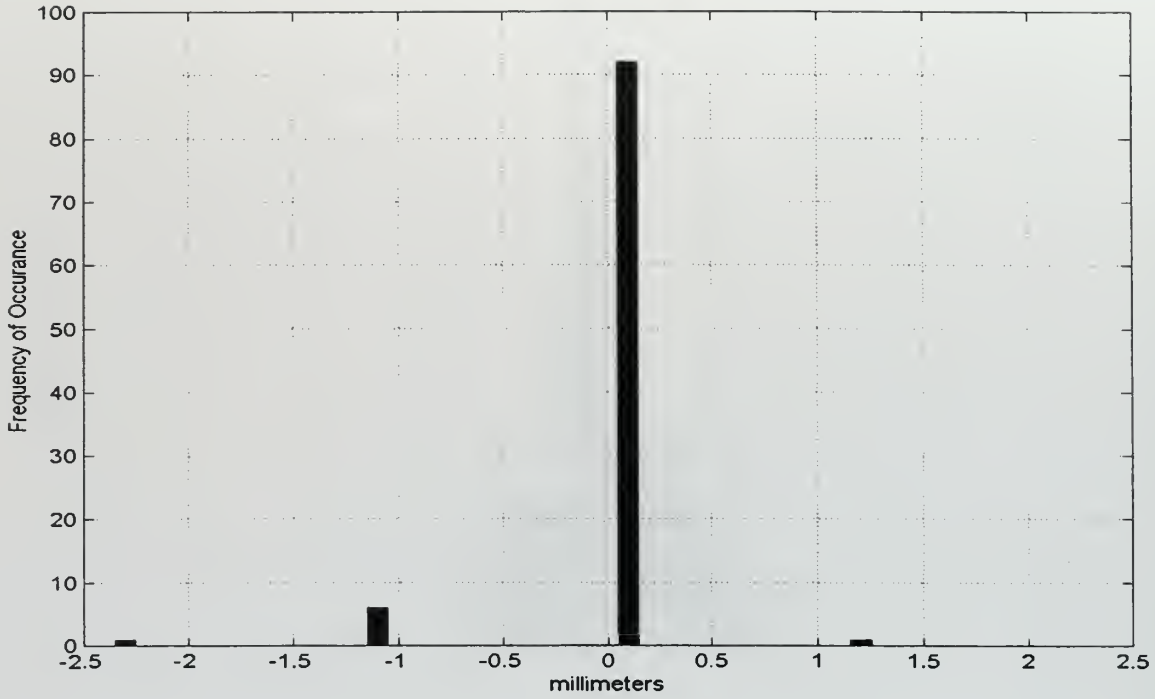

Figure B.55. Windowed Wavelet Detail Crosscorrelation Location Histogram for Carbon Fiber Rod Sensors #1 and #2, Mean = 0.000 mm, Std Dev. = 0.388 mm, Transducer Diameter = 5.080 mm.

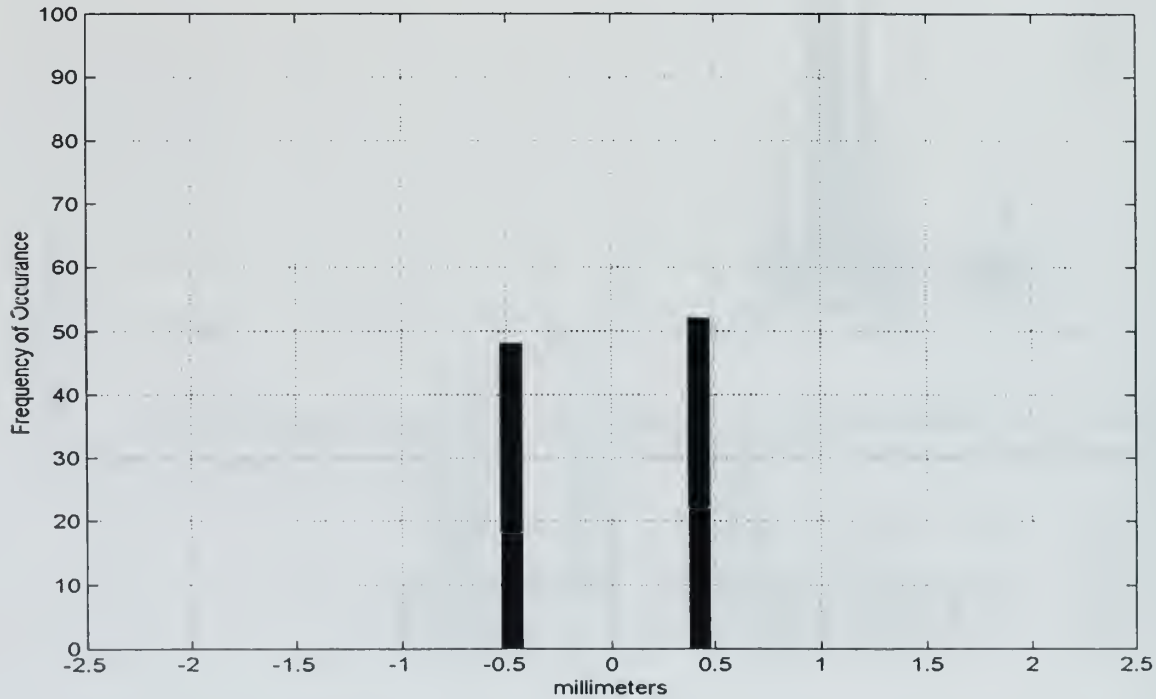

Figure B.56. Windowed Wavelet Detail Crosscorrelation Location Histogram for Carbon Fiber Rod Sensors #1 and #3, Mean = 0.000 mm, Std Dev. = 0.459 mm, Transducer Diameter = 5.080 mm.

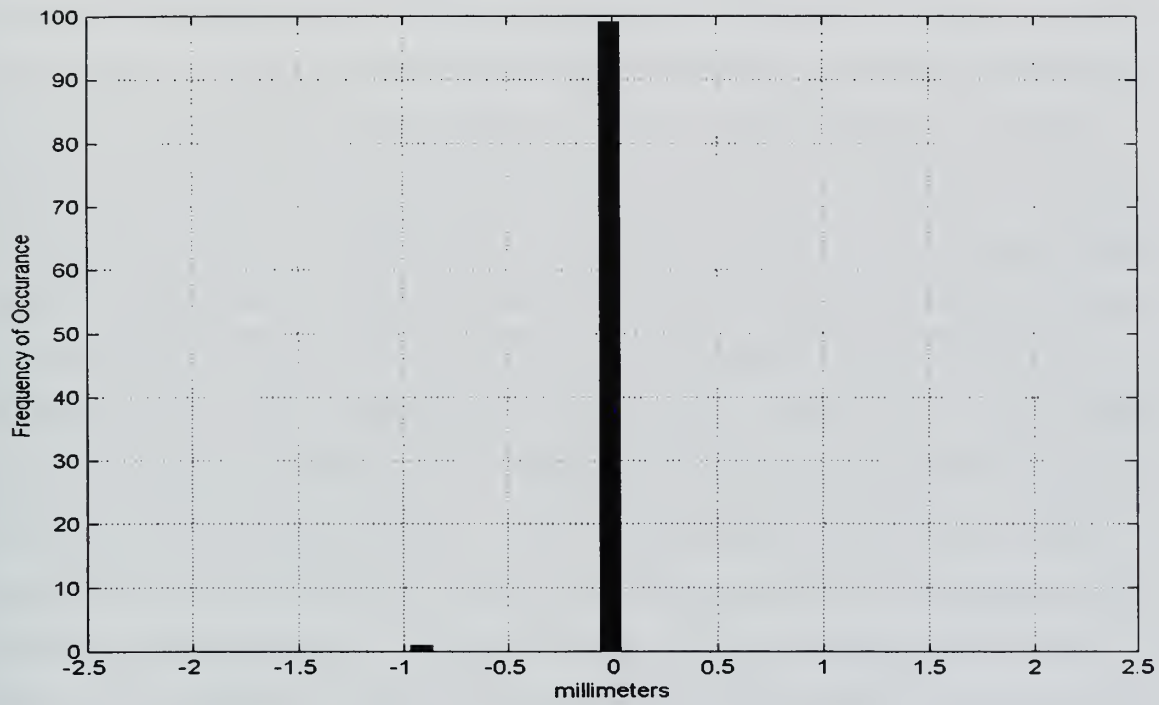

Figure B.57. Windowed Wavelet Detail Crosscorrelation Location Histogram for Carbon Fiber Rod Sensors #1 and #4, Mean = 0.000 mm, Std Dev. = 0.092 mm, Transducer Diameter = 5.080 mm.

APPENDIX C. EXPERIMENTAL METHODS

A. MAKING TEST SIGNALS

The Fracture Wave Detector hardware is set up in accordance with the FWD users guide. The step by step instructions are thorough and complete. If the specimen is not connected, begin with the large steel rod. Place the rod on the testing bench, and slide the for large transducer holders over the rod. Put the transducer holders on the rod where you want them. Place a small amount of silicon vacuum grease on each of the transducers and gently place them into the holders until the face of the transducer touches the test rod. Put a dental rubber band over the top, and attach it to the pins in the side of the transducer holders. Ensure that the rubber band lies over the top of the transducer. If two rubber bands are tied together to form a figure eight, two sets of them will maintain the contact force, and the rubber band will last longer. The large transducers and holders are sturdier than the small transducers, so they should be used until the system is familiar to the user. Connect the transducers to the preamplifiers, and the preamplifiers to the filter Trigger Modules. Verify the switch settings on the Filter Trigger Modules. The total gain should be in the range of 41 decibels to start. If the gain on the preamplifiers is 20 db, the gain *switch* on each FTM should be up, to +21 db. The gain *knob* should be fully counter-clockwise to 0 db. Double check that all four preamplifiers and all four channel on the FTM have identical settings. The filter and trigger settings are set per the FWD users guide. Plug all the power cords into a power strip, and use the switch on the power strip to turn the system on and off. The FWD hardware needs to be turned on with the computer to work properly. Acquisition of signals should be accomplished in DOS mode. The post test and location procedures may be done in Windows. When the computer finishes booting up, go the start button and select shut down. At the shut down window

toggle the radio button to "Restart in MS DOS Mode", and select OK. At the DOS prompt, change to the FWD directory by typing

C:\ cd fwd12 <return>

which will come back as

C:\FWD12\ <return>

to execute the FWD software, type

FWD96 <return>

The FWD12 window will now appear. If this is the first time using the module, take a hour to read the users guide, it will pay off in the long term. Use the mouse to select the acquisition module. Select setup and verify the settings. The pre-trigger setting should be 12.5%, the memory length 2048, and the digitization rate 10 Mhz. Check the four channel mode button, and select OK. The parametric settings are used only if there is a forcing function applied to the test specimen. Select start from the acquisition window. The window will now fill with the plot windows. Take the Pentel 0.3 mm pencil with H lead. Click five or six times on the end to extend the lead. Place the lead gently on the test specimen where the signal will originate. Hold the pencil at 30 to 45 degrees to the test surface, and increase force until the lead breaks. The trigger lights should flash, and the waveforms appear on the data windows. If there is only going to be one event per data file, select end, and name the file. Exit the acquisition module. And enter the post test module. The use of the location module is explained in the FWD users guide. In order to use the signal in MATLAB, in will need to be converted to tab delimited ASCII text. In the post test module, select File, and open the file that you just saved. On the menu bar select Export, select ASCII Text file type, retype the desired file name in the window, and hit OK. The file name will have a .txt extension automatically. Exit the post test module, and Quit the FWD program. This will return the computer to DOS. Type WIN to restart Windows. Start Excel, and open the file that was just saved. The file will have a .txt, so ensure that Excel is looking for text file types. The file will come

in as comma delimited text, and the program will step you through that. The data will be in five columns. The first column is the time, and the second through fifth columns are the signals from sensors one, two, three, and four respectively. Select Save As, and select Tab Delimited Text. The .txt extension needs to be changed to a .mat extension in order for MATLAB to read it. The file should be saved in the MATLAB directory. Exit Excel and start MATLAB. If the time column is unneeded, delete the column in Excel. The signal can be loaded into MATLAB by using the command

>> load *filemane.mat* -ascii

The MATLAB script files used in this thesis are in Appendix C. To plot the signals, wavelet decomposition's and crosscorrelation functions, use *signal_plotter.m*

APPENDIX D. MATLAB SCRIPT FILES

A. WAVEDETXCORR.M

```
%%%%%%%%%%%%%%%%%%%%%%%%%%%%%%%%%%%%%%%%%%%%%%%%%%%%%%%%%%%%%%%%%%%%%%%%%%%%
%     WAVEDETXCOR = Wavelet Detail Cross Correlation
%     Thesis1.m modified 2-20-98 to window the reconstructed details
%     from the left at the arrival of the longitudinal wave applied
%     to all levels, then from the left at the arrival of the Long.
%     and Trans. waves, finally window the detail levels which contain
%     the long. wave from the left by the long. arrival, and from the
%     right by the trans. wave arrival time, based on the theoretical
%     wave velocities.
clear;
format compact,format long g;
dataload_c;% data file of all the carbon fiber signals
location_window=zeros(100,8,3);%(100,3,10)
%%%%%%%%%%%%%%%%%%%%%%%%%%%%%%%%%%%%%%%%%%%%%%%%%%%%%%%%%%%%%%%%%%%%%%%%%%%%
%     Variable Input
k1=input('What point does the left window start?  ');
k2=input('What point does the right window end?  ');
windowed_signal=signal_setC(k1:k2,:,:);
for z=1:100% Input as 2048 pts
  [data sensor signal]=size(windowed_signal(:,:,z));
  dec_level=8;
  D=zeros(data,dec_level,sensor);
  Xcorl_0=zeros((2*data)-1,dec_level,(sensor-1));
%%%%%%%%%%%%%%%%%%%%%%%%%%%%%%%%%%%%%%%%%%%%%%%%%%%%%%%%%%%%%%%%%%%%%%%%%%%%
  %     Wavelet Decomposition
  for k=1:sensor
     [C(:,k,z),L]=wavedec(windowed_signal(:,k,z),dec_level,'db4');
  end
  %%%%%%%%%%%%%%%%%%%%%%%%%%%%%%%%%%%%%%%%%%%%%%%%%%%%%%%%%%%%%%%%%%%%%%%%%%%%
  %     Detail Reconstruction  D(i,j,k)=detail(1:2048,level,sensor#)
  for k=1:sensor
     for j=1:dec_level
        D(:,j,k)=wrcoef('d',C(:,k,z),L,'db4',j);
        %D(:,j,k)=D_temp(k1:data,j,k);%sets the window on each
        %detail level at the arrival of the long. wave at the trigger.
     end
  end
  %%%%%%%%%%%%%%%%%%%%%%%%%%%%%%%%%%%%%%%%%%%%%%%%%%%%%%%%%%%%%%%%%%%%%%%%%%%%
  %     Detail Cross Correlation
  % Xcorl(i,j,k)=Cross Correlation at each Detail level, j, between
  % Sensor 1 and the other three sensors, k.
  %      l = correlation # 1=1:2; 2=1:3; 3=1:4;
z
```

```
  for k=2:sensor
     l=k-1
     for j=1:dec_level
        Xcorl_0(:,j,l)=xcorr(D(:,j,1),D(:,j,k),'coeff');
        [max_peak(z,j,l) location_window(z,j,l)]=max(Xcorl_0(:,j,l));
     end     %2264:2515
     %      l = correlation # 1=1:2; 2=1:3; 3=1:4;
  end

end % end of signal loop
save left_window4 location_window;
```

B. WAVDETCORSTAT.M

```
function[xcorl,moa_1,moa_2,fac]=wavdetcorstat(x,dec,sen,wf)
%%%%%%%%%%%%%%%%%%%%%%%%%%%%%%%%%%%%%%%%%%%%%%%%%%%%%%%%%%%%%%%%%%%%%%%%%%%%
%     Variable Initialization
[r c s]=size(x);
t_index=(1:1:r)';
x2=zeros(r,c,s);f=zeros(c,s);mu=f;var=f;
for k=1:s
   for j=1:c
      [p(j,k) p_i(j,k)]=max(x(:,j,k));
      f(j,k)=(wf)*p(j,k);
%     Eliminate the values of the Cross Correlations below the WF.
      for i=1:r
         if x(i,j,k) >= f(j,k);
            x2(i,j,k) = x(i,j,k);
         else
            x2(i,j,k)=0.0;
         end
      end
      SIGMA=sum(x2(:,j,k));%   Area Under Curve.
      product=t_index.*x2(:,j,k);% Vectorized Product
      mu(j,k)=(sum(product))/SIGMA;
      shift=t_index-mu(j,k);
      var(j,k)=sum(((shift).^2).*x2(:,j,k));
   end
end
xcorl=x2;
moa_1=mu;
moa_2=var;
fac=f;
%%%%%%%%%%%%%%%%%%%%%%%%%%%%%%%%%%%%%%%%%%%%%%%%%%%%%%%%%%%%%%%%%%%%%%%%%%%%
%for j=1:dec_level
%   SuperXcorl(:,j)=xcorr(Xcorl(:,j,1),Xcorl(:,j,2),'coeff');
%end
%      Best Correlation Selection
%SuperXcorl=zeros(8189,dec_level,sensor-1);
```

C. SIGNAL_PLOTTER.M

```
%     Signal_plotter  Plots desired signals, details, crosscorrelations.
clear;format compact,format short g;
close(figure(1));close(figure(2));close(figure(3));close(figure(4));
close(figure(5));close(figure(6));close(figure(7));close(figure(8));
close(figure(9));
%%%%%%%%%%%%%%%%%%%%%%%%%%%%%%%%%%%%%%%%%%%%%%%%%%%%%%%%%%%%%%%%%%%
%     Variable Input
load c89.mat -ascii  % Change to load the desired file.
signal=c89(:,:);% Only sensor data kept.
[data sensor]=size(signal);
dec_level=8;%input('What level decomposition ?   ');
D=zeros(data,dec_level,sensor);
Xcorl_0=zeros((2*data)-1,dec_level,(sensor-1));
%%%%%%%%%%%%%%%%%%%%%%%%%%%%%%%%%%%%%%%%%%%%%%%%%%%%%%%%%%%%%%%%%%%
%     Wavelet Decomposition
for k=1:sensor
   [C(:,k),L]=wavedec(signal(:,k),dec_level,'db4');
end
%%%%%%%%%%%%%%%%%%%%%%%%%%%%%%%%%%%%%%%%%%%%%%%%%%%%%%%%%%%%%%%%%%%
%     Detail Reconstruction  D(i,j,k)=detail(1:2048,level,sensor#)
for k=1:sensor
   for j=1:dec_level
      D(:,j,k)=wrcoef('d',C(:,k),L,'db4',j);
   end
end
%%%%%%%%%%%%%%%%%%%%%%%%%%%%%%%%%%%%%%%%%%%%%%%%%%%%%%%%%%%%%%%%%%%
%     Detail Cross Correlation
% Xcorl(i,j,k)=Cross Correlation at each Detail level, j, between
% Sensor 1 and the other three sensors, k.
%      l = correlation # 1=1:2; 2=1:3; 3=1:4;
for k=2:sensor
   l=k-1;
   for j=1:dec_level
      Xcorl_0(:,j,l)=(xcorr(D(:,j,1),D(:,j,k),'coeff'));
      max_peak(j,l)=max(Xcorl_0(:,j,l));
   end
%      l = correlation # 1=1:2; 2=1:3; 3=1:4;
end
%%%%%%%%%%%%%%%%%%%%%%%%%%%%%%%%%%%%%%%%%%%%%%%%%%%%%%%%%%%%%%%%%%%
%     Call to WAVDETCORSTAT
%     WAVlet DETail CORrelation STATistics
wf=0.85;
[Xcorl,MoA_1,MoA_2,fac]=wavdetcorstat(Xcorl_0,dec_level,sensor,wf);
%%%%%%%%%%%%%%%%%%%%%%%%%%%%%%%%%%%%%%%%%%%%%%%%%%%%%%%%%%%%%%%%%%%
%     Determine Smallest Second Moments of the Reduced Correlations
for k=1:sensor-1
    for j=1:dec_level
       Best_parameter(j,k)=MoA_2(j,k)/max_peak(j,k);
    end
    [Min_try(k) min_index(k)]=min(Best_parameter(:,k));
```

```
end
%%%%%%%%%%%%%%%%%%%%%%%%%%%%%%%%%%%%%%%%%%%%%%%%%%%%%
%     Plotting Signals, Details, and Cross Correlations
DL=int2str(dec_level);
M1=int2str(min_index(1));M2=int2str(min_index(2));
M3=int2str(min_index(3));
%     Original Signals     %
fig=1;
figure(fig)
subplot(sensor,1,1),plot(signal(:,1),'r'),grid,hold
title('Graphite Rod Signal 89 Sensor 1 Raw Signal')
axis([0 2048 -.37 .37])
set(gca,'XTickLabel',[' '])
subplot(sensor,1,2),plot(signal(:,2),'b'),grid,hold
title('Sensor 2 Raw Signal')
axis([0 2048 -.37 .37])
set(gca,'XTickLabel',[' '])
subplot(sensor,1,3),plot(signal(:,3),'g'),grid,hold
title('Sensor 3 Raw Signal')
axis([0 2048 -.37 .37])
set(gca,'XTickLabel',[' '])
subplot(sensor,1,4),plot(signal(:,4),'m'),grid,hold
title('Sensor 4 Raw Signal')
axis([0 2048 -.37 .37])
fig=fig+1;
%
%         Details            %
for k=1:sensor
   K=int2str(k);
   figure(fig)
   subplot(dec_level,1,1),plot(D(:,1,k)),grid,hold
   set(gca,'XLim',([0 2048]))
   set(gca,'XTickLabel',[' '])
   title(['Sensor ',K,' Detail 1'])
   for j=2:dec_level-1
      DT=int2str(j);
      subplot(dec_level,1,j),plot(D(:,j,k)),grid,hold
      set(gca,'XLim',([0 2048]))
      set(gca,'XTickLabel',[' '])
      title(['Detail ',DT])
    end
    subplot(dec_level,1,dec_level),plot(D(:,dec_level,k)),grid on,hold
on
    set(gca,'XLim',([0 2048]))
    title(['Detail ',DL])
    fig=fig+1;
end

%     Cross Correlations     %
for k=1:(sensor-1)
   figure(fig)
   SN=int2str(k+1);
```

```
   subplot(dec_level,1,1),plot(Xcorl_0(:,1,k)),grid on,hold on
   plot([0 4095],[fac(1,k) fac(1,k)],'r')
   title(['Sensor 1 Cross Correlated with Sensor',SN,',Detail Level 1'])
   set(gca,'XTickLabel',[' '])
   axis([0 4095 -1 1])
   for j=2:dec_level-1
      DT=int2str(j);
      subplot(dec_level,1,j),plot(Xcorl_0(:,j,k)),grid on,hold on
      plot([0 4095],[fac(j,k) fac(j,k)],'r')
      title(['Detail ',DT])
      set(gca,'XTickLabel',[' '])
      axis([0 4095 -1 1])
   end
   subplot(dec_level,1,dec_level),plot(Xcorl_0(:,dec_level,k)),grid
on,hold on
   plot([MoA_1(dec_level,k) MoA_1(dec_level,k)],[-1 1],'r')
   title(['Detail Level ',DL])
   axis([0 4095 -1 1])
   fig=fig+1;
end  % end of signal_plotter
```

LIST OF REFERENCES

Allen, D.H., Haisler, W.E., *Introduction to Aerospace Structural Analysis*, John Wiley and Sons, 1985.

Chui, C.K., *Wavelets: A Tutorial in Theory and Applications*, Academic Press Inc.,1992.

Cohen, A., Kovacevic, J., *Wavelets: A Mathematical Background*, Proceedings of the IEEE, vol. 84, no. 4, pp. 514-522, April 1996.

Cooper, G.R., McGillem, C.D., *Probabilistic Methods of Signal and System Analysis*, pp. 110-220, Oxford University Press, 1986.

Davies, R.M., *Stress Waves in Solids*, Cambridge Monographs on Mechanics and Applied Mathematics, pp 64-138, Cambridge University Press, 1956.

Daubechies, I., *Ten Lectures on Wavelets*, Society For Industrial and Applied Mathematics, 1992.

Fracture Wave Detector Users Manual, Digital Wave Corporation, March 1996.

Gade, S., Gram-Hansen, K.,*The Analysis of Nonstationairy Signals*, Sound and Vibration, pp. 40-46, January 1997.

Gish, D.A., *Failure Site Location By Acoustic Emission For Composite Reliability Assurance*, Master's Thesis, Naval Postgraduate School, Monterey, California, September 1995.

Hess-Nielsen, N., Wickerhauser, M.V., *Wavelets and Time Frequency Analysis*, Proceedings of the IEEE, vol. 84, no. 4, pp. 523-540, April 1996.

Kolsky, H., *Stress Waves in Solids*, pp. 1-86, Oxford University Press, 1953.

Lurie, R., *Wavelet Analysis Using the MATLAB Wavelet Toolbox*, pp. 1-61, The Mathworks Incorporated, 1996.

Strang, G., Nguyen, T., *Wavelets and Filter Banks*, Wellesley-Cambridge Press, 1996.

Sweldens, W., *Wavelets: What's Next?*, Proceedings of the IEEE, vol. 84, no. 4, pp. 680-685, April 1996.

Ziola, S.M., *Source Location in Thin Plates Using Crosscorrelation*, PhD. Dissertation, Naval Postgraduate School, Monterey, California, December 1991.

INITIAL DISTRIBUTION LIST

1. Defense Technical Information Center 2
   8725 John J. Kingman Rd. STE 0944
   Ft. Belvoir, Virginia 22060-6218

2. Dudley Knox Library 2
   Naval Postgraduate School
   411 Dyer Rd.
   Monterey, California 93943-5101

3. Prof. Gerald H. Lindsey 1
   Code AA/Li
   Department of Aeronautical Engineering
   Naval Postgraduate School
   Monterey, California 93943-5000

4. Prof. Edward M. Wu 3
   Code AA/Wu
   Department of Aeronautical Engineering
   Naval Postgraduate School
   Monterey, California 93943-5000

5. Army Research Office 1
   Engineering and Environmental Science Division
   Post Office Box 12211
   Research Triangle Park, North Carolina 27709-2211
   Attn: Dr. Kailasam Iyer

6. Naval Research Laboratory 1
   Mechanics of Materials Branch Code 6380
   Washington D.C. 20375
   Attn: Dr. Robert Badaliance

7. Army Research Laboratory 1
   Bldg 4600
   Aberdeen Proving Ground, Maryland 21005-5069
   Attn: Dr. S.C. Chou

8. Digital Wave Corporation.....1
   14 Inverness Drive East
   Building B, Suite 120
   Englewood, Colorado 80112
   Attn: Dr. Steven Ziola

9. LCDR Joseph G. Jerauld 3
   5636 Nokomis Drive
   La Mesa, California 92041